Photocopy and Use Authorization

In presenting this thesis in partial fulfillment of the requirements for an advanced degree at Idaho State University, I agree that the Library shall make it freely available for inspection. I further state that permission to download and/or print my thesis for scholarly purposes may be granted by the Dean of the Graduate School, Dean of my academic division, or by the University Library. It is understood that any copying or publication of this thesis for financial gain shall not be allowed without my written permission.

Signature_____

Date_____

Neutron Beam Characterization at the Neutron Radiography Reactor at the Idaho National Laboratory

By

Sam Henry Giegel

A thesis

submitted in partial fulfillment

of the requirements of the degree of

Master of Science in the Department of Nuclear Science and Engineering

Idaho State University

Spring 2018

Committee Approval

To the Graduate Faculty:

The members of the committee appointed to examine the thesis of Sam H. Giegel find it satisfactory and recommend it be accepted.

_____

Dr. Chad Pope,

Major Advisor

_____

Dr. George Imel,

Committee Member

_____

Dr. Aaron Craft,

Committee Member

_____

Dr. Seyed Mousavinezhad,

Graduate Faculty Representative

Acknowledgments

I would like to thank Dr. Aaron Craft, Dr. Chad Pope and Dr. George Imel for advising me through the past couple years on this project. Their patience and guidance has helped me develop professionally and academically in this field of expertise. I would also like to thank the NRAD team of engineers and operators who spent some sleepless nights performing these experiments and making sure I received the data in a timely manner. The Department of Energy should also be acknowledged for recognizing the importance of this work and providing funds for the project through the Laboratory Directed Research and Development program (LDRD 16-070).

Vita

I was born in Greenville, Pennsylvania on December 1st, 1992. I graduated from Reynolds High School in 2011 and enrolled at Idaho State University (ISU) as an undergraduate in nuclear engineering. During my undergraduate career I became an NRC certified reactor operator for the AGN-201 reactor at ISU and worked for the Technical Safety office performing radiation surveys of lab rooms and instrument calibrations. I also had the opportunity to be involved in an internship with Idaho National Laboratory the summer of 2015. I graduated with a bachelor's of science in nuclear engineering in 2016. I immediately enrolled in the graduate program at ISU where I met my future wife, Larinda Nichols, who was also enrolled in the nuclear engineering graduate program. I plan on graduating in May of 2018 and could not be more thankful for the opportunities that ISU has presented me with over the 7 years I have been enrolled.

Dedication

All of the hard work put into this project is dedicated to my loving and supporting family. My Pennsylvania family (Mom, Dad, Lucy and Jacob) who has supported me in my all my decisions and shaped me into the person I am today and to my Idaho family (Larinda, Dennis and Ayla) who have opened my eyes to see the bright and beautiful future that I have in the gem state.

Table of Contents

List of Figures viii

List of Tables x

Abstract xi

1 Introduction 1

2 Background 3

2.1 NRAD Facility Description 3

2.2 Description of Beamlines 4

2.3 Neutron Radiography: Techniques and Methods 6

2.4 Neutron Beam Characteristics 7

2.4.1 L/D Ratio 8

2.4.2 Neutron Beam Flux 12

2.4.3 Neutron Beam Flux Profile 13

2.4.4 Cadmium Ratio of the Neutron Beam Flux 15

2.4.5 Image Quality 17

2.4.6 Neutron Energy Spectrum 20

2.4.7 Gamma Energy Spectrum 22

3 Methods & Materials 26

3.1 L/D Ratio 26

3.2 Neutron Beam Flux 28

3.3 Neutron Beam Flux Profile 32
3.4 Cadmium Ratio of the Neutron Beam Flux 33
3.5 Image Quality 34
3.6 Neutron Energy Spectrum 34
3.6.1 Foil Activation Description 34
3.6.2 Unfolding with MAXED and GRAVEL 39
3.6.3 Monte Carlo N-Particle Transport Description 42
3.6.4 Comparison of MCNP and UMG Codes 48
4 Results & Discussion 50
4.1 Neutron Beam Flux 50
4.2 Neutron Beam Flux Profile 52
4.3 Cadmium Ratio of the Neutron Beam Flux 53
4.4 Image Quality 54
4.5 Neutron Energy Spectrum 57
4.5.1 Bare Foil Results 57
4.5.2 Cadmium Covered Foil Results 69
4.5.3 Sensitivity Analysis of GRAVEL Spectrum 73
4.5.4 Comparison of MCNP and UMG Energy Spectra 74
5 Summary and Conclusions 82
6 Future Work 84

7 References 85

8 Appendices 90

Appendix A: Self-shielding and Scattering Correction Factors 90

Appendix B: UMG input files..... 91

Appendix C: Cadmium Covered Foil Response Functions 95

Appendix D: MCNP input file of ERS model 98

Appendix E: MCNP vs UMG Analysis. 112

Appendix F: Experimental Validation of the MCNP6 East Beam Line Model 115

Appendix G: Shielding Analysis in ERS for an HPGe Detector 120

List of Figures

Figure 1. Top View of the NRAD reactor core [2] 3

Figure 2. Picture of the umbra concept. 9

Figure 3. Pictures of a typical NU device [7]. 10

Figure 4. Cadmium sheet NU device with different diameters [8]. 11

Figure 5. Gd and Hf wedge dimensions and experimental orientation. 11

Figure 6. a) Horizontal plot profile b) Vertical plot profile [10]. 14

Figure 7. Microscopic absorption cross-section of Cd vs Au [14]. 16

Figure 8. a) Beam purity indicator b) Sensitivity indicator. 18

Figure 9. L/D apparatus setup in the East Radiography Station. 27

Figure 10. 21-gold foil array setup. 28

Figure 11. Example gamma energy spectrum of a ^{198}Au [27]. 29

Figure 12. Cadmium covered gold foil and cadmium covered array. 33

Figure 13. General response ranges for the selected foils. 36

Figure 14. Experimental setup of multi-foil array (dimensions are in inches). 37

Figure 15. Labeled diagram of multi-foil setup 37

Figure 16. ERS MCNP6 model (plan view). 43

Figure 17. F2 surface tally in NRAD reactor MCNP model. 44

Figure 18. Beam filter window where F2 tallies were taken of reactor source. 45

Figure 19. Modified F4 tally of (n, γ) reaction in indium foil. 46

Figure 20. Elevator tube and image plane where MCNP6 tallies are taken. 46

Figure 21. Neutron flux as a function of position on the image plane in the ERS. 52

Figure 22. 3-Dimensional representation of neutron flux profile in ERS 53

Figure 23. Neutron radiographs of IQIs. From left to right: Indium Foil, Dysprosium Foil. 56
Figure 24. Energy-normalized default spectrum per source particle. 60
Figure 25. Response functions of foils 1, 2, 4, 7, and 9 (bare). 62
Figure 26. Response functions of foils 12, 16, 17, 20, and 21 (bare). 63
Figure 27. Response functions of foils 3, 5, 8, 10, 11, 13, and 14 (bare). 64
Figure 28. UMG output of initial solution spectrum. 65
Figure 29. MCNP tally used to calculate inelastic cross-section of ^{115}In. 66
Figure 30. Lethargy-normalized neutron energy spectrum comparison (ERS - bare). 67
Figure 31. Energy-normalized neutron energy spectrum comparison (ERS - bare) 68
Figure 32. Raw neutron energy spectrum comparison (ERS - bare) 68
Figure 33. MAXED output spectrum based on cadmium covered and bare foil measurements. . 72
Figure 34. GRAVEL output spectrum based on cadmium covered and bare foil measurements. 72
Figure 35. Source vs Image Plane comparison in the original MCNP model. 75
Figure 36. Visual derivation of the source definition for the hybrid spectrum. 77
Figure 37. Activity comparison between three simulated spectrum and measured data. 78
Figure 38. Neutron energy spectrum at the image plane of the ERS facility (energy-normalized). 80
Figure 39. Neutron energy spectrum at the image plane of the ERS facility (raw neutron flux). 81

List of Tables

Table 1. Definitions of D parameters [15]. 19

Table 2. H and G values [15]. 19

Table 3. Description of categorized facilities based on image quality [15]. 20

Table 4. Foil information for the neutron spectrum measurements. 35

Table 5. Uncertainties in measured parameters used to calculate neutron flux. 50

Table 6. Neutron flux measurements at the image plane (ERS). 51

Table 7. Cadmium covered gold foil activity measurements (ERS). 54

Table 8. Beam purity indicator densities. 55

Table 9. IQI determined values vs a category I radiographic facility. 55

Table 10. Measured responses of the bare multi-foil array. 58

Table 11. SPR results from measured data and MCNP (bare foils). 59

Table 12. MCNP calculated default energy spectrum in the east beamline. 61

Table 13. MCNP vs measured activities from In-115(n,n')In-115m reaction. 66

Table 14. Measured responses of the cadmium covered multi-foil array. 70

Table 15. SPR results from measured data and MCNP (cadmium covered). 71

Table 16. Chi-square values of the GRAVEL spectrum as a function of perturbing the foil response 74

Table 17. Attenuation factors and GRAVEL source definitions for the ERS beam line MCNP model 76

Table 18. Ratio of measured data to GRAVEL and Hybrid spectra for the bare foil set. 79

Neutron Beam Characterization at the Neutron Radiography Reactor at the Idaho National Laboratory

Thesis Abstract – Idaho State University (2018)

The Neutron Radiography Reactor (NRAD) at the Idaho National Laboratory (INL) has two beamlines extending out of the east and north faces of the reactor core. The control rod withdrawal procedure has been altered recently, potentially changing the physics of the neutron beams, requiring re-characterization. The characterization of the East Radiography Station (ERS) involved experiments used to measure the following characteristics: Neutron flux, neutron flux profile, cadmium ratio, image quality and the neutron energy spectrum. The thermal neutron flux was measured using gold foil activation and determined to be $9.61 \times 10^6 \pm 2.47 \times 10^5$ *n/cm*^{2}*-s* with a relatively uniform profile across the image plane. The cadmium ratio measurement was performed using bare and cadmium covered gold foils and measured to be 2.05 ± 2.9%. The ERS is a category I facility signifying it has the highest possible rank a radiography station can achieve.

The neutron energy spectrum was measured using foil activation coupled with unfolding algorithms provided by the software package unfolding with MAXED and GRAVEL (UMG). The Monte-Carlo N-Particle (MCNP6) transport code was used to assist with the unfolding process. UMG, MCNP6, and measured foil activities were used to determine a neutron energy spectrum which was implemented into the MCNP6 model of the ERS to contribute to future studies.

Key Words: Neutron Beam Characterization, Neutron Radiography, NRAD, Neutron Energy Spectrum, Neutron Flux.

1 Introduction

The Neutron Radiography Reactor (NRAD) plays an important role at Idaho National Laboratory (INL) by contributing to the non-destructive analysis of used nuclear fuel and other irradiated items. There are many ways to examine spent fuel but most require destructive examination to observe the phenomena that occurred on the inside, destroying the sample and limiting its use for future experiments. The NRAD facility allows the fuel to be examined by neutron radiography. The experimenter studying the fuel can observe what is happening inside the cladding by looking at a radiograph produced by the beamline. The nondestructive nature of neutron radiography allows the spent fuel to be further examined. The NRAD facility has an ideal location directly underneath the Hot Fuel Examination Facility (HFEF) that was built to safely handle highly radioactive samples. An elevator in the ERS provides access to HFEF and positions samples in the beamlines for neutron radiography.

The NRAD reactor's fuel was converted to low-enriched uranium and upgraded from a 60-fuel element core (Highly Enriched Uranium) to a 64-fuel element core (Low Enriched Uranium) in 2012. The east neutron beam was characterized after the upgrade to record how the beam properties changed [1]. Recently, the NRAD reactor engineers have changed the way the control rods are withdrawn in the reactor core, which may impact the neutron intensity in the two beam line. The banking of the control rods has most likely changed the characteristics of many parameters of the neutron beams and for this reason the beams must be characterized again.

The characterization involved measuring the L/D ratio of the beam, the neutron beam flux and spatial variance, the neutron energy spectrum, gamma energy spectrum, cadmium ratio, and the image quality the beam can provide. The project scope covered a two-to-three-year period where a student from Idaho State University prepared a literature review of the various techniques

then designed and performed an assortment of experiments to characterize the neutron beamlines at the NRAD facility. Additionally, a report was composed to guide future neutron beam characterization efforts.

These characterization efforts serve two major purposes for INL. The first purpose of the project was to characterize the two neutron beamlines in the NRAD facility to give the engineers and scientists a valuable understanding of how the beam characteristics have changed. The second purpose of this effort was to develop a suite of procedures to be used in future neutron beam characterization efforts to provide future users and developers with a reference guide to characterize the beams when parameters in the reactor core change. The reference guide will be a general guide for all neutron beams at INL, not just the NRAD facility.

2 Background

2.1 NRAD Facility Description

The NRAD facility is a TRIGA-Mark II reactor design that produces power up to 250 kW_{th}. It sits below the HFEF providing easy access to the radioactive materials the NRAD facility might need to image. The reactor is water and graphite moderated and contains a total of 64 cylindrical fuel elements. Figure 1 shows the configuration of the fuel elements, along with 4 graphite elements, 2 shim control rods and one regulating rod.

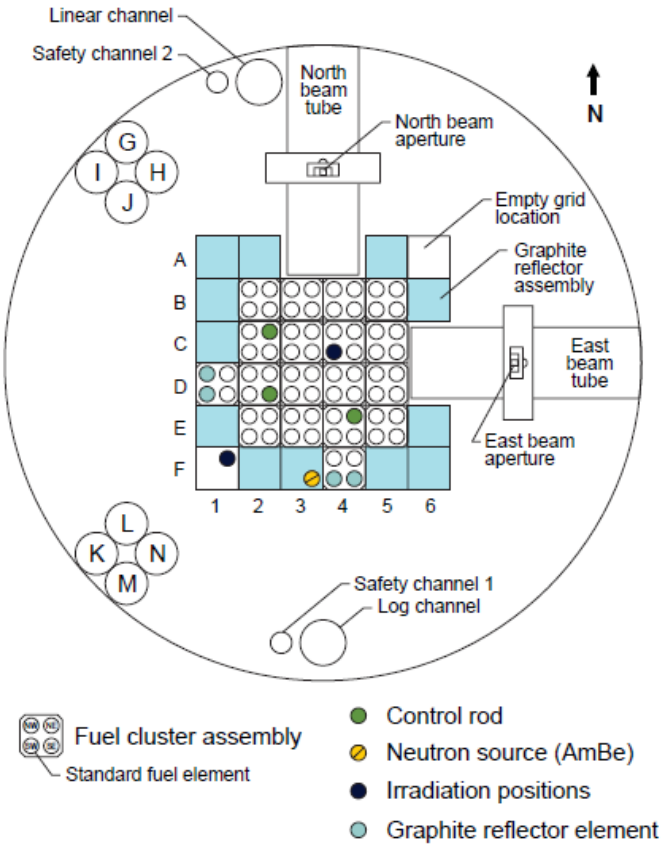

Figure 1. Top View of the NRAD reactor core [2].

Each fuel rod contains 19.75% enriched uranium which is approximately 30% of the fuel in the assembly. The uranium is mixed with zirconium, hydrogen, and natural erbium (UZrH-Er) that acts as a burnable poison to compensate for the excess reactivity in the core [2]. The fuel rods

have a 1.37-inch (3.4798 cm) diameter and a total length of 23.125 inches (58.738 cm). NRAD contains 3 boron-carbide (B_4C) control rods with slightly different physical dimensions from the fuel elements. A graphite reflector surrounds the reactor core to reduce leakage of neutrons. The reactor is initially brought to start-up conditions using a 5 Ci americium-beryllium neutron source. The start-up source emits 10^7 neutrons per second and remains in the core during operation until the reactor is shutdown [2].

2.2 Description of Beamlines

The neutron radiography facility has two beam ports facing east and north of the reactor core. The East Radiography Station (ERS) is a 15-foot, air and helium filled, aluminum tube starting at the outer east edge of the reactor core. The apertures for the beam are placed about halfway in between the outer edge of the reactor core and the outer wall of the reactor vessel. The aperture devices are made of boron nitride with three circular holes cut out to collimate the beam. The holes come in three different size diameters: 3.5, 1.39, and 0.59 inches. The length of the beam, from the aperture to the image plane (L) and the diameter of the aperture (D) can be used to describe a specific characteristic of particle beams called the L/D ratio. This characteristic will be described in more detail later. L/D ratios for the ERS are calculated out to be 50, 125, and 300, corresponding to the three aperture diameters listed previously. The ERS also has an elevator shaft, filled with argon gas, directly connected to the hot cells above which allow easy access to used fuel or other highly radioactive materials. The elevator shaft lowers material directly in front of the beam line to allow images to be taken [2].

The North Radiography Station (NRS) is located at the north end of the reactor and has a beam line length of approximately 55 feet. The aperture dimensions are 3.5, 2.105, and 0.902 inches and the corresponding L/D ratios are calculated to be 185, 300, and 700. The elevator shaft

lowers into the NRS and is not connected to the hot cells but to a room above allows materials to be lowered down into the station [3]. The elevator shaft has a mechanism attached to it allows objects to be rotated while being imaged in the beam. This rotation enables a three-dimensional tomographic reconstruction of the object to be produced.

Both beam facilities use an indirect method (e.g. transfer method) to produce neutron radiographs. This method is discussed further in the next section. A pair of tracks lead into the beam facility from the outside room where the cassette foils are loaded and unloaded. After the object has been exposed in the beam, the irradiated foils behind the object get transferred back to the outside room via the rails. The foils are taken into a dark room where they are sealed next to a piece of film that interacts with the beta particles emitted from the foils to produce an image. Dysprosium and indium foils are used at the NRAD facility for radiography. The dysprosium foil is placed first behind the object being irradiated; this is due to dysprosium's high thermal neutron absorption cross-section. A cadmium foil is placed behind the dysprosium to block the remaining thermal neutrons so, theoretically, only epi-thermal and fast neutrons interact with the next foil which is indium. Although indium has a large thermal absorption cross-section it also has a larger absorption cross-section at a much higher energy, including a broad resonance absorption peak at 1.46 eV. The indium foil absorbs neutrons at the epi-thermal and fast energy levels. Another cadmium foil is placed behind the indium which is used to stop any remaining neutrons from back scattering and interacting with the foils [3].

The NRAD facility has performed two complete neutron beam characterization efforts in the past 30 years, once in 1992 [4] and again in 2013 [1]. Each characterization was performed when properties in the reactor core were changed in a way that affects the neutron beams.

2.3 Neutron Radiography: Techniques and Methods

Neutron radiography is the process creating two-dimensional projection radiographs of an object with a beam of neutrons. Neutrons can either pass through an object or become attenuated by the material in the object. A material placed behind the object is exposed to the passing neutrons and is activated, emitting some type of ionizing radiation when subsequent decay occurs [5]. The radiation emitted interacts either directly or indirectly with a piece of film providing a negative image of the exposed object. The whiter parts of this film signify the areas in the object that were not able to attenuate the neutrons while the darker areas of the film are the areas that interacted with the neutrons, not allowing them to activate the material placed behind the object [5].

Indirect, direct, radioscopy and computed tomography are just a few of the more common techniques involved in obtaining images using neutron radiography. The indirect method (e.g. transfer method) involves exposure of an object in front of a converter screen which then becomes activated by the neutrons. The converter screen is collected after exposure and placed in contact with an x-ray film for a set period of time. The beta radiation being emitted from the screen interacts with the film producing an image. The benefits and applications of this technique come from the ability to take images of highly radioactive fuels or other radioactive materials without exposing the film to gamma radiation which can distort the image [6]. Direct methods of neutron imaging entails much of the same process described in the indirect method but the film and converter screen are in contact with each other during the entire exposure process, meaning the film is also being exposed to the neutron beam and the object being imaged. The direct method offers higher detection efficiency and better spatial resolution compared to the indirect method. The direct method also cuts down on the amount of time needed to process an image compared to

the multiple steps it takes for the indirect method. The first step is exposing the converter screen in the beam and the second step is putting the converter screen in contact with the film.

Radioscopy was mentioned as another common type of neutron imaging technique. Radioscopy is unique because it allows the image to be processed and seen while the object is being exposed to the neutron beam. This process works by setting a fluorescent screen behind the object being imaged, allowing the fluorescent screen to interact with the neutrons (e.g. produce light) and then using a neutron image intensifier to convert incoming thermal neutron images into a bright light images which is observed by a charged coupled device (CCD) camera. A mirror is used to reflect the emitting light towards a CCD camera placed behind shielding to avoid over exposure from the neutron beam [6]. The CCD camera produces a real-time image of the object. Some useful applications for radioscopy involve following fluid movements through engines or movement of moisture.

Neutron computed tomography offers its own unique applications. Tomographic images are different than the usual radiographic image because it supplies a cross-sectional view of the object being exposed to the neutron beam. The process for neutron tomography includes rotating the object while it is being exposed to the beam and setting up an array of detectors behind the object being imaged. The measurements taken from the array of detectors are then reconstructed using a computer to produce the image of the object [6].

2.4 Neutron Beam Characteristics

The following sections will cover multiple characteristics that were measured and calculated for the ERS and NRS at INL's NRAD facility. The sections will describe the specific characteristic and its significance to the facilities. A list of different measurement techniques will

be illustrated for each characteristic along with an explanation of how it relates to neutron radiography.

2.4.1 L/D Ratio

Radiography requires that the path of the particles be as parallel to one another as possible to produce an image with good definition or sharpness. A measurement of neutron beam collimation is the length-to-diameter (L/D) ratio of the beam. A neutron-absorbing plate is placed in between the neutron source and the object being imaged, this plate is called the aperture. The plate has a circular opening with a specific diameter and the distance between this plate and the image plane in the facility is the length. The L/D ratio is simply the length of the beam divided by the diameter of the opening the beam is being collimated through [5]. The effective L/D ratio differs from the physical dimensions of the beam for two reasons: the neutrons back scattering into the image plane from objects behind and the collimator not effectively absorbing all neutrons passing through (i.e. neutrons with different energies) [5]. This can contribute to a smaller L/D ratio, but is effectively eliminated in the NRAD facility due to the last cadmium foil in the radiograph cassette. The cadmium foils layered in between the imaging foils of dysprosium and indium eliminate most back scatter while the beam stop behind the elevator tube effectively stops any remaining back scatter. This leaves the main contribution to the effective L/D ratio to be from the absorbing material in the aperture which is not a perfect absorber. The effective diameter of the aperture is slightly larger than the machined diameter.

The American Standard Test Method (ASTM) suggests using a no umbra (NU) device for measuring the effective L/D ratio [7]. Radiographs are taken of this device at the image plane and the effective L/D ratio can be obtained from a visual inspection of the developed images.

Umbras are primary shadows occurring when neutrons are striking the object from many different angles. The goal is to find the width that does not display this scattering event. The widths in the processed image will display a white line in their centers, the further the objects are from the collimator the smaller the white line will appear. Figure 2 shows a depiction of the umbral shadow with a wire. Equation 1 can be used to find the effective L/D ratio. The wire that does not display this white line can be used to find the value of *b* in Equation 1 [7].

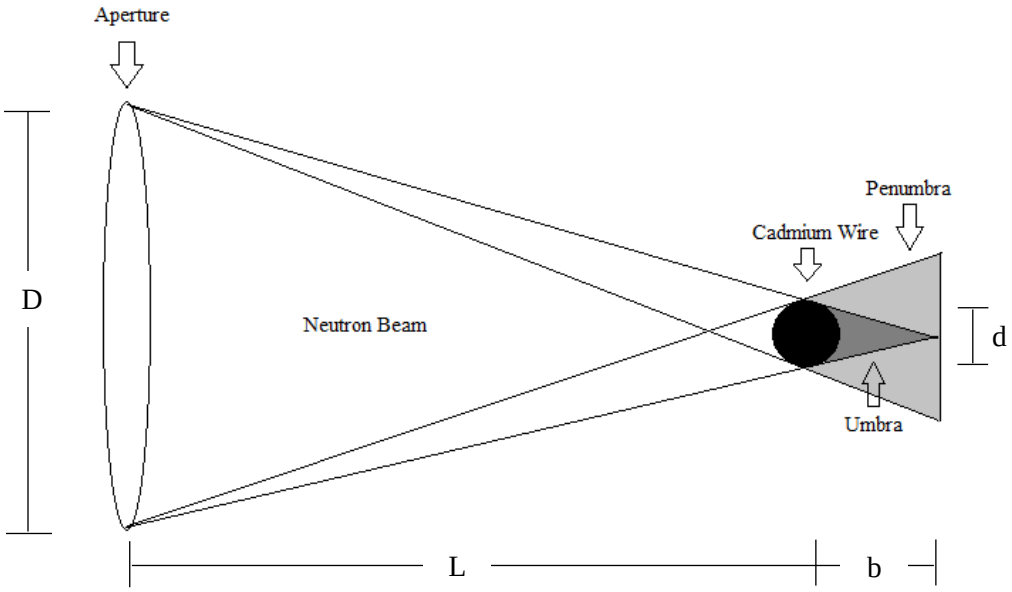

Figure 2. Picture of the umbra concept.

$$\frac{L}{D} = \frac{b}{d} \tag{1}$$

The technique mentioned above is the visual analysis performed on the processed film; another, more accurate method can be done using a microdensitometric device to analyze the image. Wave forms of two rods must be scanned with the microdensitometer, one close to the film plane and the other near but not past the point where the umbral image disappears. The wave forms are then analyzed and the value for *b* can be found and applied to Equation 1 [7].

The NU device has a few different geometries shown by the figures below. Figure 3 displays the ASTM standard L/D device. V or u-shaped grooves are machined into the device with equal spacing between each one. Neutron absorbing wires such as cadmium or nylon are placed in these grooves. The device is then placed at a 45-degree angle which allows the wires to be set at specific distances from the collimator. An NU device works using the following logic: The cadmium wires placed in the v-grooves strongly absorb neutrons, so the neutron flux behind the cadmium is lower than anywhere else in the image plane. As the wire moves away from the image plane and the umbra width decreases, the shadow becomes lighter until the umbra reaches zero and there is no more shadow.

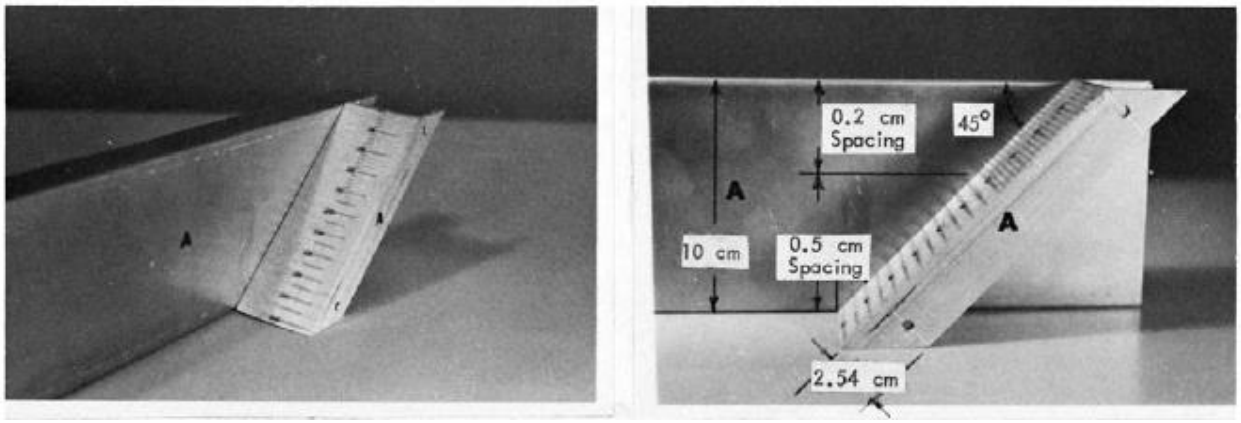

Figure 3. Pictures of a typical NU device [7].

Another geometry consists of a flat cadmium plate with holes of different diameters mounted at a specified distance from the image plane. In this scenario, the distance of the NU device (*b*) stays constant and the diameter of the holes (*d*) will change. The diameters span both the vertical and horizontal directions of the plate because the effective L/D of the beam may change slightly based on position in the image plane. The effective L/D at any point on the image plane can be found by measuring the change in L/D with position and extrapolating the results to any position. Figure 4 shows the L/D device [8].

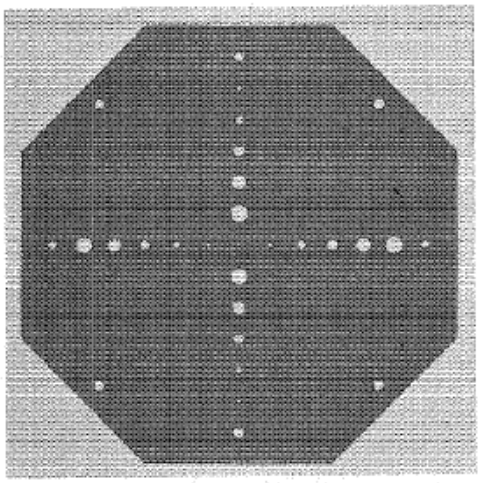

Figure 4. Cadmium sheet NU device with different diameters [8].

The final geometry of the NU device can consist of sheets of gadolinium and hafnium cut into wedge shapes and placed a specified distance (*b*) from the image plane. Figure 5 shows the dimensions and orientation of the wedges.

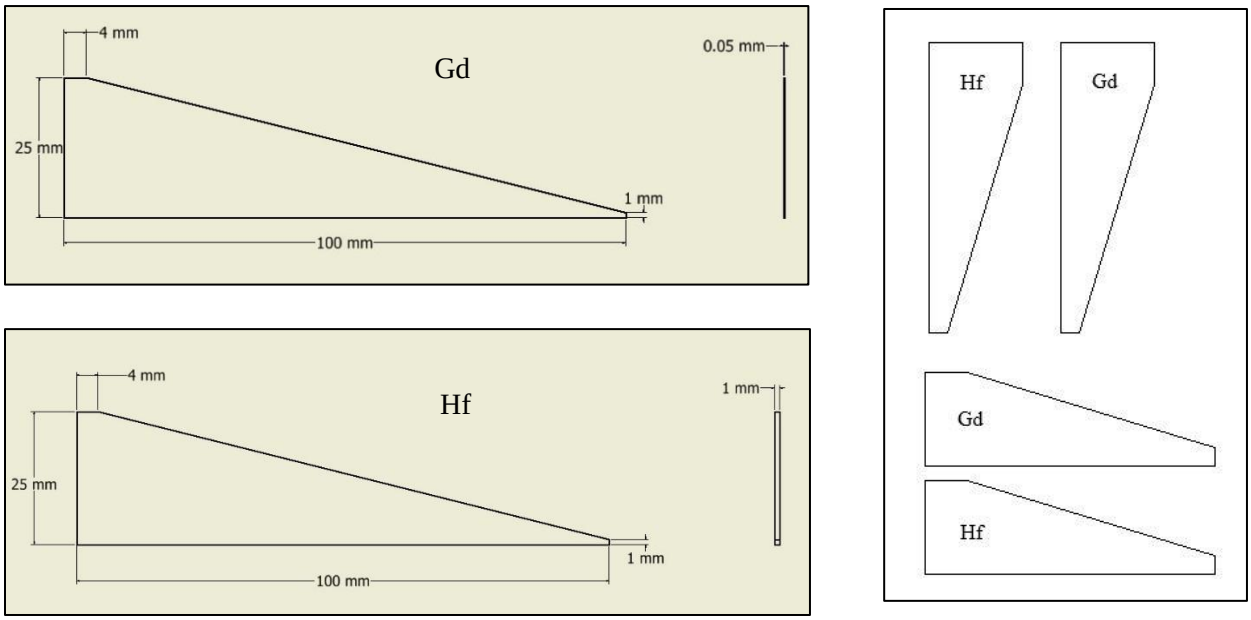

Figure 5. Gd and Hf wedge dimensions and experimental orientation.

The geometry shown above in the figure allows for a continuous change in diameter (*d*) as the width of the wedge decreases along the length. The wedges should be placed vertical and

horizontal in the image plane and gadolinium can be used to measure the effective thermal L/D and the hafnium wedge can be used to measure the effective epi-thermal L/D.

2.4.2 Neutron Beam Flux

The neutron flux incident on the image plane has a significant impact on the radiographic images. Higher neutron flux can reduce exposure times or improve signal-to-noise ratio for longer exposures. There are several ways to measure the neutron flux from a neutron source but only a few will be listed in this subsection based on applicability and practicality.

The first method described in this section is the use of fission threshold detectors to measure the thermal neutron flux of the beam. The detectors are built with an inner lining of fissile material that interacts with the neutrons passing through. The neutrons cause fissions and the fission fragments interact with the gas in the chamber to produce a current that is correlated to the number of neutrons passing through the detector [9]. This method can be used to find the number of thermal neutrons passing through the detector if U-235 is used or the fast neutron flux can be found by using U-238 as the lining on the detector. Because of the small size of these detectors, several could be used along the image plane to get a better idea of the average thermal and fast neutron flux on the image plane. Thermal and fast neutron flux could be found at individual points as well. The fission chambers can be used to measure the thermal flux and the thermal flux can be used to derive the total flux of the beam based on cadmium ratio measurements discussed later in this paper.

Another method involves calculating flux values based on activation reaction rates from irradiated foils with high thermal neutron absorption cross-sections. Gold foils are one of the standard foils used for this type of measurement [10] [1] [11]. An array of these foils should be placed at the image plane in the neutron radiography facility and be irradiated by the neutron beam

for a set period of time. The foils would then be transferred from the radiography station to a counting lab where the count rates (i.e. activity) would be found using a gamma spectroscopy instrument, for example a high purity germanium (HPGe) detector. The activity of the nuclide in the foil can then be directly correlated to the amount of neutrons incident on the foil.

2.4.3 Neutron Beam Flux Profile

The beam flux profile is a measure of the uniformity of the neutron flux at the image plane. Unfortunately, an equally distributed neutron flux across the image plane does not normally happen due to asymmetries caused by the neutron beam interacting with surrounding material. Some examples are back scattering of neutrons off the beam stop or irregular scattering off the walls of the collimator [12]. Asymmetries in the neutron beam can cause a peak in the middle and the flux is not as intense towards the edges of the image plane [1]. The L/D ratio mentioned in the previous section can affect the uniformity of the neutron beam as well. If the effective L/D ratio is not in use the images can become blurry and this is caused by irregularities in the beam profile [12].

Neutron activation analysis can be used in the exact same way as described in section 2.4.2 to measure the beam flux profile over the image plane. An array of gold foils will be equally distributed at the image plane and can then be exposed to the neutron beam. The foils are counted and the average flux of each foil is compared to the position that foil was placed on the image plane. The correlation between the neutron flux and the position will give a flux profile of the beam incident on the image plane [10].

Activation analysis is a quick way to obtain a coarse view of the flux profile shape but to obtain a more accurate representation of the profile a blank radiographic image can be taken of the converter screens in the facility. The blank image of the converter screen can be scanned by a film

scanner and analyzed using imaging software. The analyzing involves correlating the film density to neutron intensity. The image is read by looking for lighter areas, these areas signify a decrease in film density and hence a decrease in neutron intensity. To obtain a better understanding of which areas are lighter or darker than others, the scanned image grayscale values can be plotted with the distance away from the center of the image. Figure 5 shows examples of the plots taken during the 2015 characterization effort on the NRAD facility.

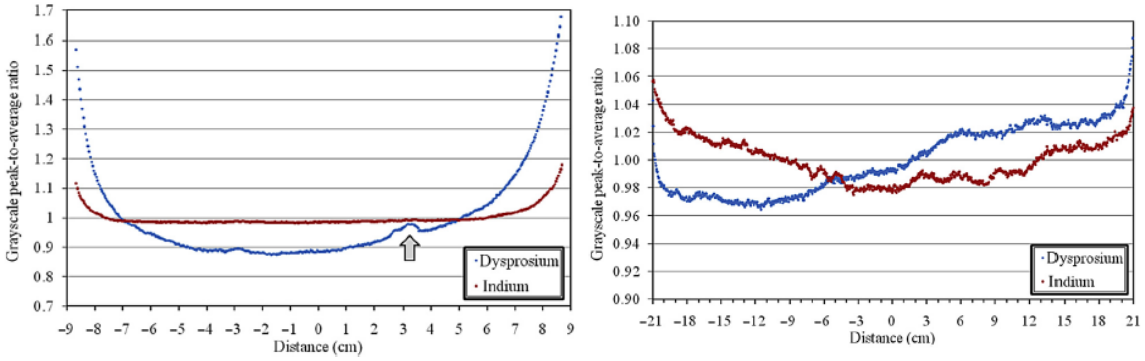

(a) (b)

Figure 6. a) Horizontal plot profile b) Vertical plot profile [10].

The main advantage to this method is one scan and one neutron image can give the needed information to obtain a beam flux profile of this entire image plane. This process can save on time and operational costs. Another method is used to measure the neutron flux profile across the image plane could be the use of small, gas filled neutron detectors. This method was used in 2014 at the Beryllium-oxide Reflected and High-Density Polyethylene (HDPE) Moderated Multiplying Assembly (BRAHMMA). The team wanted to take measurements of this sub-critical assembly's neutron flux profile to obtain a better knowledge about its shape. They used custom built, He-3 filled detectors to take these flux measurements. The detectors were 70 mm long and had an outer diameter of 6.3 mm. They were taking measurements in neutron fields of 10^3 to 10^7 *n/cm*^{2}*-s*. The

detectors were placed in certain experimental channels and manually moved across the assembly's core while taking measurements every 70 mm [13].

This method could be adapted to the NRAD facility by connecting a series of detectors to motorized grippers that could slowly move the detectors across the image plane in the vertical and horizontal directions. Measurements could be received in the room just outside the radiography stations and a flux profile could be obtained from the recordings. The detectors would also have to accumulate a certain amount of counts to assure the uncertainties of the values are within range. The main disadvantage to this method would be the amount of time it would take to obtain all the needed measurements.

2.4.4 Cadmium Ratio of the Neutron Beam Flux

The cadmium ratio is defined as the ratio of the reaction rates induced by thermal neutrons and epi-thermal neutrons. The larger the ratio value, the larger the thermal flux is compared to the epi-thermal flux. It is called the cadmium ratio because cadmium has a special property that allows it to absorb most neutrons below a specific energy. This energy depends on several factors, the main one being cadmium thickness. If a gold foil is covered in a cadmium sheet, theoretically, the only neutrons that will be incident on the gold foil will be epi-thermal neutrons or neutrons with higher energies [11]. Figure 7 shows the microscopic absorption cross-sections for gold and cadmium. It can be seen from this figure that the cadmium will absorb a majority of the thermal neutrons before they can make it to the gold foil.

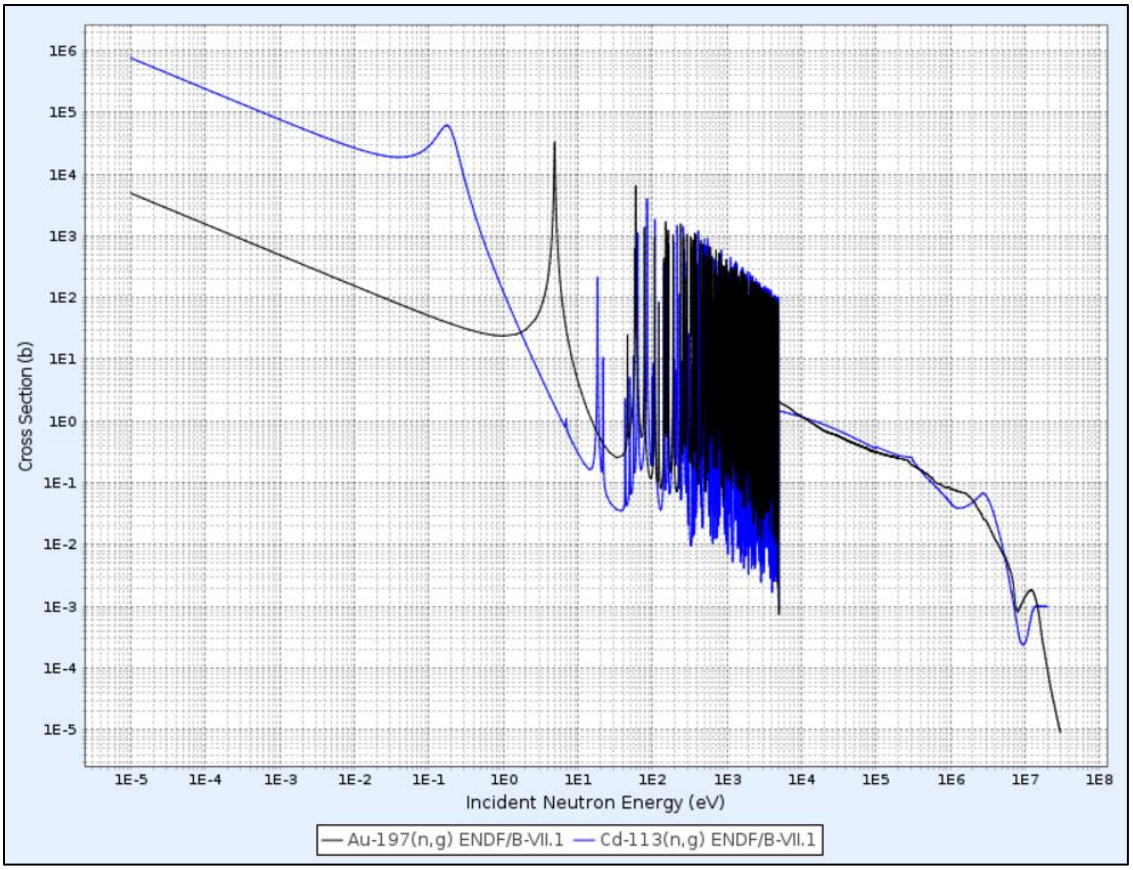

Figure 7. Microscopic absorption cross-section of Cd vs Au [14].

The thermal neutron absorption is mainly due to the high thermal neutron absorption cross-section of the cadmium sheet. The ratio can then assist in developing an idea of how many thermal neutrons are interacting at the image plane compared to epi-thermal or fast neutrons. The purpose of this characteristic goes back to the resolution of the neutron beam. Thermal neutrons are less likely to make it through an object designed to absorb thermal neutrons (i.e. nuclear fuel rods) [3], this makes it advantageous to have a high epi-thermal and fast flux of neutrons that can make it through the object to the imaging foils. The cadmium ratio should give the NRAD facility a good idea of how many epi-thermal and fast neutrons there are at the image plane, which will assist in future modifications to the beam lines, if need be.

A method for determining the cadmium ratio in a neutron flux is described in ASTM E261-10 [11]. Bare and cadmium-covered foils are exposed to the neutron flux in identical conditions

(i.e. same position, same foil weight, same exposure time). The reaction rates of the foils are then measured using a gamma spectrometer and then compared using Equation 2.

$$R = \frac{R_B}{R_{Cd}} = \frac{A_B}{A_{Cd}} \tag{2}$$

The reaction rate of the bare foil is R_b and the reaction rate for the cadmium covered foil is R_{Cd} [11].

2.4.5 Image Quality

The image quality is an important metric to characterize for neutron beams used for neutron radiography. According to ASTM E545-05 the beams image quality is found by measuring four different characteristics using image quality indicators (IQI's) [15]. There are two types of image quality indicators used, the beam purity indicator (BPI) and the sensitivity indicator (SI).

The SI is used to measure the sensitivity to detail the beam can produce. It is a step-wedge device that contains small gaps and holes. The SI device can be visually analyzed to determine the sensitivity of the radiograph (i.e. the smaller the gaps and holes one can distinguish, the more sensitive the radiograph). The BPI is a polytetrafluoroethylene block with different materials of known dimensions that can be radiographed and analyzed to obtain pertinent information that help categorize the facility. Drawings of the two devices are shown in Figure 8.

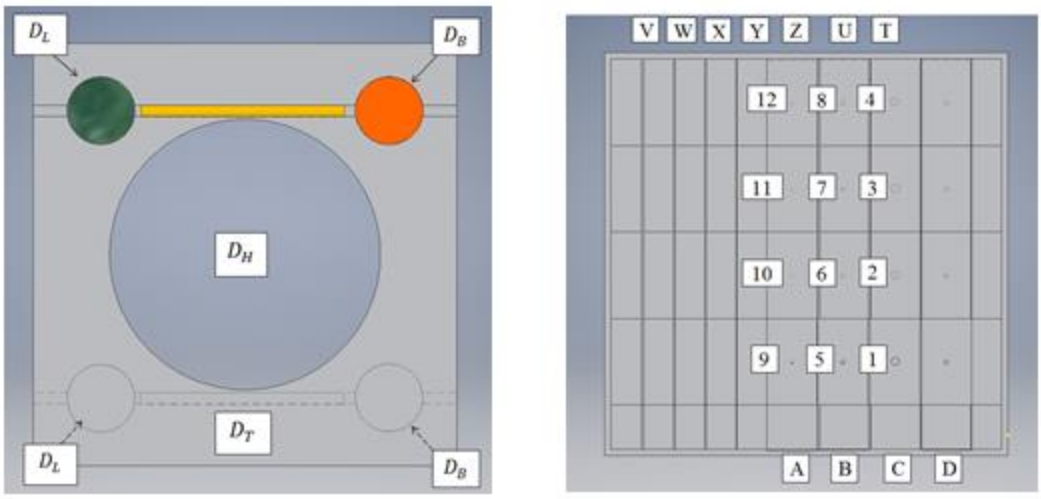

(a) (b)

Figure 8. a) Beam purity indicator b) Sensitivity indicator.

The BPI is used to measure the thermal neutron content (NC), the scattered neutron content (S), the effective gamma content (γ), and the pair production content (P). The last two terms mentioned are applicable to direct conversion techniques only. The NRAD facility operates as an indirect conversion facility so the amount of photons incident on the conversion foils have no effect on the development of the neutron radiograph. The gamma content and the pair production content will be ignored for all image quality measurements taken.

The equations used to find the values to these terms are listed below in Equation 3 and Equation 4. Table 1 gives a brief description of the terms in the equations along with what type of material will be inserted into the various openings in the device.

$$NC = \frac{D_H - (higher D_B + \Delta D_L)}{D_H} \times 100 \tag{3}$$

$$S = \left(\frac{\Delta D_B}{D_H}\right) \times 100 \tag{4}$$

Table 1. Definitions of D parameters [15].

$\boldsymbol{D_B}$	Film densities measured through the images of the boron nitride disks
$\boldsymbol{D_L}$	Film densities measured through the images of the lead disks
$\boldsymbol{D_H}$	Film density measured at the center of the hole in the BPI
$\boldsymbol{D_T}$	Film density measured through the image of the polytetrafluorethylene
$\boldsymbol{\Delta D_L}$	Difference between the D_L values
$\boldsymbol{\Delta D_B}$	Difference between the D_B values

The SI device is used to measure the two other characteristics shown in Table 3, the largest consecutive numbered hole that is visible (H) and the smallest gap seen at all absorber thicknesses (G) [15]. Table 2 shows the values that the number of visible holes and steps represent of the SI device.

Table 2. H and G values [15].

Value of H	Shim	Value of G	Gap
1	C	1	T
2	C	2	U
3	C	3	V
4	C	4	W
5	B	5	X
6	B	6	Y
7	B	7	Z
8	B		
9	A		
10	A		
11	A		
12	A		

The combination of these two devices offers a qualitative understanding of the capabilities of the neutron radiography facility. A ranking system has been developed by ASTM using the parameters calculated from the indicators described. The quality level of a facility on a scale from category I to category V can be determined using Table 3.

Table 3. Description of categorized facilities based on image quality [15].

CATEGORY	NC	H	G	S	γ	P
I	65	6	6	5	3	3
II	60	6	6	6	4	4
III	55	5	5	7	5	5
IV	50	4	5	8	6	6
V	45	3	5	9	7	7

2.4.6 Neutron Energy Spectrum

The neutron energy spectrum of a beam provides information on the intensities of a wide range of energy bins. General information such as thermal and epi-thermal neutron flux can be derived from irradiating gold foils and using cadmium covers. The cadmium ratio can be calculated from these results but to obtain a neutron flux at a specific energy, one must have a knowledge of the entire spectrum.

Foil activation is a proven and very common method of measuring neutron energy spectra. By using many foils comprised of different materials, an energy spectrum can be unfolded based on the response each foil has to the spectrum. There are three regions in the neutron energy spectrum measured using this technique: thermal (0 – 0.025 eV), intermediate (0.025 eV – 10 keV), and fast (10 keV – 20 MeV). This method has been used many times over [16-18] and has been proven to give satisfactory results. The foils are exposed to a neutron energy spectrum and the response of each one is calculated using the measured activity and known physical features of the foils. Computer codes such as Monte Carlo N-Particle (MCNP) and unfolding with MAXED and GRAVEL (UMG) can be used to determine the guess energy spectrum and the unfolded energy spectrum, respectively.

Another technique used to measure the neutron energy spectrum is the Bonner sphere approach. This technique consists of 12 moderating polyethylene spheres with diameters ranging

from 3-12 inches. These spheres have a thermal neutron detector placed inside; the fast neutrons incident on the sphere become moderated and are then measured by the detector. The degree of moderation is small for a small sphere. This means if a neutron is detected in the small Bonner sphere then it is a low energy neutron that was detected. The larger rem balls have considerably more moderation so if a neutron is detected in those then it is assumed to have more energy when it started to penetrate, correlating to a higher energy neutron. The combination of the thermal neutron detector and the multiple levels of moderation allow the Bonner sphere set to detect neutrons at multiple energies [19].

Before neutron spectrum measurements can be taken the response function of the Bonner sphere set must be found for each thickness. The response function of the Bonner sphere set is usually dependent upon the moderator sphere's density and the type of thermal neutron detector being used in the spheres. Many Bonner sphere sets have been analyzed for this purpose which allows the use of predetermined response functions to be used for efforts without the tedious task of calculating them.

Measurements must be taken with one sphere at a time and one constant, normalizing sphere to account for fluctuation in reactor power. The reactor must be operating at a low level of power to avoid large dead times, pulse pileup and high levels of radiation exposures. A count time must be long enough to obtain a reasonable uncertainty for the particles counted by the detector. When the data for the spheres are collected, the unfolding process mentioned for the foil activation technique can be used to find the energy spectrum for the beam [19].

The last method analyzed for measuring the neutron energy spectrum is the velocity selector. A velocity selector is a cylindrical, motorized device that can discriminate neutrons based on their energy's wave lengths. To explain the general workings of a velocity selector, a single

helical slot selector will be used as a simplified example. The device works by cutting a tiny helical slot into a high neutron absorbing material. As the device rotates the rotational speed of the motor, the angle the helical slot is cut into the material and the length of the cylinder can all be related to the speed of neutron traveling parallel to the selector. There are also multi-disk velocity selectors which have better resolution and transmissions. The velocity selector method could help measure the neutron energy spectrum in the neutron beam at the NRAD facility. The device could be set to allow only neutrons with a specified energy to pass through and attenuate all other energy levels. A detector could be placed at the image plane and it could be assumed the neutrons passing through the detector are of a pre-set energy level. The spectrum could be completed through a tedious process using the velocity selector, but with great accuracy. Multiple papers have been written, reviewing and establishing the principles behind the velocity selector but none have produced a concise process on measuring the energy spectrum of a neutron beam facility [20-22].

The NRAD facility does not have the resources or adequate space for a velocity selector in the ERS at this time and the spheres of polyethylene in the Bonner sphere method are too large to insert them where the measurements at the image plane are to be taken. The foil activation analysis was determined to work best for this facility due to its ability to fit into the tight space between the elevator tube and the image plate and for the ease of repeating the experiment if needed. Two measurements are needed for the foil activation analysis unlike the velocity selector and the Bonner spheres which would require several reactor shut downs and restarts to accumulate the necessary data.

2.4.7 Gamma Energy Spectrum

The gamma content of a neutron beam can play a significant role on how the images look after they are processed. If the gamma content is too high the images will be distorted and the

resolution will suffer. The NRAD facility uses an indirect transfer method for taking neutron radiographs which means the film is processed, analyzed, and is never directly exposed to the gamma radiation from the neutron beam or the objects being imaged (i.e. used nuclear fuel). NRAD is planning to convert the ERS to a digital radiography station in the future which can be affected by large doses of gamma radiation. The gamma energy spectrum will inform future efforts on what type of radiation is incident on the system and how much protection it would need.

There are several different instruments used to measure the gamma energy spectrum of a source but for the application in the tight quarters of the NRAD imaging stations, a small, portable detector would be ideal. The detector must cover a wide range of energies up to a few MeV and it must have a high enough resolution to show distinguishable peaks of the different photons emitted from the core and the surrounding materials.

Sodium iodide (NaI) with a thallium dopant is a common gamma spectrometer in the health physics field. This instrument has been proven and enhanced to capture a wide range of energies for gamma spectroscopy. The NaI detector is a scintillation-based system, it detects the light given off from excited electrons. Ionizing radiation penetrates the detector and interacts with the fluorescent material inside. The radiation excites the electrons which then give off a photon as they return to their ground state. In order for the photon to be detected a photomultiplier tube must be used to boost the signal and then a preamplifier is used to even further boost it to detectable levels [9]. A NaI detector was used to measure a gamma spectrum in 1968 in the High Flux Isotope Reactor (HFIR) at the Oak Ridge National Labs. They performed these measurements at low reactor powers to minimize the exposure to photons and neutrons emitted by the activated materials close to the core [23]. A Li-6 shield was placed around the NaI detector to shield it from

neutrons. The detector was chosen by the scientists at HFIR because of its sensitivity and gamma efficiency as a function of energy.

Temperature moderated gamma spectrometers (i.e. HPGe Detectors) could pose a problem due to the amount of space they require to operate. A CdZnTe (CZT) semiconductor detector requires a very small amount of space and no cooling system to operate. The two main advantages to the CZT detectors is the low amount of energy needed to create electron/hole pairs and the ability to operate at room temperature conditions [24]. A typical semiconductor detector works by allowing the charged particle to pass through the crystal inside the detector, affecting what is known as a band gap, which is a gap of energy between stable and excited electrons. This gap energy is the energy needed by the electron to become excited and jump the gap. The charged particle moves through the detector and excites stable electrons along the way. The detector is electrically biased creating an electrical potential within the volume forcing the negatively charged electrons to migrate towards the positive end. The excited electron will move across the band gap and leave a vacancy where it was stable. This is known as an electron-hole pair. The electron travels down one side of the detector while the hole is filled by one stable electron after another resulting in the movement of the vacancy down the opposite direction of the detector. The electrons collected at one end and the absence of electrons collected at the other end can produce a current directly related to the energy of the incoming radiation [9].

The CZT detectors have deficiencies as well. The electron-hole pairs are trapped rather quickly and cannot always make it to the boundaries to produce a reading, this leads to incomplete formation of gamma energy spectrums. Another disadvantage comes from the formation of larger, homogeneous crystals for the detectors. The lack of size contributes to the inefficiencies and resolution of the gamma spectrum readings [24]. With these deficiencies mentioned the CZT

detector still out performs any scintillator in resolution and efficiency due to the semiconductor properties it possesses. Shielding will be required for this detector due to the large neutron flux of the beam.

It has been mentioned several times in this section that High Purity Germanium detectors would not be plausible due to their size and the large amount of the detector that would be exposed to the beam to obtain a reading. An experiment was found that used an HPGe detector to measure the gamma spectrum from a neutron beam. The experiment was conducted at the High Flux Reactor (HFR) in Petten, the Netherlands. The neutron beam, where the measurements were taken, had a neutron flux of 3.8×10^8 n/cm^2-s [25]. The ERS neutron beam flux was last measured to have a full reactor power flux of about 4×10^6 n/cm^2-s making it considerably less harmful environment to the detector. The neutron beam was shielded with a polyethylene block and most of the parts to the HPGe detector were shielded with lead apart from the detector itself. The detector was set up about 6.5 feet away from the neutron beam entrance, with the shielding in between. It was mentioned that low level gamma rays would have been shielded by the polyethylene but this was disregarded due to the low level rays already being attenuated from the liquid in the collimator of the beam.

The experiments performed in the HFR is a good example that a gamma energy spectrum can be obtained using an HPGe detector for neutron beam application. The HPGe detector would be the ideal choice for gamma spectroscopy because of the high resolution and efficiency proven to obtain a more precise and resolute gamma energy spectrum than the NaI (Tl) detector [9]. The HPGe detector has a higher resolution and efficiency compared to the CZT detector as well [24].

3 Methods & Materials

3.1 L/D Ratio

The third NU device mentioned in Section 2.4.1 was chosen for the L/D measurement in the beamlines. This method requires only one image to be taken with each aperture setting and does not require adjusting after each shot and demands very little space to set up. The arrangement was placed 1 meter (3.3 feet) in front of the image plane and had to be positioned 20.32 cm (8 inches) off the ground to be directly in the middle of the neutron beam. The placement should theoretically result in zero umbral shadows at the 8-mm mark on the gadolinium and hafnium foils using an L/D of 125. The setup was exposed for the standard neutron radiograph imaging time for each aperture setting: 4 minutes, 22 minutes, and 60 minutes for aperture settings 50, 125, and 300, respectively. A picture of the apparatus and the corresponding setup can be seen in Figure 9 and Figure 10.

Figure 9. L/D apparatus setup in the East Radiography Station.

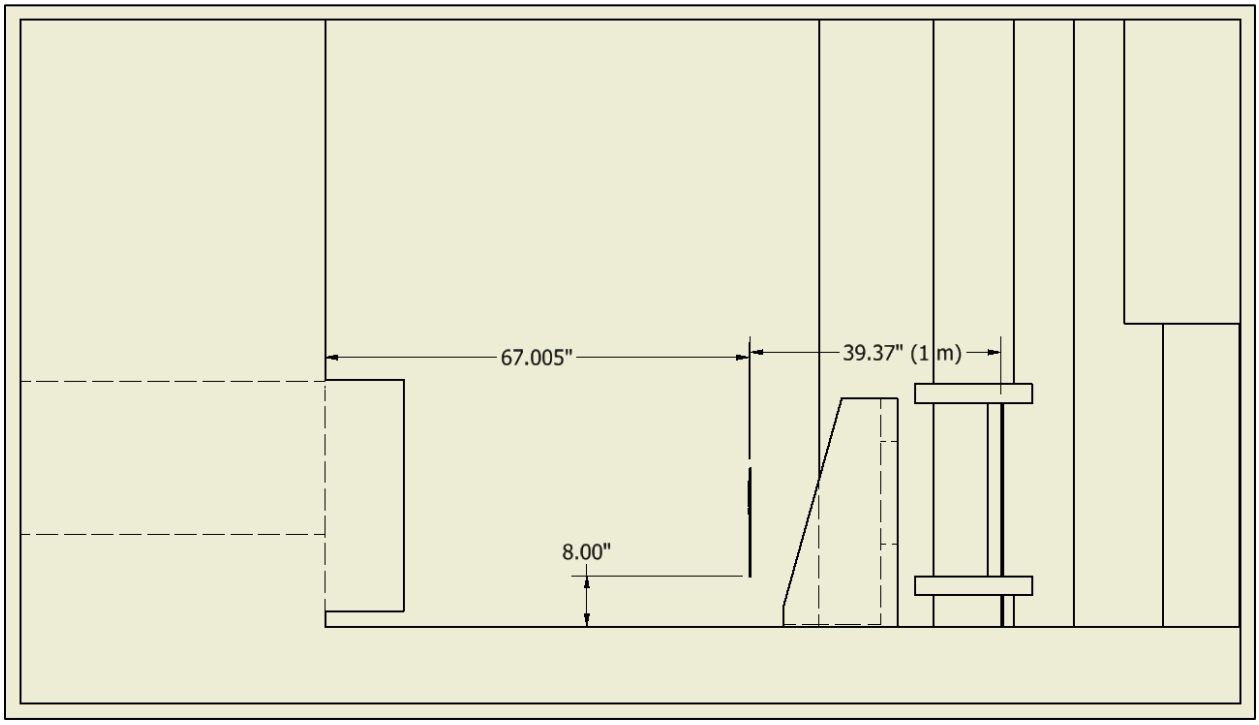

Figure 10. L/D dimensional setup in the ERS.

3.2 Neutron Beam Flux

Neutron activation analysis with gold foils was determined to be the most appropriate neutron flux measurement technique for the neutron beams at NRAD. An array of 21 gold foils was attached to an aluminum plate that could fit into the cassette device. This device would remotely place the foils up against the image plane directly in the path of the neutron beam. The foils were then exposed to the neutron beam for 5 hours with the reactor power level at 250 kW_{th}. A drawing that displays the dimensions and layout of the 21-gold foil array can be seen in Figure 11 along with a picture of the actual setup. The foils were wrapped in aluminum foil and aluminum tape was used as the adhesive to ensure the gold foils stayed on the plate.

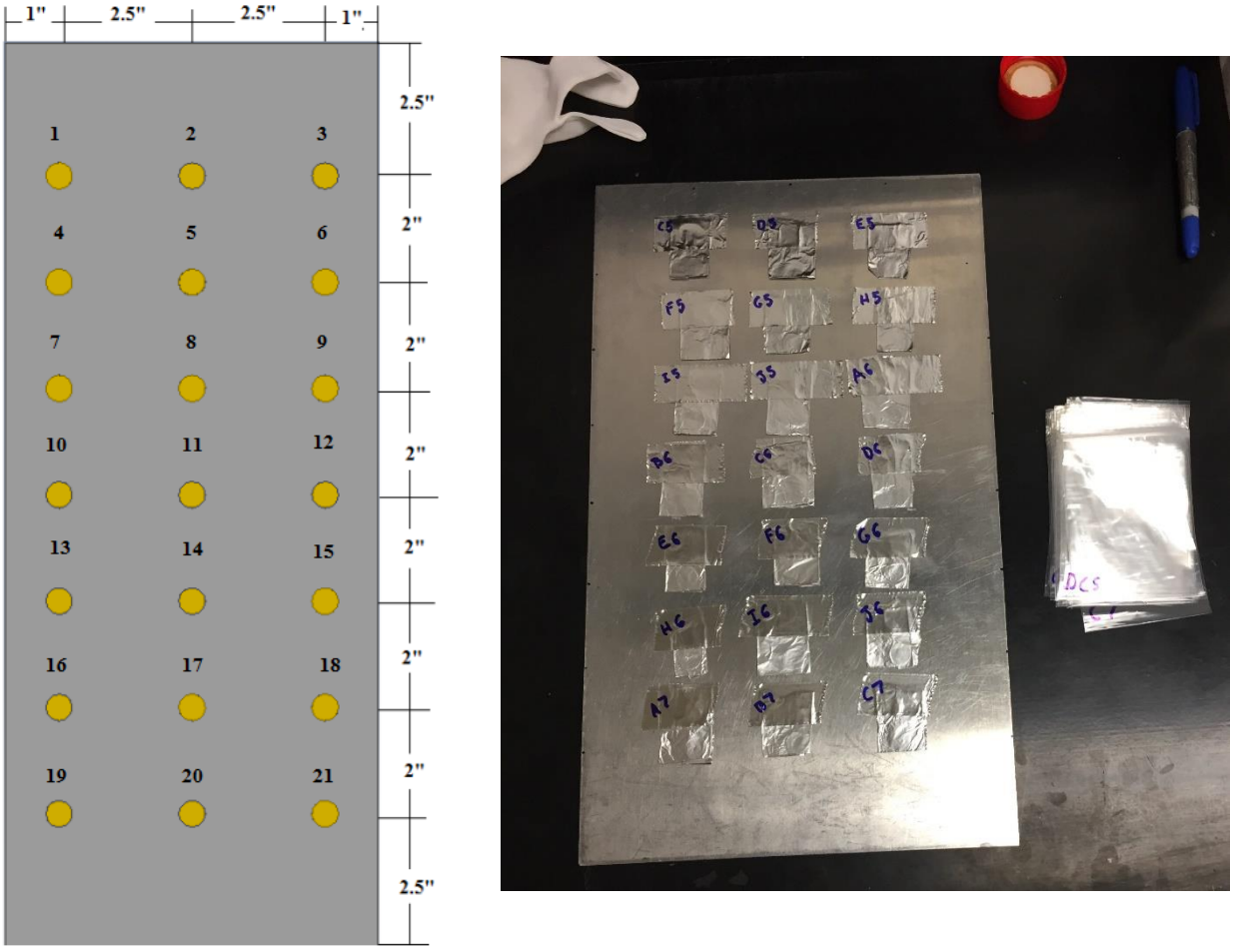

Figure 11. 21-gold foil array setup (left) and picture (right).

The foils were taken off the aluminum plate after the exposure time was reached and taken to the Analytical Laboratory at MFC to measure the activity emitted from the reaction caused by the neutrons: $^{197}Au(n,\gamma)^{198}Au$. The radionuclide produced from the neutron interaction (^{198}Au) has a half-life of about 2.7 days and emits a gamma-ray in the decay process with an energy of 411.8 keV [26]. This gamma energy is unique to the decay process of ^{198}Au and can be used to determine the activity of the activated gold foil. The figure below shows a typical HPGe detector output when analyzing an activated gold foil.

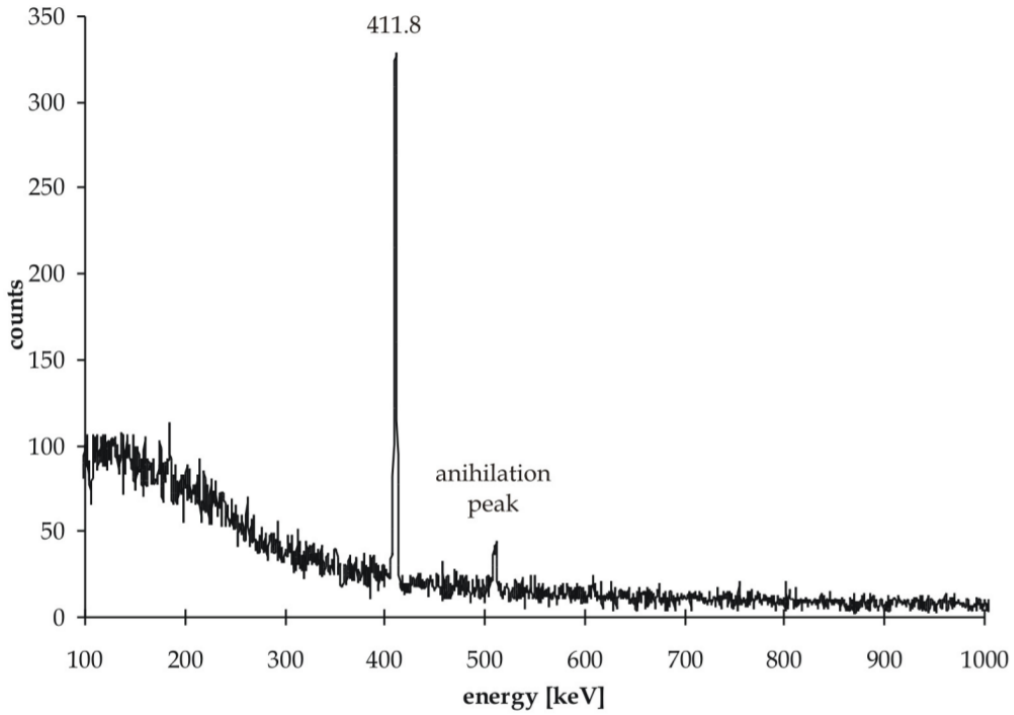

Figure 12. Example gamma energy spectrum of a ^{198}Au [27].

An HPGe instrument can be used to detect the gamma-ray emitted from the gold foil. The HPGe detector used to in this part of the project was an Ortec brand detector with a relative efficiency of 50%. The Analytical Laboratory used a Canberra Apex software to determine the number of decays (i.e. gamma-rays) per second emitted from the gold foil. This detector was calibrated with a ^{152}Eu source which was also used as a control during the counting process [28].

The activity of each foil was then correlated to the average thermal neutron flux incident on the image plane.

The average neutron flux for each individual foil was found by solving the differential equation seen in Equation 5.

$$\frac{dn}{dt} = -\lambda n + R \tag{5}$$

The term, $\frac{dn}{dt}$, is the time rate of change of the radioactive nuclide being produced in the foil, $-\lambda n$ is the rate of loss of the radioactive nuclide (λ is the decay constant of the specified nuclide) and *R* is the production rate of the nuclide. If the integral of this equation is taken and it is assumed the foil is not initially radioactive, the activity of the foil can be calculated from Equation 6.

$$A = R\left(1 - e^{-\lambda t}\right) \tag{6}$$

The number of radioactive nuclides produced is directly related to the activity of the foil after activation [29]. The term *A* represents the activity of the foil after the exposure time *t*. The saturation activity of the nuclide (*R*) represents the maximum activity the nuclide can achieve given the following constraints:

$$R = \sigma \phi N \tag{7}$$

N is the atom density of the nuclide being irradiated, σ is the microscopic cross-section of the desired reaction and ϕ is the neutron intensity (e.g. neutron flux) incident on the foil. The equation used to calculate the neutron flux incident on the foils can be found by substituting Equation 7 into Equation 6 and then solving for ϕ.

$$\bar{\phi} = \frac{A}{N\sigma\left(1 - e^{-\lambda t_{exp}}\right)} = \frac{\phi}{f_s} \tag{8}$$

A self-shielding correction factor was deemed necessary to add to the flux term. It will be correcting for the decrease in the neutron flux due to the high thermal neutron absorption cross-section of the gold foils. Neutrons scattering inside the gold foil should also be accounted for to ensure all necessary steps are taken and the most accurate flux can be determined. The correction factors can be found using Equation 9.1 and Equation 9.2 [30]. The term *x* refers to the thickness of the foil in centimeters and Σ_t is the macroscopic cross-section for gold. The flux value calculated from Equation 8 can be divided by the final correction term to find the neutron flux incident on the foils [10].

$$f = \frac{1 - e^{\Sigma x}}{\Sigma x} \tag{9.1}$$

$$f_s = \frac{f}{\left(1 - \frac{\Sigma_s}{\Sigma_t}(1 - f)\right)} \tag{9.2}$$

Two sets of gold foils were irradiated resulting in a total of 42 foils used to measure the neutron flux at the image plane. This also allows two sets of data to be compared with a better statistical value for the final result.

The uncertainty for the measured flux incident on each foil is a combination of the physical parameters of the foil, measurable aspects of the experiment setup, and the error associated with the measurement of radioactive decay in the foils.

Radioactive decay is a random process and is always subject to some degree of uncertainty when being measured. It is assumed that the counts measured on each foil represent a normal distribution detected by the HPGe detector. The normal distribution of the amount of decays can be used to calculate the predicted standard deviation of each activity measurement. Equation 10 and 11 can be used to derive the standard deviation (σ) of a measurement (i.e. uncertainty) by

relating it to the variance and the expected sample variance (s^2) to the predicted variance (σ^2) [9]. The number of counts is the measured radioactive decay emitted from the foil.

$$s^2 = \sigma^2 = (\#\ of\ counts) \tag{10}$$

$$\sigma_A = \sqrt{\#\ of\ counts} \tag{11}$$

The uncertainties in this thesis are reported at a 2σ value. This value represents a confidence level of 95% indicating that measurements should fall in the range of the mean, plus-or-minus two standard deviations.

The physical feature of the foils that had measured uncertainties was the weight (*w*). The measured uncertainties in the experimental setup included time (*t*) of irradiation and the physical placement (*P*) of the foils on the image plane. Equation 12 was used to calculate the total uncertainty in each flux based on the parameters described. This equation is used because the neutron flux equation multiplies and divides these parameters requiring a fractional error to be calculated.

$$\left(\frac{\sigma_\phi}{\phi}\right)^2 = \left(\frac{\sigma_w}{w}\right)^2 + \left(\frac{\sigma_A}{A}\right)^2 + \left(\frac{\sigma_t}{t}\right)^2 + \left(\frac{\sigma_P}{P}\right)^2 \tag{12}$$

3.3 Neutron Beam Flux Profile

Neutron activation analysis was also used to measure the neutron beam flux profile. The 21 gold foils used to measure the neutron flux were plotted to measure the flux profile across the image plane. It can be seen from Figure 11 that the foils were spaced equal distances apart and cover the entire image plane. The results of each foil's measured activities will be compared to their position to determine if there is a relatively uniform beam over the entire 119 in^2 (767 cm^2) image plane.

3.4 Cadmium Ratio of the Neutron Beam Flux

The same techniques used to measure the flux and flux profile of the beam were used for this measurement with a few differences. The 21-gold foil array was setup the same way it was shown in Figure 11 but this time each gold foil was inserted into a cadmium cover that would shield the gold from the low-level neutrons of the beam. Figure 13 show the cadmium cover and the array of cadmium covered gold foils set to be irradiated.

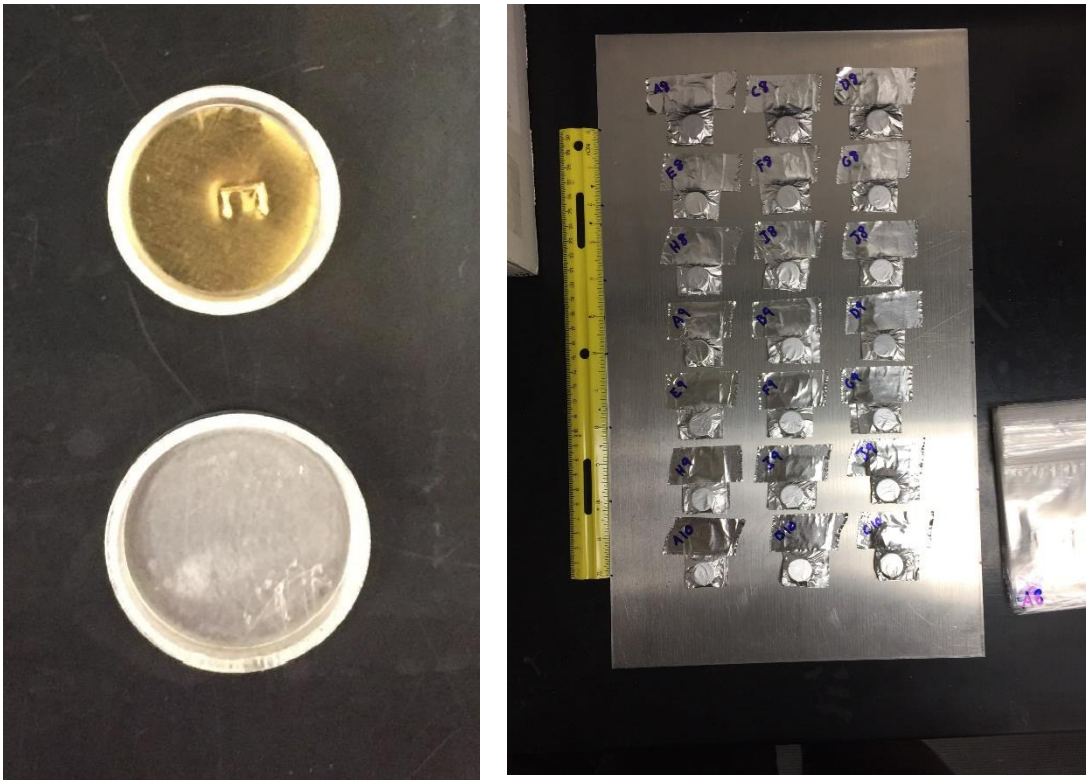

Figure 13. Cadmium covered gold foil and cadmium covered array.

This set of foils were irradiated for the same amount of time as the bare gold foils (5 hours) to ensure the data could be compared as few changes as possible. Two sets of cadmium covered gold foils were irradiated for the same reasons given in Section 3.2. The cadmium ratio was then calculated using Equation 2 and the average activity determined at each position.

3.5 Image Quality

The image quality of the beam was determined using the methods described in ASTM standards [15]. Neutron radiographs were taken of the two image quality indicators (IQI) using the L/D setting of 125 and an exposure time of 22 minutes. The BPI surface was positioned parallel against the film cassette and the cadmium wires in it were oriented so their longitudinal axis is perpendicular to the nearest film edge. The SI device was positioned in the image plane so its thickest step is not adjacent to the BPI and it was ensured that the SI no less than 25 mm away from the edge of the exposed area. The images of the IQI's were then analyzed visually and using a densitometer to determine the values described in section 2.4.5.

3.6 Neutron Energy Spectrum

3.6.1 Foil Activation Description

Foil activation analysis requires a number of foils that react with all parts of the neutron energy spectrum (i.e. thermal, intermediate, and fast). Two foil kits were purchased from Shieldwerx^{TM}, a company that supplies several different types of materials made for radiation environments. A list of the foils can be seen in the Table 4 with their corresponding neutron energy ranges [26, 31-33]. The energy ranges of interest for each foil can be seen in Figure 14.

Table 4. Foil information for the neutron spectrum measurements.

		Bare		Cadmium Covered	
Foil	**Reaction**	**E_L (MeV)**	**E_H (MeV)**	**E_L (MeV)**	**E_H (MeV)**
Gold (Au)	Au-197(n,γ)Au-198	5.00E-08	4.50E-06	3.80E-06	9.20E-06
Cobalt (Co)	Co-59(n,γ)Co-60	1.00E-09	2.50E-06	6.90E-07	1.43E-04
Copper (Cu)	Cu-63(n,γ)Cu-64	9.00E-09	1.50E-03	5.25E-07	9.60E-03
Iron (Fe)	Fe-58(n,γ)Fe-59	9.00E-09	4.00E-04	5.25E-07	1.00E-02
Indium (In)	In-115(n,γ)In-116m	4.50E-08	3.00E-06	9.00E-07	2.00E-06
Lutetium-Aluminum (5.2%Lu-Al)	Lu-175(n,γ)Lu-176m	1.00E-09	7.50E-05	2.50E-06	1.25E-03
Maganese-Copper (8.7%Mn-Cu)	Mn-55(n,γ)Mn-56	9.00E-09	4.00E-04	4.75E-07	1.10E-03
Molybdenum (Mo)	Mo-98(n,γ)Mo-99	1.00E-09	2.00E-03	1.50E-07	6.75E-03
Sodium Chloride (NaCl)	Na-23(n,γ)Na-24	1.00E-09	1.50E-07	5.25E-07	3.00E-03
Scandium (Sc)	Sc-45(n,γ)Sc-46	7.00E-09	6.00E-06	4.00E-07	4.75E-04
Tungsten (W)	W-186(n,γ)W-187	9.00E-08	3.50E-05	1.20E-05	3.80E-05
Aluminum (Al)	Al-27(n,α)Na-24	3.00E+00	1.00E+01		
Copper (Cu)	Cu-63(n,α)Co-60	1.19E+01	1.63E+01		
	Cu-63(n,2n)Cu-62				
Iron (Fe)	Fe-54(n,p)Mn-54	2.30E+00	7.40E+00		
	Fe-56(n,p)Mn-56				
Indium (In)	In-115(n,n')In-115m	1.20E+00	5.80E+00		
Magnesium (Mg)	Mg-24(n,p)Na-24	6.50E+00	1.13E+01		
Nickel (Ni)	Ni-58(n,p)Co-58	1.31E+01	1.69E+01		
	Ni-58(n,2n)Ni-57				
Sodium Chloride (NaCl)	Cl-35(n,α)P-32	5.00E+00	1.00E+01		
Sulfur (S)	S-32(n,p)P-32	2.30E+00	7.30E+00		
Titanium (Ti)	Ti-47(n,p)Sc-47	3.70E+00	9.20E+00		
	Ti-48(n,p)Sc-48				
Vanadium (V)	V-51(n,α)Sc-48	1.20E-02	1.00E+01		
Zinc (Zn)	Zn-64(n,p)Cu-64	2.60E+00	7.40E+00		
Zirconium (Zr)	Zr-90(n,2n)Zr-89	1.27E+01	1.67E+01		

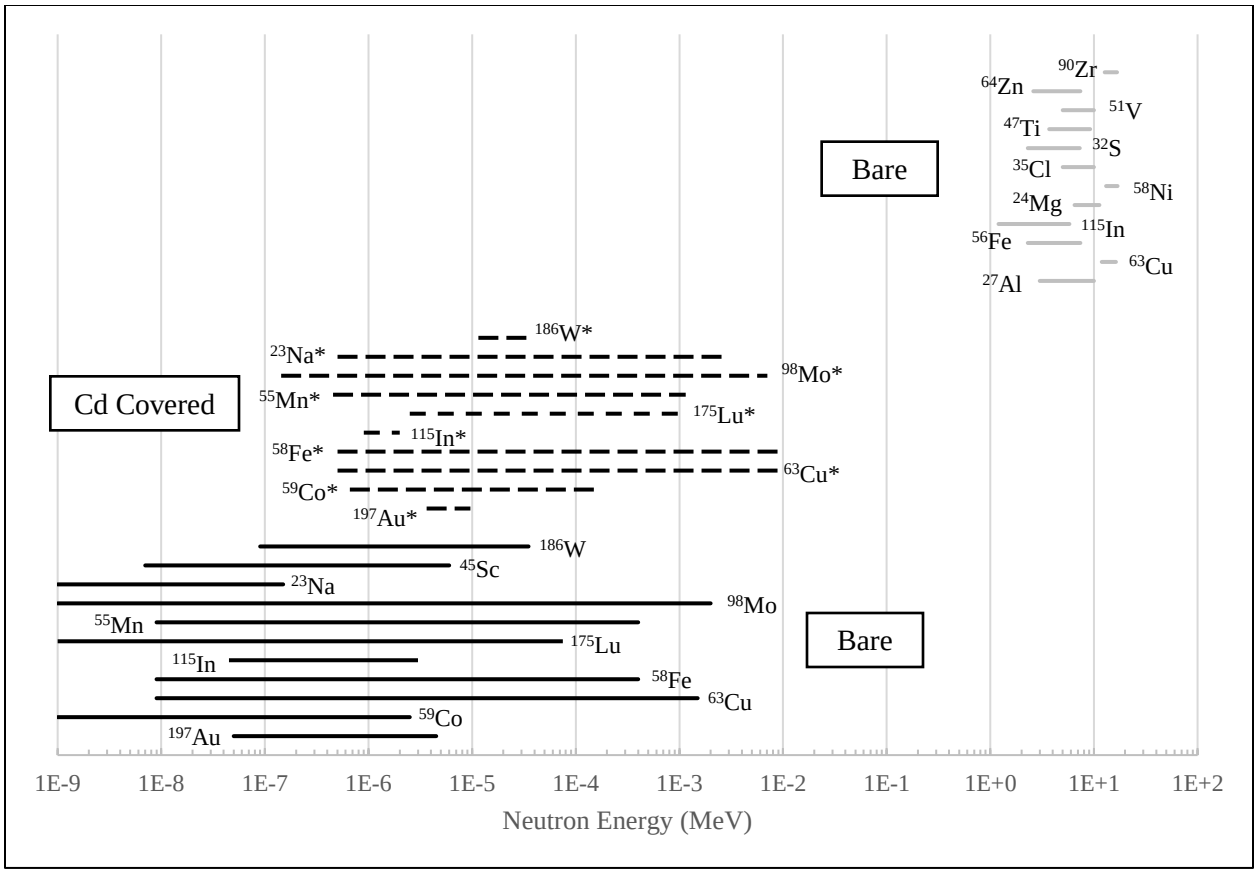

Figure 14. General response ranges for the selected foils.

It should be noted that energy response ranges for foil activation are highly dependent on the environment the detectors are subjected to. The values shown in Table 4 and Figure 14 were taken from spectral measurements performed at other facilities where the neutron beams have different features than the ERS.

The foils listed above were individually wrapped in aluminum foil and then attached to the center of an aluminum sheet with aluminum tape. Aluminum was used because of its transparency to neutrons. The foils were then exposed to the east radiography neutron beam for ten hours at a reactor power level of 250 kW_{th}. A picture of the setup can be seen in Figure 15 accompanied by the dimensions of the array. Figure 16 shows the related foil description for each position on the aluminum sheet.

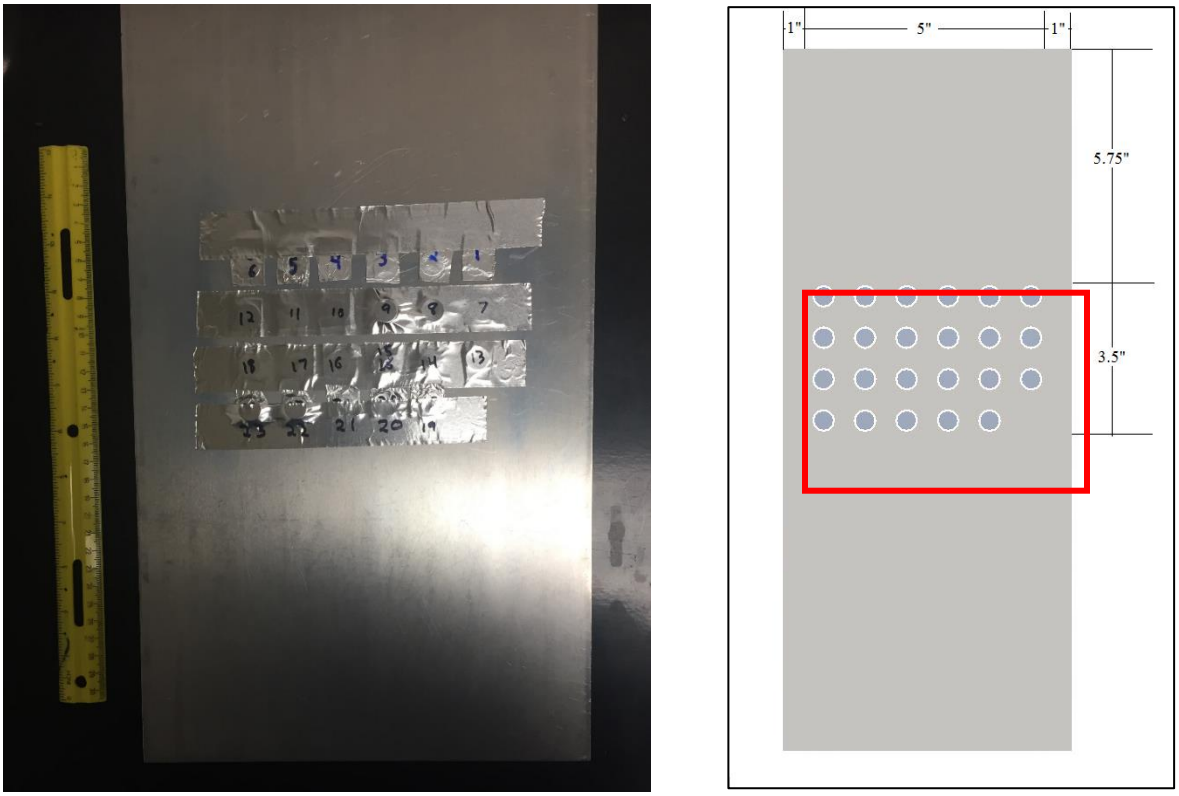

Figure 15. Experimental setup of multi-foil array (dimensions are in inches).

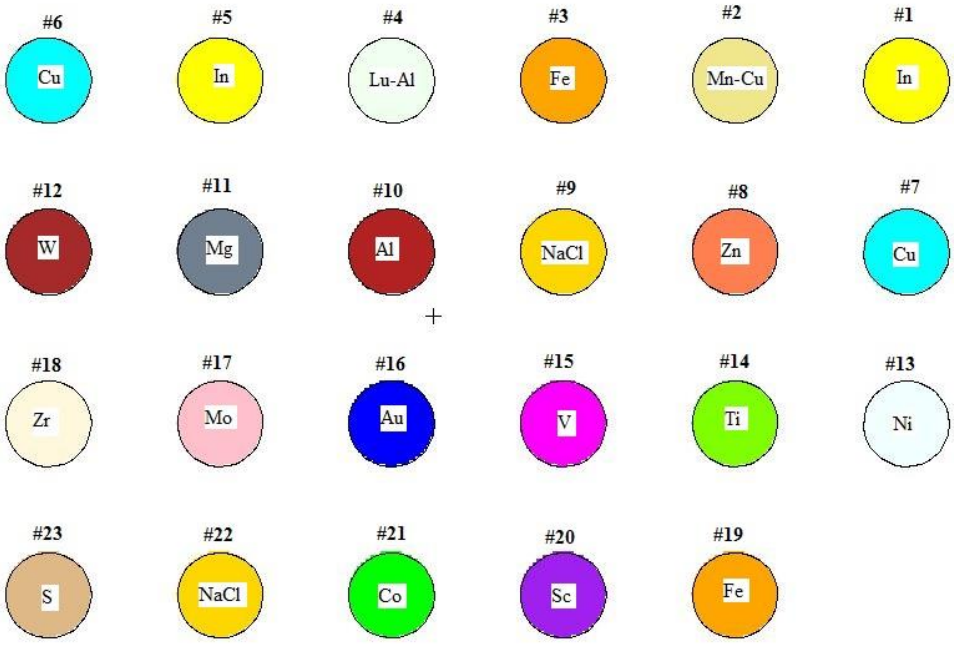

Figure 16. Labeled diagram of multi-foil setup in Figure 15.

The foils were carefully taken off the aluminum sheet after the irradiation period and transported directly to the analytical lab, so the activities of the specified reactions could be determined. There were two types of detectors used to measure the count rates of the foils: A High Purity Germanium (HPGe) detector, to measure the gamma-rays and a gas flow proportional counter to measure the charged particles. The HPGe detector has a relative efficiency of 50% and was calibrated using a ^{152}Eu source, while the proportional counter was a Protean Gas Flow detector, model 9604, calibrated using ^{99}Tc and ^{239}Pu sources [28].

Many of the neutron interactions with a target nuclide produce a gamma-ray at some point along the decay chain of the radionuclide produced. The gamma-ray will have an energy unique to the reaction between the neutron and the target nuclide. The multi-channel analyzer connected to the HPGe detector will correlate the height and width of this energy peak to the number of reactions occurring in the target sample. There are two reactions that take place in foil #22 and #23 (sulfur and sodium chloride) that do not produce gamma rays. The proportional counter was used to determine the activity of the beta radiation emitted from these foils.

The activities can be used to calculate the response of each foil, this response will be used in the unfolding software later in the experiment. The foils can be treated as detectors, each with they're unique response to the neutrons crossing the plane. The response of each foil can be found by using the following equation [34]:

$$R = \int_0^\infty dE\, \mathcal{R}(E)\phi(E) \tag{13}$$

The $\mathcal{R}(E)$ value in Equation 13 is the response function, which in the case of neutrons is simply the microscopic cross-section (σ) of the desired reaction integrated over all energy groups. Equation 6 can be used to solve for this response producing Equation 14.

$$R = \sigma\phi = \frac{A * f_s}{N(1 - e^{-\lambda t})} \quad (14)$$

Macroscopic cross-sections used in Equation 9.2 to find the scattering correction factor will be determined using MCNP. It is more accurate to use continuous-energy cross-sections using a realistic energy spectrum because it provides a better representation of the neutron spectrum than the averaged thermal cross-sections tabulated in text books. The energy-averaged macroscopic cross-sections will be calculated by performing tallies in MCNP to determine the reaction rate and flux on each foil.

A second set of foils were irradiated in the ERS using the same methods described above. This time each foil was placed inside a cadmium casing, the same casing used in previous measurements for the cadmium ratio of the gold foils.

3.6.2 Unfolding with MAXED and GRAVEL

UMG is an unfolding software package developed at the Physikalisch-Technische Bundesanstalt (PTB) laboratory in Germany. It requires a Windows XP operating system to run properly and it also needs the following three input files: Measured foil responses, response functions of each foil, and a default neutron energy spectrum to begin the process. UMG is comprised of two types of unfolding packages, MAXED (Maximum Entropy Deconvolution) uses a maximum entropy algorithm based on information theory and statistical mechanics to calculate a relatively unbiased neutron energy spectrum from the three input parameters mentioned above. Equation 15 represents a general detector and how to calculate the energy spectrum based on the detector's response.

$$N_k + e_k = \sum_l R_{kl}\phi_l \tag{15}$$

The term N_k is the number of counts in channel *k*, R_{kl} is the response of channel *k* to the particles in energy bin *l*, ϕ_l is the solution spectrum. The value of e_k is the difference between the measured value and the predicted value of the detector [35]. Equation 16 is used to constrain the e_k value allowing the software to solve Equation 17 using a given chi-square value. The chi-square value represents the difference between the measured counts and the expected counts if there were no relationship in the population.

$$\chi^2 = \sum_k \frac{e_k^2}{\sigma_k^2} \tag{16}$$

$$S = -\sum_i \phi_i \ln\left(\frac{\phi_i}{\phi_i^{DEF}}\right) + \phi_i^{DEF} - \phi_i \tag{17}$$

Equation 14 is the maximum entropy equation that uses the default spectrum (e.g. initial guess spectrum) and the solution spectrum that is dependent upon the default and the response functions. The final solution to the spectrum is chosen according to which one maximizes the entropy (*S*) of the distribution [35] [36]. Maximizing *S* in Equation 17 by choosing the correct solution spectrum will ensure an unbiased solution relying maximally on the measured data (i.e. foil activities) and minimally on the calculated data (i.e. default spectrum, response functions) [37].

The GRAVEL method is a modification of SAND-II and relies mostly on the default spectrum given in the input file. It will use the default spectrum and the measured activities from the foils to perform an iterative procedure that will converge on a solution spectrum based on the assumption that the default spectrum is near the exact solution.

$$\phi_i^{J+1} = \phi_i^J \exp\left(\frac{\sum_k W_{ik}^J \, log\left(\frac{N_k}{\sum_{i'} R_{ki'}\phi_{i'}^J}\right)}{\sum_k W_{ik}^J}\right) \tag{18}$$

$$W_{ik}^J = \frac{R_{ki}\phi_i^J}{\sum_{i'} R_{ki'}\phi_{i'}^J}\frac{N_k^2}{\sigma_k^2} \tag{19}$$

Where R_{ki} is the response function of foil *k* for the i^{th} energy bin, ϕ_i^J is the solution flux in i^{th} energy bin of the J^{th} iteration. A detailed derivation of the maximum entropy equations can be found in the following references [38] [39].

MAXED and GRAVEL operate using the same input files and both sets of codes use chi-square values for their convergence criteria. One of the input parameters for the control files in UMG asks the user to specify the chi-square per degree of freedom (PDF) value. The *e* term in Equation 16 is the difference between the measured response of detector *k* and the calculated response of detector *k* using the new solution spectrum. If both sets of data matched, the summation would be equal to the total number of detectors used. The chi-square PDF is the chi-square value normalized to the number of detectors. In an ideal scenario with a perfect match between measured and calculated, the chi-square PDF would be equal to unity [40].

A sensitivity analysis was performed on the chosen unfolded spectrum to demonstrate how sensitive the spectrum is to the measured responses of the foils. The response of each foil was perturbed by its corresponding uncertainty and the UMG software was used to calculate a new chi-square value for the perturbed spectrum. These chi-square values were then compared to the unperturbed chi-square value to determine how large of an effect the uncertainty of the measurements have on the unfolded spectrum.

3.6.3 Monte Carlo N-Particle Transport Description

Monte Carlo N-Particle (MCNP) is a general-purpose particle transport software that allows users to track the physics of a particle whether it be alphas, electrons, photons, or neutrons. The software can record a variety of information about the desired particle based on statistical methods and random sampling [41]. A simplified form of the Monte Carlo process consists of simulating a number of particle histories by using a pseudorandom number generator. The random numbers are generated in each particle history and used to sample probability density functions for scattering angles and track length distances, just to name a couple. The particles energy, position, and direction are determined using random sampling and the particles history is only complete when it is captured or escapes the specified system [42]. Monte Carlo N-Particle version 6 was used for this project and can be obtained for free from the Radiation Safety Information Computational Center (RSICC).

The input deck includes three types of cards for the software to read: surface cards, cell cards, and data cards. The surface cards describe the environment the user wishes to simulate particles. Surface cards describe very basic geometrical shapes such as cylinders, planes, and cones, among many others. These cards have a list of optional parameters that help specify the size of these shapes [41]. Data cards describe the materials, source information, and tally types of the problem and cell cards combine the surface and data cards to form an environment for the desired particles to interact and simulate phenomena. MCNP has been used many times to simulate neutron flux and energy spectra from a reactor [43 – 45] and response functions for different materials in neutron fields [17] [16].

An MCNP6 model was built to assist in the neutron energy spectrum calculations. This model includes the east beamline modified from an existing model built by John Bess at INL [46], and the east radiography station. A snapshot of the model can be seen in Figure 15.

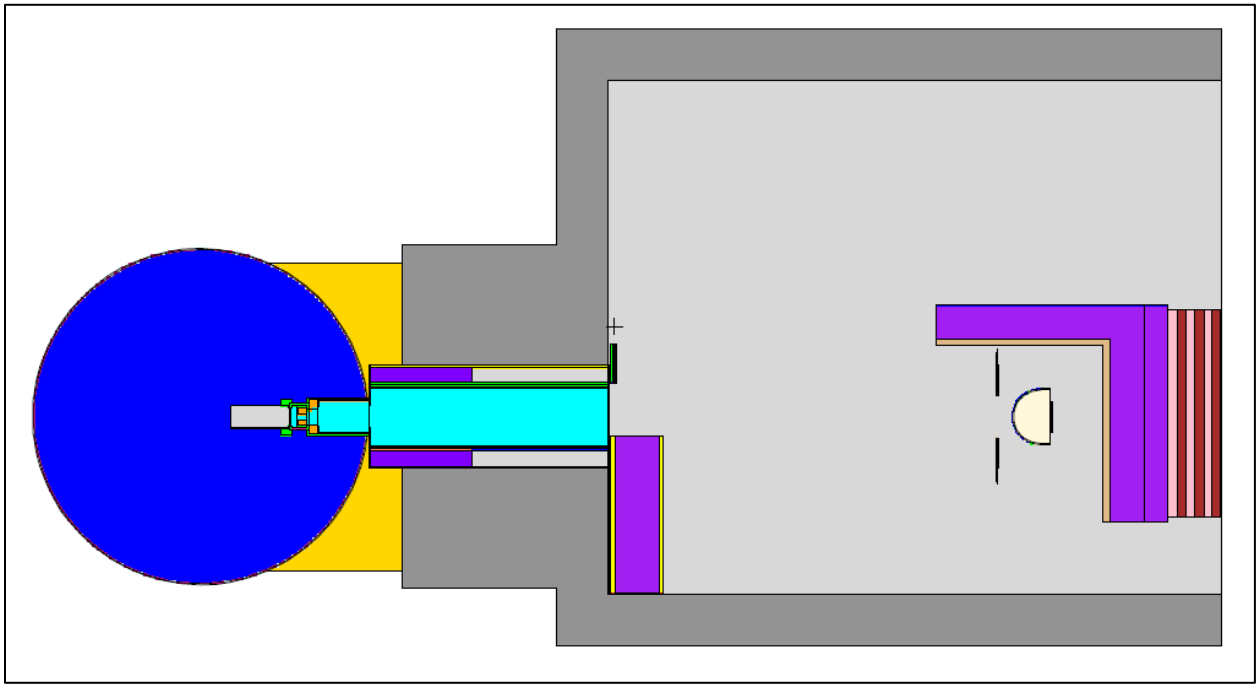

Figure 17. ERS MCNP6 model (plan view).

The NRAD reactor core was excluded from the model to perform calculations in a reasonable amount of time on the computer operating systems available. A disc source was created from the original NRAD reactor model and inserted into the new east beamline to simulate the neutrons heading towards the ERS. This source was obtained using an F2 surface tally and running a k-code calculation using 6,500 generations with 60,000 particles per generation.

The flux tallies used for a majority of the calculations performed in the model are the area integrated scalar flux (F2) and the volume integrated scalar flux (F4). The equations used in MCNP to calculate these tallies can be seen below.

$$F2 = \frac{1}{A}\int dE \int dt \int dA \int d\Omega \; \Psi(\vec{r}, \hat{\Omega}, E, t) \tag{20}$$

$$F4 = \frac{1}{V}\int dE \int dt \int dV \int d\Omega\ \Psi(\vec{r}, \hat{\Omega}, E, t) \tag{21}$$

The two tallies are calculated using the physical parameters of volume (cm^3) and area (cm^2) along with the following [41]:

r	=	particle position vector (cm)
$\hat{\Omega}$	=	direction vector
E	=	energy (MeV)
t	=	time (sh = 10^{-8} s)
Ψ	=	angular flux

The F2 tally can be seen in the figure below.

```
F12:n  677
*C12   90.000  50.000  30.000 25.000 21.875  18.75  15.625
       12.5    9.375   6.25   3.125   0
C
F22:n  677
*C22   90  0
E22    1.00E-09  1.75E-09  3.07E-09  5.39E-09  9.45E-09  1.66E-08
       2.91E-08  5.10E-08  8.94E-08  1.57E-07  2.75E-07  4.82E-07
       8.45E-07  1.48E-06  2.60E-06  4.56E-06  7.99E-06  1.40E-05
       2.46E-05  4.31E-05  7.55E-05  1.32E-04  2.32E-04  4.07E-04
       7.14E-04  1.25E-03  2.20E-03  3.85E-03  6.75E-03  1.18E-02
       2.08E-02  3.64E-02  6.38E-02  1.12E-01  1.96E-01  3.44E-01
       6.03E-01  1.06E+00  1.85E+00  3.25E+00  5.70E+00  1.00E+01
```

Figure 18. F2 surface tally in NRAD reactor MCNP model.

An angular tally was taken of the neutrons (F12) as well as an energy distribution tally (F22). The angle modification performed on the F22 tally ensured only the neutrons traveling towards the ERS were tallied and not the ones scattering back towards the reactor. Figure 19 is a screenshot of the NRAD core model and it shows the location where the tallies were taken and later used as the source location in the ERS model.

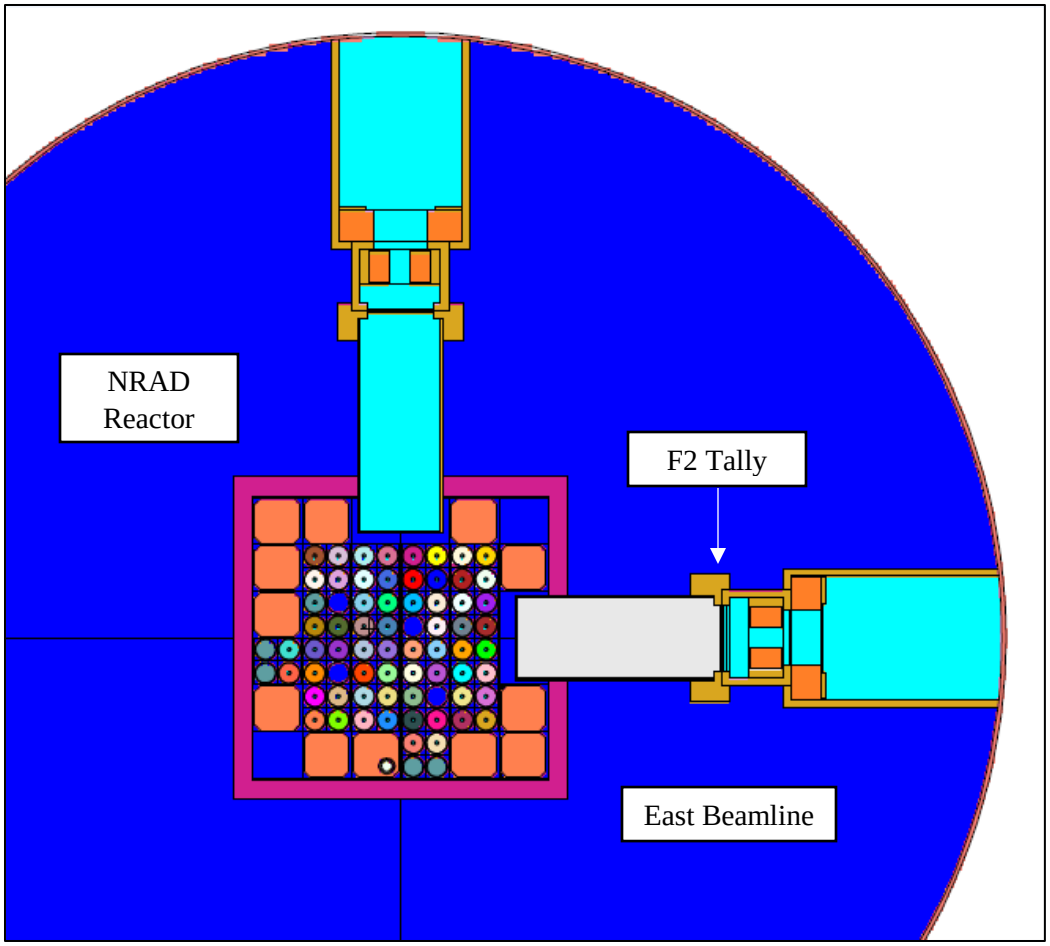

Figure 19. Beam filter window where F2 tallies were taken of reactor source.

The results displayed by MCNP6 are normalized to one source particle. The F2 tally units are *n/cm*^{2}*-sp*, in order to convert them into units of neutron flux a de-normalization factor was created. A source particle rate (SPR) term can be found for each foil by dividing the measured activity of each foil by the MCNP6 calculated activity of the same foil. The resulting units of this calculation will be *sp/s*. The average SPR can then be used to convert F2 and F4 tally values to *n/cm*^{2}*/s* by simply multiplying the value by the average SPR.

The UMG software required two sets of input data calculated by MCNP. The first set was the default spectrum at the image plane used as the initial guess spectrum for both GRAVEL and MAXED. The spectrum was found in MCNP6 using an F2 surface tally placed on the image plane

where the foils were set up in the experiment. This tally has the same energy distribution as the tally shown in Figure 18, but with no angular conditions. The second set of input data UMG requires is a response function of each foil used in the measurements. The response function is the energy dependent cross-section of the reaction of interest and can be determined in MCNP6 by using modified F4 tallies. Figure 20 shows the F4 tally used to calculate the response function of the neutron capture reaction in one of the indium foils and Figure 21 shows where the tally was taken in the model.

```
F14:n 5106
FM14 1 335 102
FC14 "(n,gamma) Reaction Rate of In Foil"
FT14 scx 3
```

Figure 20. Modified F4 tally of (n, γ) reaction in indium foil.

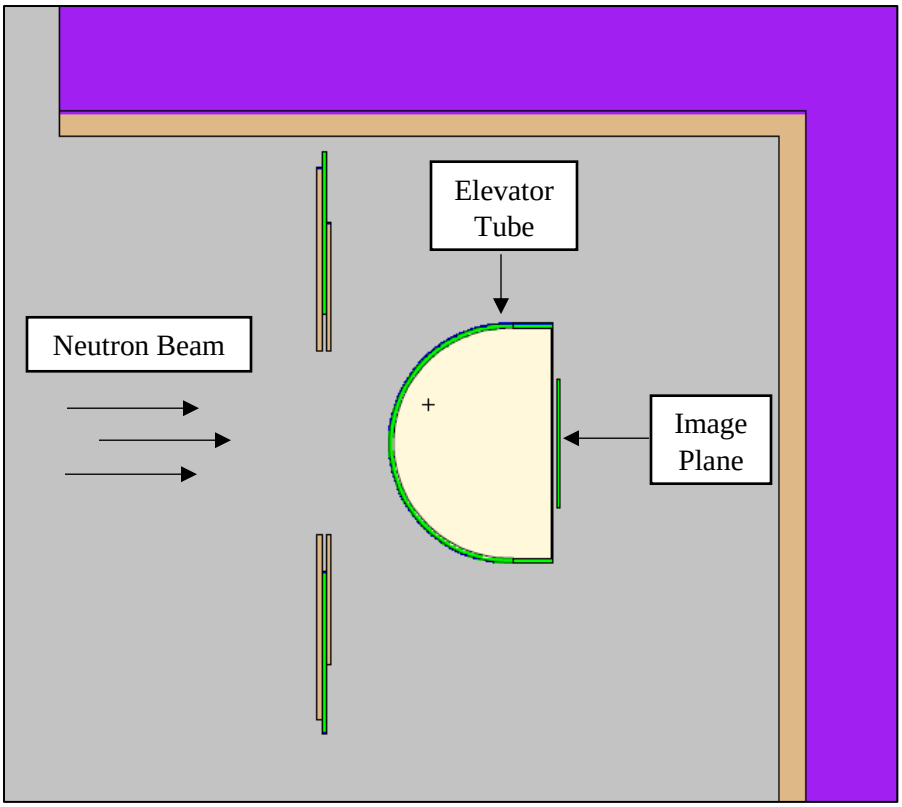

Figure 21. Elevator tube and image plane where MCNP6 tallies are taken.

The terms in the FM14 line should be interpreted as follows: 1 represents a scalar value, this can usually be a normalizing factor but in this particular case the tally will be multiplied by 1 to avoid confusion. The second term is the material number which should represent the isotope of interest in the particular foil. For instance, the titanium foil used is made of the naturally occurring isotopes ^{46}Ti, ^{47}Ti, ^{48}Ti, ^{49}Ti, and ^{50}Ti but the reactions of interest in the foil only include ^{47}Ti(n,p)^{47}Sc and ^{48}Ti(n,p)^{48}Sc. A separate list of material cards were written in the input file to ensure only these reactions contributed to the tallies. The third term uses this material number to find the energy dependent cross-sections for the reaction of interest. Figure 20 shows this value to be 102 which represents the reaction (n,γ). A list of values and their corresponding reaction can be found in the appendix of the MCNP6 user manual under the document number LA-UR-13-21822 [47]. The third line in the figure is a comment and the fourth line is a special treatment of the F14 tally that splits it into the same energy distribution as the source in the model.

The modified F4 tally represents Equation 11 and must be divided by the unperturbed flux incident on the foils. This flux was calculated in MCNP by taking an F4 tally of the region directly behind the foils designated by the red box in Figure 15. The material in the cell used to calculate the unperturbed flux must be set to a void to be truly unperturbed. The equation used to calculate the energy dependent response function of each foil in MCNP6 can be seen below along with the corresponding units.

$$\mathcal{R}(E_i) = \frac{Modified\ F4_i}{Unperturbed\ F4_i} = \frac{\left[\frac{b-n}{cm^2-sp}\right]}{\left[\frac{n}{cm^2-sp}\right]} = barns \tag{22}$$

The MCNP6 tally set up and Equation 22 were used for each of the 23 foils used in the measurement. The default spectrum, the response functions and the measured responses for all the foils were then uploaded to UMG to unfold the neutron energy spectrum.

3.6.4 Comparison of MCNP and UMG Codes

The goal, after accurately measuring the neutron energy spectrum at the image plane, is to produce an MCNP6 model that can accurately simulate the same neutron beam in the ERS. Creating an MCNP model validated by measured results can be a very useful tool for experiment preparation in the future of this facility. A method has been developed to implement the unfolded spectrum, which is mostly based on measured results, into the MCNP model and create a new source definition that will simulate a more accurate neutron beam in the ERS. This method involves calculating the amount of attenuation each neutron energy bin experiences as it travels from the entrance of the beam filter tube (i.e. source plane) to the image plane behind the elevator in the MCNP model. This amount of attenuation, which will be called the attenuation factor, was applied to the unfolded spectrum to obtain an estimate of the new source definition. The assumption used in this method is the attenuation factor is independent of the spectrum magnitude. The equation below shows how this factor was calculated.

$$Attenuation\ Factor_k = \frac{F2_{IP,k}}{F2_{SP,k}} \tag{23}$$

$F2_{IP,k}$ is the surface tally result for energy bin k at the image plane and $F2_{SP,k}$ is the tally at the source plane. This assumption can be used to calculate a new source term based on the shape of the unfolded spectrum. Each value in the UMG solution spectrum was divided by its corresponding attenuation factor. These results can be normalized to one source particle and provide a new list of neutron energy probabilities.

$$UMG\ Source_k = \frac{UMG\ Image\ Plane_k}{Attenuation\ Factor_k} \tag{24}$$

The new source term was inserted back into the MCNP model to predict the activities of the foils. A reaction rate tally similar to the one described in Figure 20 was performed on each foil for both bare and cadmium covered sets. This tally was then used to calculate the activity of the given foil. These activities were calculated using a modified version of Equation 6 and Equation 7. The MCNP tallies are the modifications in Equation 25. The results of these computations were compared to measured results to determine how well the model simulates the neutron beam.

$$A_i = \left(SPR * N_j * FM4_j * V_j\right) * \left(1 - \exp\left(-\lambda_j t\right)\right) \tag{25}$$

SPR	=	Average source particle rate
N_j	=	Atom density of the foil j
$FM4_j$	=	Total modified F4 tally of foil j described in Equation 19
V_j	=	Volume of foil j
λ_j	=	Decay constant of foil j

4 Results & Discussion

4.1 Neutron Beam Flux

Measured uncertainties for each parameter described in sections 3.2 can be seen in Table 5. These uncertainties were used in Equation 12 to produce an average flux uncertainty of 2.6%. The uncertainty for the weight of each foil was provided by the manufacturing company. The placement error was measured using the smallest possible measurement that could be taken on the ruler used to place the foils on the aluminum sheet, and the time uncertainty was provided by the NRAD operators using the smallest possible time measurement on the timer. The measured results for the neutron flux at the image plane are shown in the Table 6.

Table 5. Uncertainties in measured parameters used to calculate neutron flux.

Parameter	(±)	(%)
Foil Weight (g)	0.0005	0.42%
Activity (dps)*	--	1.5%
Time (s)	0.001	0.10%
Placement (in)	0.0625	1.04%

**Error reported at 2σ*

Table 6. Neutron flux measurements at the image plane (ERS).

	Trial #1			Trial #2			Average
Position	**Activity (dps)**	**Flux (n/cm^2/s)**	**Error @ 2σ**	**Activity (dps)**	**Flux (n/cm^2/s)**	**Error @ 2σ**	**Flux (n/cm^2/s)**
1	1.795E+04	9.591E+06	2.6%	1.828E+04	9.753E+06	2.6%	9.672E+06
2	1.765E+04	9.410E+06	2.6%	1.799E+04	9.635E+06	2.6%	9.522E+06
3	1.743E+04	9.479E+06	2.6%	1.836E+04	9.769E+06	2.6%	9.624E+06
4	1.769E+04	9.604E+06	2.6%	1.821E+04	9.533E+06	2.6%	9.568E+06
5	1.813E+04	9.722E+06	2.6%	1.865E+04	9.813E+06	2.6%	9.768E+06
6	1.736E+04	9.399E+06	2.6%	1.780E+04	9.512E+06	2.6%	9.456E+06
7	1.788E+04	9.713E+06	2.6%	1.839E+04	9.591E+06	2.6%	9.652E+06
8	1.806E+04	9.715E+06	2.6%	1.832E+04	9.630E+06	2.6%	9.672E+06
9	1.799E+04	9.691E+06	2.6%	1.832E+04	9.661E+06	2.6%	9.676E+06
10	1.784E+04	9.692E+06	2.6%	1.865E+04	9.845E+06	2.6%	9.769E+06
11	1.802E+04	9.695E+06	2.7%	1.843E+04	9.480E+06	2.7%	9.588E+06
12	1.780E+04	9.672E+06	2.6%	1.821E+04	9.381E+06	2.6%	9.527E+06
13	1.784E+04	9.668E+06	2.6%	1.828E+04	9.434E+06	2.6%	9.551E+06
14	1.839E+04	9.902E+06	2.5%	1.832E+04	9.552E+06	2.5%	9.727E+06
15	1.806E+04	9.838E+06	2.6%	1.906E+04	9.827E+06	2.6%	9.832E+06
16	1.780E+04	9.713E+06	2.6%	1.799E+04	9.333E+06	2.6%	9.523E+06
17	1.765E+04	9.560E+06	2.6%	1.865E+04	9.656E+06	2.6%	9.608E+06
18	1.780E+04	9.664E+06	2.6%	1.802E+04	9.421E+06	2.6%	9.542E+06
19	1.758E+04	9.504E+06	2.6%	1.765E+04	9.138E+06	2.6%	9.321E+06
20	1.795E+04	9.568E+06	2.6%	1.839E+04	9.453E+06	2.6%	9.511E+06
21	1.825E+04	9.460E+06	2.6%	1.791E+04	9.857E+06	2.6%	9.659E+06

The measured activities can be seen in the second and fifth columns of Table 6, they represent the activities of the foils at the end of irradiation. Using Equation 8 mentioned above in section 3.2 the neutron flux was calculated. It should be noted that this these flux values were calculated using the average thermal microscopic cross-section of gold which 98.7 barns. This cross-section will only account for the neutrons at the thermal and epi-thermal energy levels of roughly 1 eV or less [26]. It was determined after analyzing the data that the total thermal averaged flux of the neutron beam is $9.61 \times 10^6 \pm 2.47 \times 10^5$ *n/cm^2/s*.

4.2 Neutron Beam Flux Profile

It can be seen from the figures below and from Table 6 that the neutron flux profile of the beam is relatively flat across the surface of the image plane. This is a good indicator that any object being radiographed will be exposed to roughly the same number of neutrons regardless of where it is at on the image plane. The peak-to-average ratio of the flux measurements was 1.031 indicating very small deviation from the average.

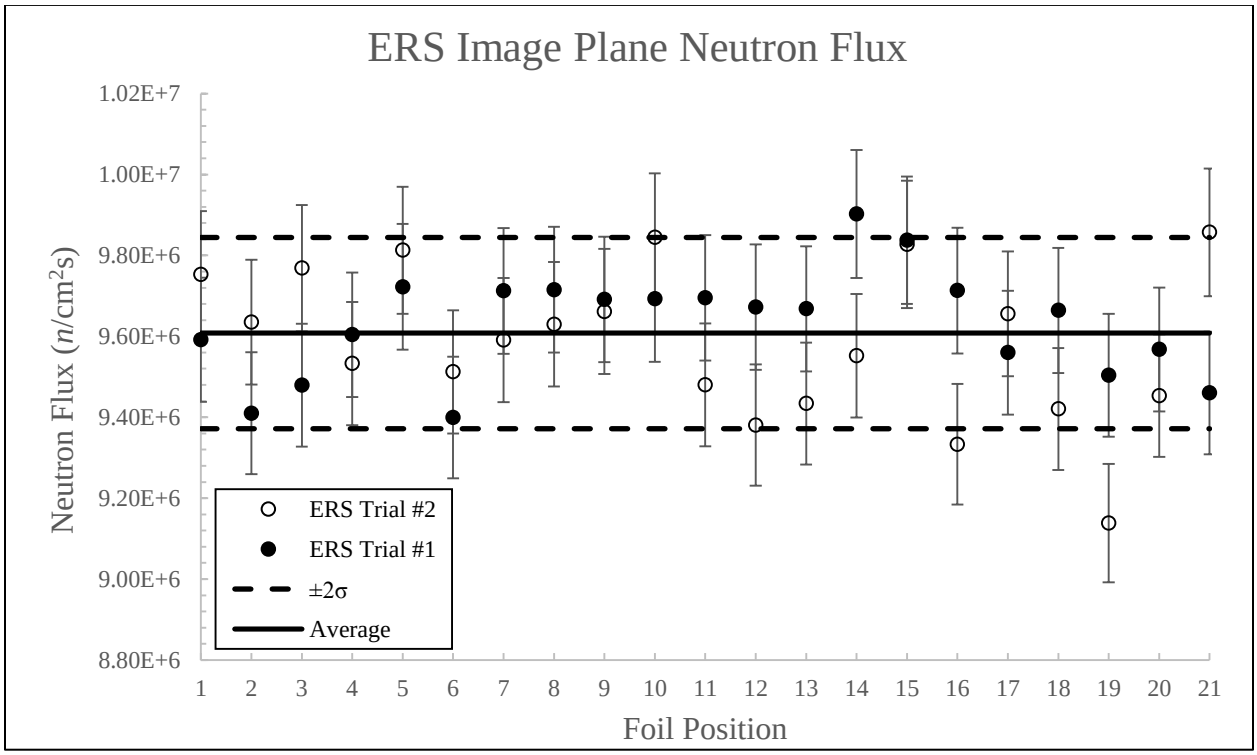

Figure 22. Neutron flux as a function of position on the image plane in the ERS.

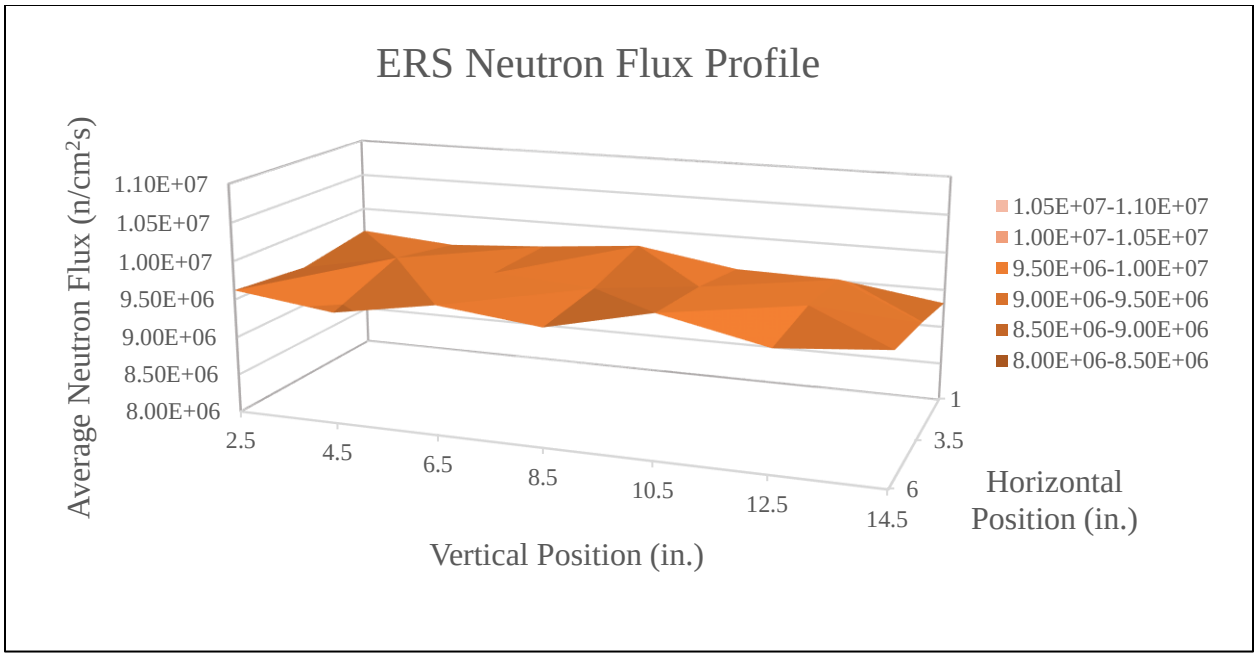

Figure 23. 3-Dimensional representation of neutron flux profile in ERS.

4.3 Cadmium Ratio of the Neutron Beam Flux

The cadmium ratio of the neutron beam at the image plane was found after irradiating 42 gold foils covered with cadmium and then comparing the activities between the two sets of foils, bare versus covered. Table 7 shows the activities of the covered foils and their resulting cadmium ratio calculated using the average activity at each position. The data was reviewed from Table 7 and it was concluded that the cadmium ratio of the gold foils was 2.05 ± 2.9%. This number verifies the ERS neutron beam has a high epi-thermal neutron content which is ideal for imaging spent nuclear fuel.

Table 7. Cadmium covered gold foil activity measurements (ERS).

	Trial #1		Trial #2		Averaged	
Position	**Activity (dps)**	**Error @ 2σ**	**Activity (dps)**	**Error @ 2σ**	**Cd Ratio**	**Error @ 2σ**
1	8.96E+03	2.9%	8.33E+03	2.9%	2.10	2.9%
2	8.96E+03	2.9%	8.48E+03	2.9%	2.04	2.9%
3	8.73E+03	2.9%	8.44E+03	2.9%	2.08	2.9%
4	8.62E+03	2.9%	8.29E+03	2.9%	2.12	2.9%
5	8.81E+03	2.9%	8.55E+03	2.9%	2.12	2.9%
6	8.92E+03	2.9%	8.62E+03	2.9%	2.00	2.9%
7	8.88E+03	2.9%	8.33E+03	2.9%	2.11	2.9%
8	9.44E+03	2.9%	8.48E+03	2.9%	2.03	2.9%
9	1.05E+04	2.9%	8.62E+03	2.9%	1.90	2.9%
10	8.92E+03	2.9%	8.62E+03	2.9%	2.08	2.9%
11	8.62E+03	2.9%	8.81E+03	2.9%	2.09	2.9%
12	9.18E+03	2.9%	8.66E+03	2.9%	2.02	2.9%
13	8.73E+03	2.9%	8.48E+03	2.9%	2.10	2.9%
14	8.92E+03	2.9%	8.44E+03	2.9%	2.12	2.9%
15	1.01E+04	2.9%	8.62E+03	2.9%	1.98	2.9%
16	8.66E+03	2.9%	8.77E+03	2.9%	2.05	2.9%
17	9.25E+03	2.9%	8.85E+03	2.9%	2.01	2.9%
18	8.92E+03	2.9%	8.51E+03	2.9%	2.06	2.9%
19	9.10E+03	2.9%	8.62E+03	2.9%	1.99	2.9%
20	9.29E+03	2.9%	8.59E+03	2.9%	2.03	2.9%
21	8.92E+03	2.9%	8.70E+03	2.9%	2.05	2.9%

4.4 Image Quality

The film densities of the beam purity indicator can be found in Table 8, and the values obtained from visual analysis of the sensitivity indicator can be found in Table 9. The two neutron radiographs can be seen in Figure 24. The densities were found using an Xrite model 301 densitometer that correlates the amount of light transmitted through the film to the density of the film [48]. It can be seen from the measured parameters in Table 9 that the ERS facility scores in the category I range for neutron content, scattering content and the amount of visible gaps and

holes. The pair production and gamma content do not apply to the ERS because the facility uses an indirect method for developing radiographs and the films are never exposed to gamma-rays in the beam.

Table 8. Beam purity indicator densities.

BPI Parameters		
$\mathbf{D_B}$	0.47	0.44
$\mathbf{D_L}$	2.13	2.23
$\mathbf{D_H}$	2.77	
$\mathbf{D_T}$	2.19	
$\mathbf{\Delta D_L}$	0.1	
$\mathbf{\Delta D_B}$	0.03	

Table 9. IQI determined values vs a category I radiographic facility.

	ERS	Category I
NC	79	≥ 65
S	1	≤ 5
P	NA	≤ 3
γ	NA	≤ 3
G	7	≥ 6
H	7	≥ 6

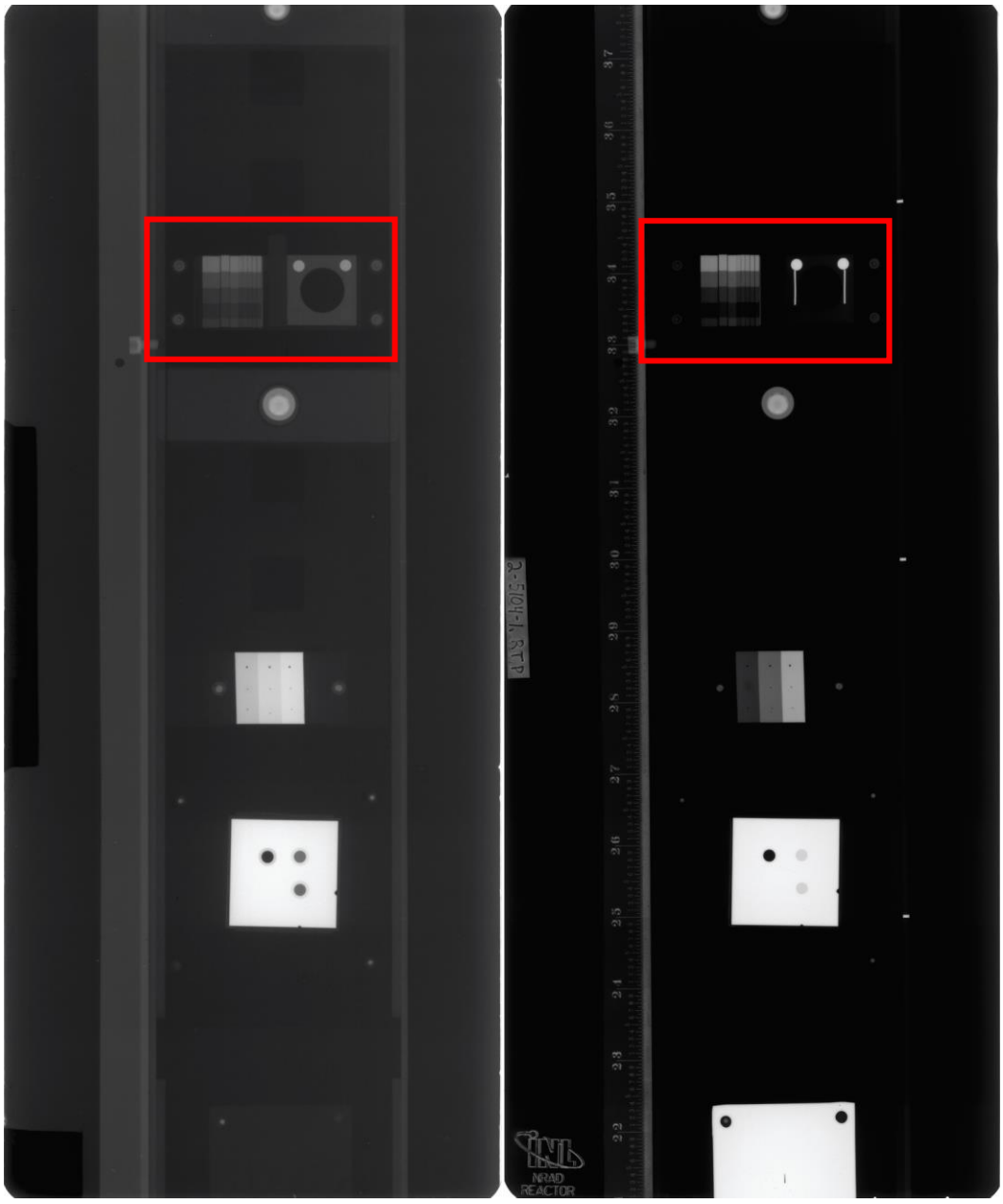

Figure 24. Neutron radiographs of IQIs. From left to right: Indium Foil, Dysprosium Foil.

4.5 Neutron Energy Spectrum

This section will describe how the three sets of data were collected for the UMG software. The foil responses were measured first and then an MCNP6 model of the ERS was created and the response functions for the foils and the initial guess spectrum were calculated from the model.

4.5.1 Bare Foil Results

The unfolding software requires three sets of data to be determined before the neutron energy spectrum solution can be calculated. The first set of data was the measured responses of the irradiated foils. The scattering and self-shielding correction factors were first determined for each foil using the MCNP model and process described in section 3.6.1. The table in Appendix A shows the energy-averaged cross-sections calculated by MCNP and the resulting correction factors. The response of each foil was found using Equation 14 and the results can be seen in Table 10.

Table 10. Measured responses of the bare multi-foil array.

Foil	Reaction	Response {[n -b/cm^2-s]}	Error @ 2σ
Indium (In)	In-115(n,γ)In-116m	9.928E+08	3%
Manganese-Copper (8.7%Mn-Cu)	Mn-55(n,γ)Mn-56	7.448E+07	3%
Iron (Fe)	Fe-54(n,p)Mn-54	--	NA
	Fe-56(n,p)Mn-56	1.007E+05	5%
Lutetium-Aluminum (5.2%Lu-Al)	Lu-175(n,γ)Lu-176m	5.263E+08	10%
Indium (In)	In-115(n,n')In-115m	1.174E+07	9%
Copper (Cu)	Cu-63(n,α)Co-60	--	NA
	Cu-63(n,2n)Cu-62	--	NA
Copper (Cu)	Cu-63(n,γ)Cu-64	2.784E+07	3%
Zinc (Zn)	Zn-64(n,p)Cu-64	2.840E+06	3%
Sodium Chloride (NaCl)	Na-23(n,γ)Na-24	2.564E+06	3%
Aluminum (Al)	Al-27(n,α)Na-24	2.339E+04	14%
Magnesium (Mg)	Mg-24(n,p)Na-24	1.141E+05	13%
Tungsten (W)	W-186(n,γ)W-187	4.414E+08	3%
Nickel (Ni)	Ni-58(n,p)Co-58	8.081E+06	3%
	Ni-58(n,2n)Ni-57	--	NA
Titanium (Ti)	Ti-47(n,p)Sc-47	1.624E+06	5%
	Ti-48(n,p)Sc-48	2.046E+04	7%
Vanadium (V)	V-51(n,α)Sc-48	--	NA
Gold (Au)	Au-197(n,γ)Au-198	6.604E+08	3%
Molybdenum (Mo)	Mo-98(n,γ)Mo-99	9.764E+06	3%
Zirconium (Zr)	Zr-90(n,2n)Zr-89	--	NA
Iron (Fe)	Fe-58(n,γ)Fe-59	--	NA
Scandium (Sc)	Sc-45(n,γ)Sc-46	1.231E+08	4%
Cobalt (Co)	Co-59(n,γ)Co-60	2.215E+08	5%
***Sodium Chloride (NaCl)**	Cl-35(n,α)P-32	1.088E+07	7%
***Sulfur (S)**	S-32(n,p)P-32	2.189E+06	7%

Only eighteen of the original twenty-seven reactions had reasonable activities that could be used to unfold the spectrum. The remaining nine reactions had activities too low for the detectors to accurately count the gamma-rays emitted from the foils. The Cl-35(n,α)P-32 and S-32(n,p)P-32 reactions that required the proportional counter to determine the activity were also dropped from

the usable list of reactions. This was decided after discovering different activated nuclides in the foils were emitting beta particles making it very difficult to distinguish the activity produced strictly from the desired reactions.

The F2 tally described in section 3.6.3 was used to find the default spectrum. The average source particle rate was calculated first in order to de-normalize the tally output. Equation 6 and Equation 7 were to calculate the activity of each reaction from the reaction rate tallies used in MCNP6. The SPR for each foil was determined by using the process described in section 3.6.3. The results can be seen in the Table 11 along with the average SPR, which was then used to calculate the neutron flux per energy bin. There were five reactions left out of the SPR calculations, the reason for this will be explained later in this section.

Table 11. SPR results from measured data and MCNP (bare foils).

Reaction of Interest	MCNP Activity (decays/sp)	Measured Activity (dps)	SPR (sp/s)
In-115(n,γ)In-116m	4.301E-08	6.401E+05	1.488E+13
Mn-55(n,γ)Mn-56	1.969E-09	3.056E+04	1.552E+13
Lu-175(n,γ)Lu-176m	1.475E-09	2.446E+03	1.658E+12
Cu-63(n,γ)Cu-64	7.412E-10	1.084E+04	1.463E+13
Zn-64(n,p)Cu-64	1.688E-11	1.265E+03	7.498E+13
Na-23(n,γ)Na-24	6.800E-10	4.662E+03	6.855E+12
W-186(n,γ)W-187	3.520E-09	3.215E+04	9.135E+12
Ni-58(n,p)Co-58	6.302E-13	6.327E+01	1.004E+14
Ti-47(n,p)Sc-47	1.502E-12	1.735E+01	1.155E+13
Au-197(n,γ)Au-198	1.283E-09	2.538E+04	1.978E+13
Mo-98(n,γ)Mo-99	1.040E-11	1.373E+02	1.32E+13
Sc-45(n,γ)Sc-46	1.715E-11	2.775E+02	1.618E+13
Co-59(n,γ)Co-60	1.096E-12	2.198E+01	2.005E+13
		Average SPR	2.452E+13

The default spectrum can be seen in Figure 25 with the corresponding values for each energy bin shown in Table 11. The energy bin structure was divided into 42 equal-lethargy bins, the smaller energies have smaller bin sizes while the larger energies have larger bin sizes. The default spectrum was normalized to show a visually correct shape by dividing the tally value by the size of its energy

bin, producing units of *n/cm^2-sp/MeV [49]*. Neutron energy spectra can also be displayed using units of neutron flux per lethargy. Lethargy represents the average logarithmic energy loss of neutrons and is the difference between the natural logarithmic values of the upper and lower energy bins *[49]*. Energy-normalized plots should be used when the x-axis and the y-axis are both logarithmic and lethargy-normalized plots should be used when the x-axis is logarithmic and the y-axis is linear.

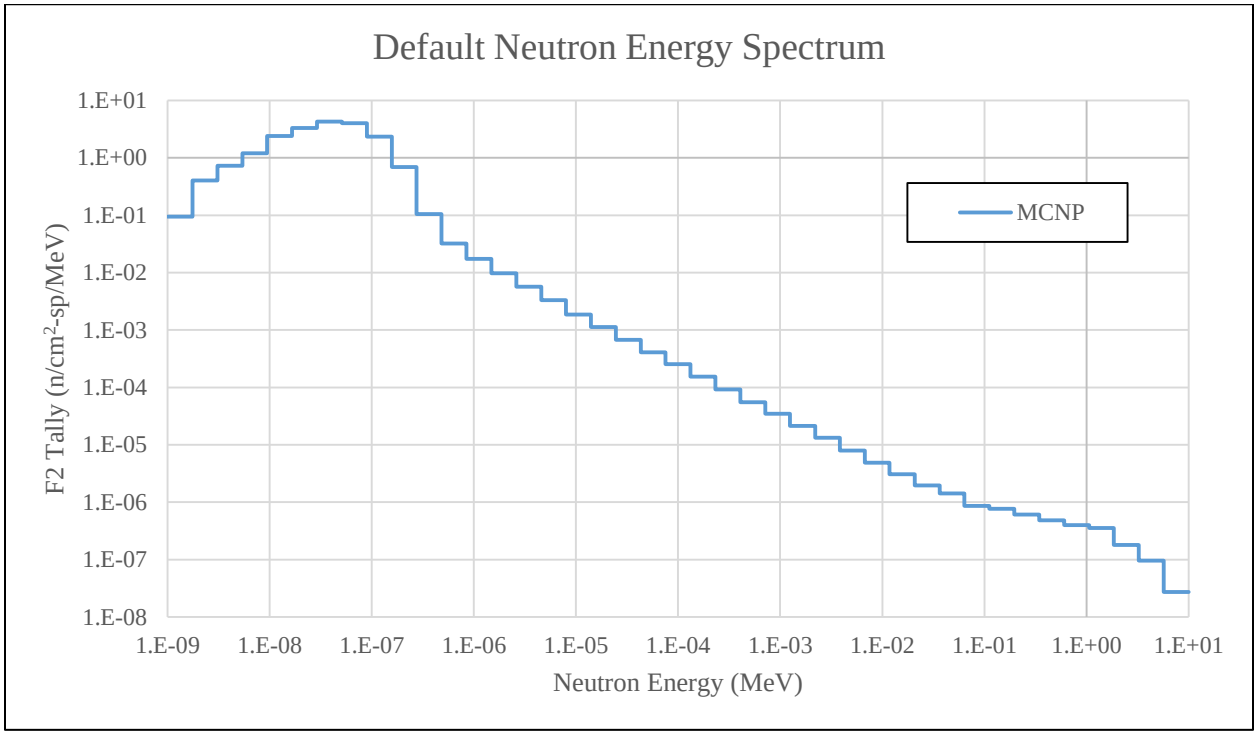

Figure 25. Energy-normalized default spectrum per source particle

Table 12. MCNP calculated default energy spectrum in the east beamline.

Energy Bin (MeV)	F2 Tally Results (n/cm^2-sp)	Error	Energy Bin (MeV)	F2 Tally Results (n/cm^2-sp)	Error
1.00E-09 - 1.75E-09	3.01E-10	1.13%	1.32E-04 - 2.32E-04	9.23E-09	0.27%
1.75E-09 - 3.07E-09	9.57E-10	0.62%	2.32E-04 - 4.07E-04	9.63E-09	0.27%
3.07E-09 - 5.39E-09	2.80E-09	0.37%	4.07E-04 - 7.14E-04	1.07E-08	0.26%
5.39E-09 - 9.45E-09	9.73E-09	0.25%	7.14E-04 - 1.25E-03	1.14E-08	0.25%
9.45E-09 - 1.66E-08	2.37E-08	0.13%	1.25E-03 - 2.20E-03	1.26E-08	0.24%
1.66E-08 - 2.91E-08	5.34E-08	0.10%	2.20E-03 - 3.85E-03	1.31E-08	0.24%
2.91E-08 - 5.10E-08	8.77E-08	0.07%	3.85E-03 - 6.75E-03	1.41E-08	0.23%
5.10E-08 - 8.94E-08	9.05E-08	0.07%	6.75E-03 - 1.18E-02	1.55E-08	0.21%
8.94E-08 - 1.57E-07	4.66E-08	0.11%	1.18E-02 - 2.08E-02	1.77E-08	0.20%
1.57E-07 - 2.75E-07	1.24E-08	0.21%	2.08E-02 - 3.64E-02	2.22E-08	0.20%
2.75E-07 - 4.82E-07	6.68E-09	0.29%	3.64E-02 - 6.38E-02	2.38E-08	0.19%
4.82E-07 - 8.45E-07	6.30E-09	0.30%	6.38E-02 - 1.12E-01	3.70E-08	0.17%
8.45E-07 - 1.48E-06	6.22E-09	0.30%	1.12E-01 - 1.96E-01	5.09E-08	0.15%
1.48E-06 - 2.60E-06	6.37E-09	0.31%	1.96E-01 - 3.44E-01	7.19E-08	0.12%
2.60E-06 - 4.56E-06	6.47E-09	0.30%	3.44E-01 - 6.03E-01	1.04E-07	0.10%
4.56E-06 - 7.99E-06	6.40E-09	0.31%	6.03E-01 - 1.06E+00	1.63E-07	0.07%
7.99E-06 - 1.40E-05	6.78E-09	0.30%	1.06E+00 - 1.85E+00	1.42E-07	0.07%
1.40E-05 - 2.46E-05	7.16E-09	0.30%	1.85E+00 - 3.25E+00	1.35E-07	0.07%
2.46E-05 - 4.31E-05	7.61E-09	0.29%	3.25E+00 - 5.70E+00	6.71E-08	0.08%
4.31E-05 - 7.55E-05	8.23E-09	0.28%	5.70E+00 - 1.00E+00	1.81E-08	0.15%
7.55E-05 - 1.32E-04	8.76E-09	0.28%			

The response function for each of the eighteen remaining reactions were calculated using MCNP6. These functions can be seen in Figures 24 – 26.

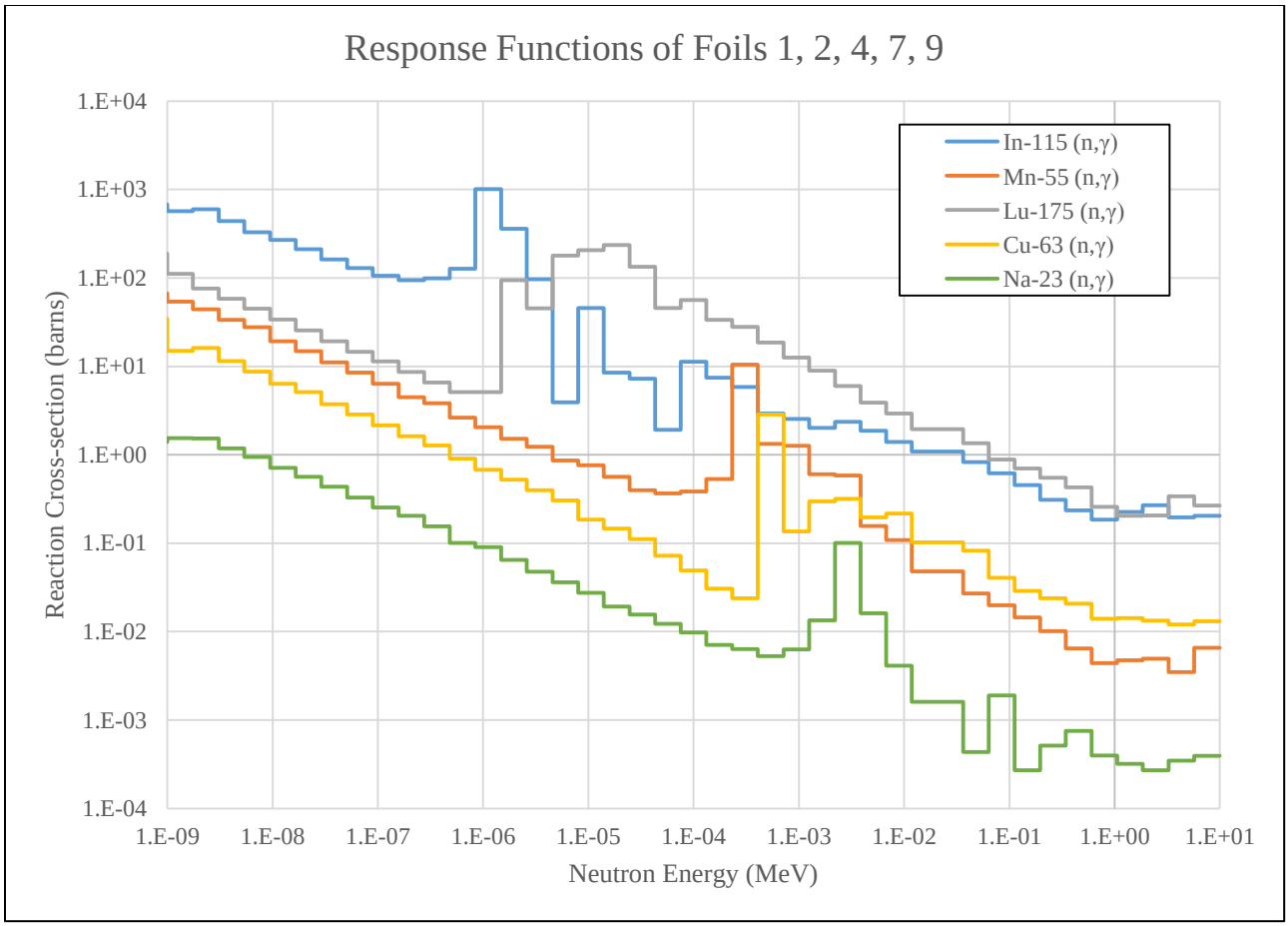

Figure 26. Response functions of foils 1, 2, 4, 7, and 9 (bare).

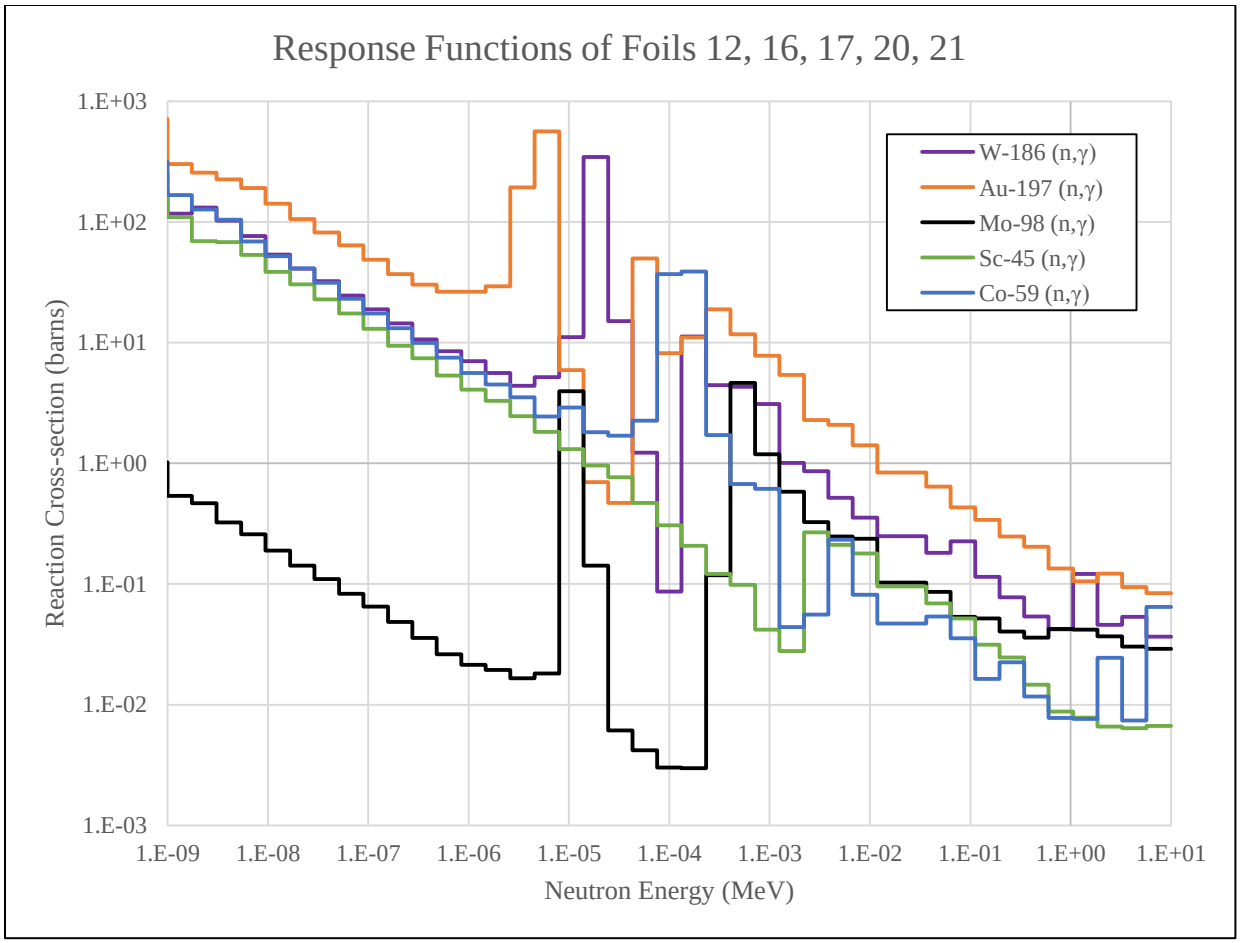

Figure 27. Response functions of foils 12, 16, 17, 20, and 21 (bare).

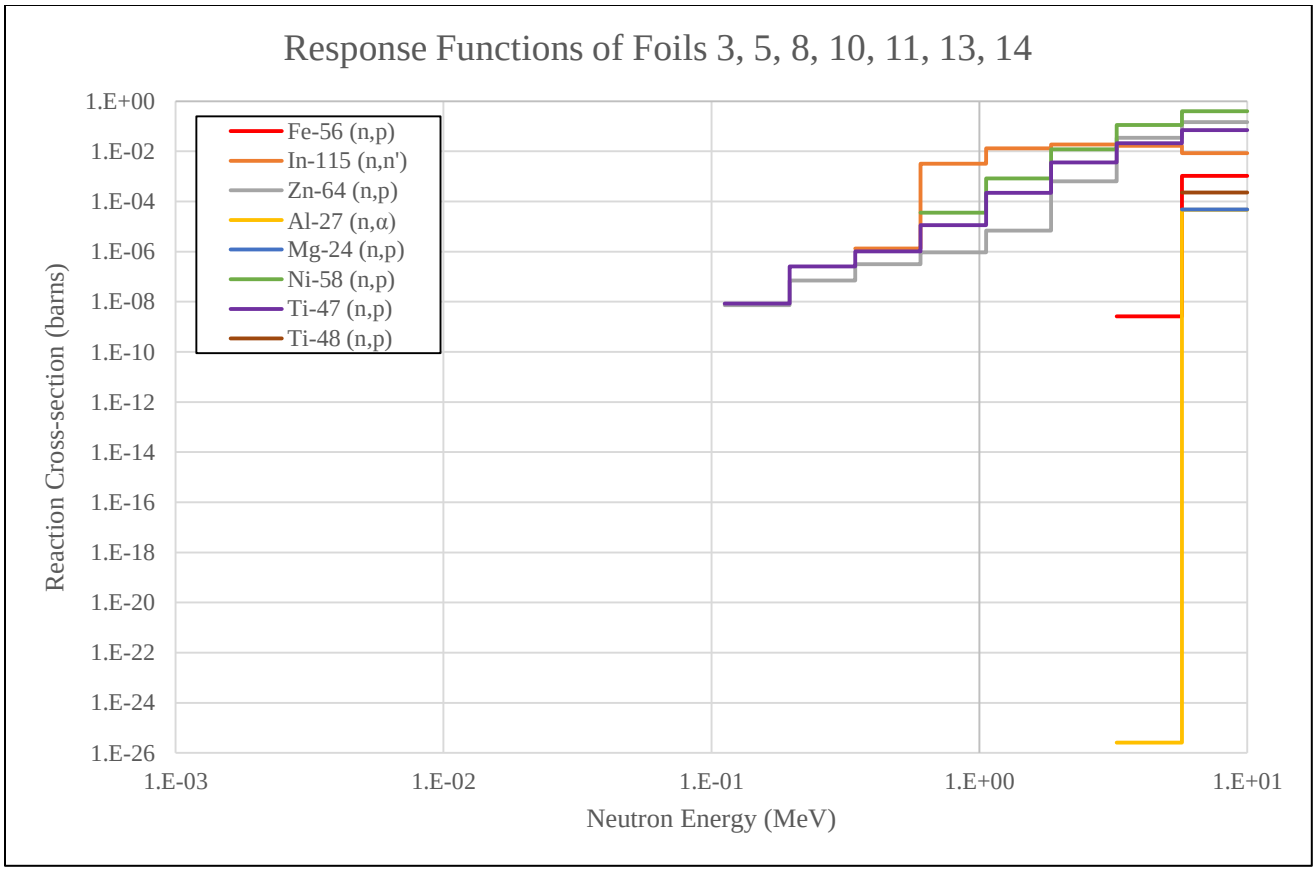

Figure 28. Response functions of foils 3, 5, 8, 10, 11, 13, and 14 (bare).

The initial solution spectrum calculated using the UMG software and data from the 18 measured reactions can be seen in Figure 29. The spectrum was plotted on a log-log scale using the UMG plot application in order to capture the total calculated spectrum. The y-axis is neutron flux per unit lethargy and the x-axis is neutron energy (MeV). The two unfolding packages show large fluctuations in the spectrum and no real conclusions can be made about the output.

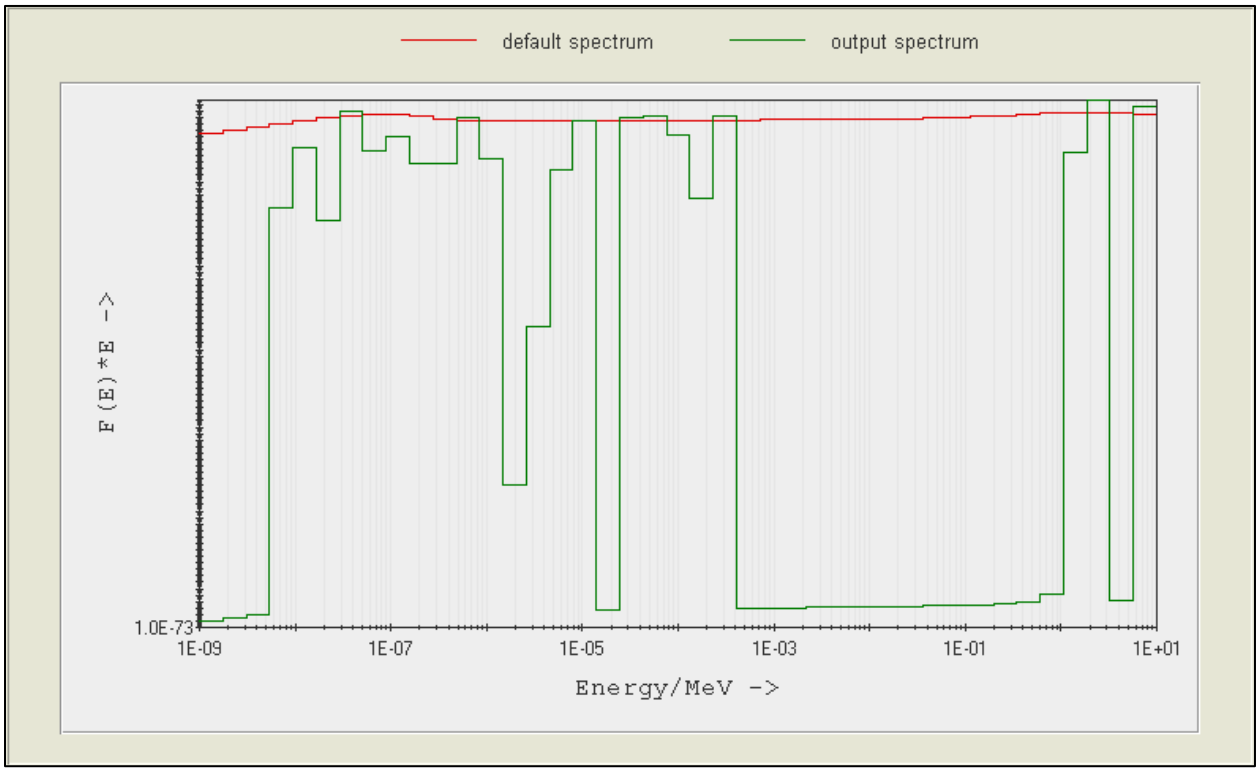

Figure 29. UMG output of initial solution spectrum.

A total of five reactions were omitted from the data used in UMG to obtain a more reasonable solution spectrum. The following reactions were the ones not included in future studies:

- Fe-56(n,p)Mn-56
- In-115(n,n')In-115m
- Al-27(n,α)Na-24
- Mg-24(n,p)Na-24
- Ti-48(n,p)Sc-48

^{56}Fe, ^{27}Al, ^{24}Mg, and ^{48}Ti were taken out because their response functions had three or less data points which could lead to large errors when folding the measured responses with the response functions. The uncertainties for the ^{27}Al and ^{24}Mg, 14% and 13% respectively, may have also contributed to the fluctuations displayed in Figure 29.

The reaction from the fifth foil, indium, was difficult to capture in MCNP. The inelastic scattering reaction of ^{115}In was simulated using a tally setup shown in Figure 30.

```
F54:n 5110
FM54 1 335 51
FC54 "(n,n') Reaction Rate of In Foil"
FT54 scx 3
C
F254:n 5110
FM254  1 335 4
FC254  "(n,n') Reaction Rate of In Foil"
FT254  scx 3
```

Figure 30. MCNP tally used to calculate inelastic cross-section of ^{115}In.

These two tallies measure two separate reactions in MCNP. The 51 reaction represents all neutron interactions that lead to the first excited state of ^{115}In while the number 4 represents the total inelastic cross-section. The MCNP6 output only shows results for the 51 reaction type which was used in UMG software. The activity measured from the indium foil and the MCNP calculated activity can be seen in Table 13 with their corresponding errors. The measured activity is roughly 50 times larger than the MCNP activity, indicating the 51 reaction is not simulating all possible reactions with the foil. The inelastic reaction from indium was taken out of the unfolding process because of this large discrepancy.

Table 13. MCNP vs measured activities from In-115(n,n')In-115m reaction.

MCNP Activity (dps)	Error	Measured Activity (dps)	Error
1.06E+02	0.72%	5.96E+03	9%

Three plots are shown in Figures 31-33 depicting the solution spectra calculated using GRAVEL and MAXED packages and the data collected from the bare foils. Energy-normalized, lethargy-normalized, and raw neutron flux for each energy bin were all plotted to provide a graphic of the neutron energy spectrum in the east radiography station.

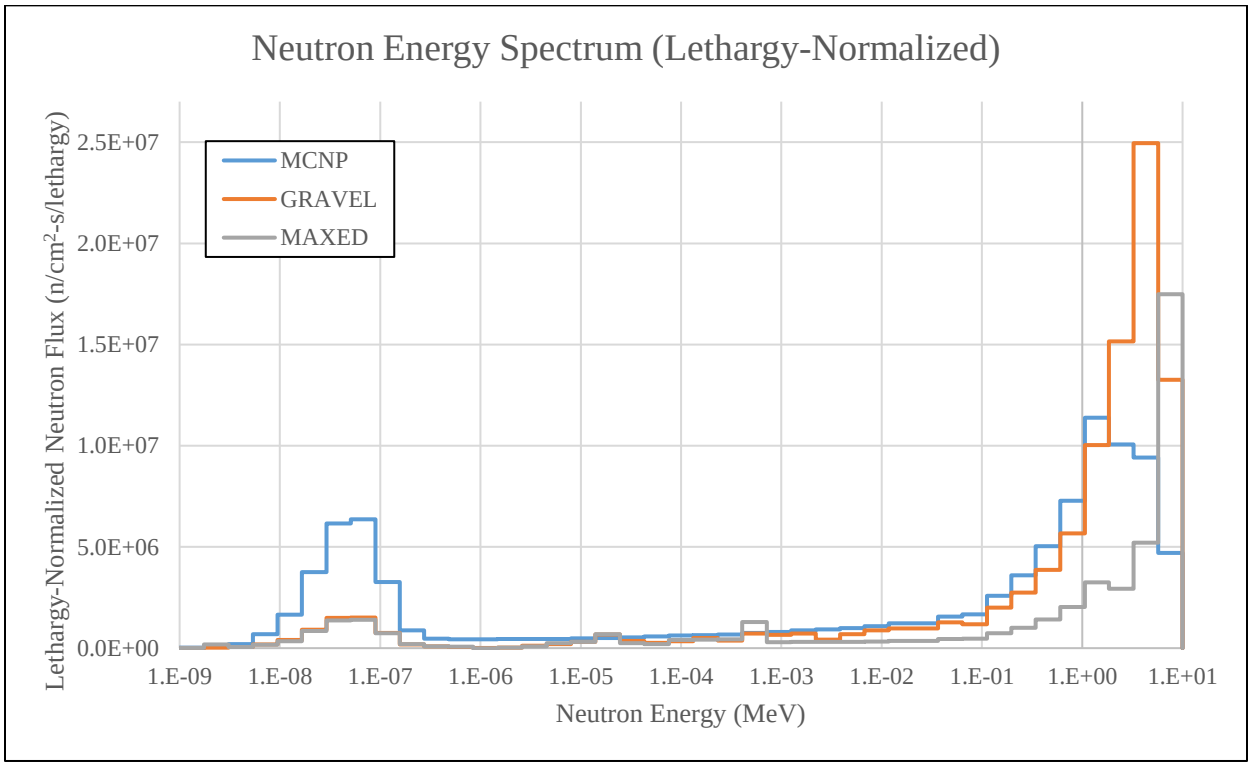

Figure 31. Lethargy-normalized neutron energy spectrum comparison (ERS - bare).

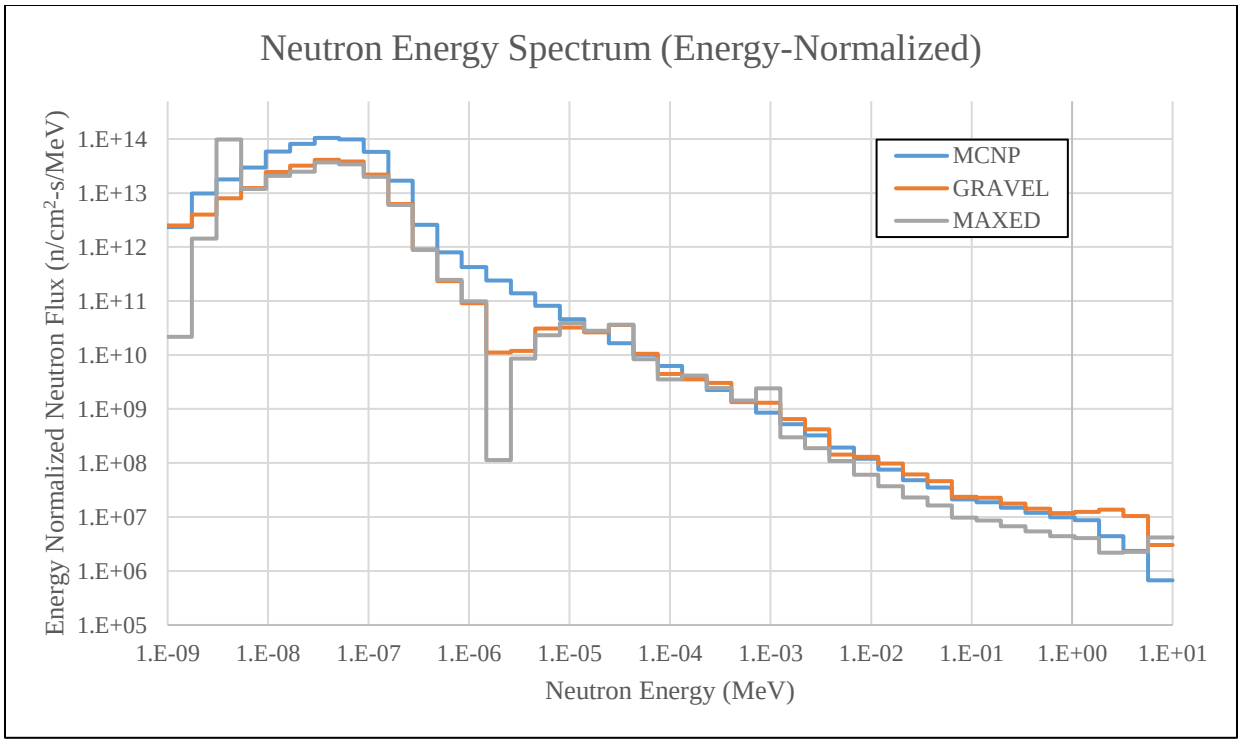

Figure 32. Energy-normalized neutron energy spectrum comparison (ERS - bare).

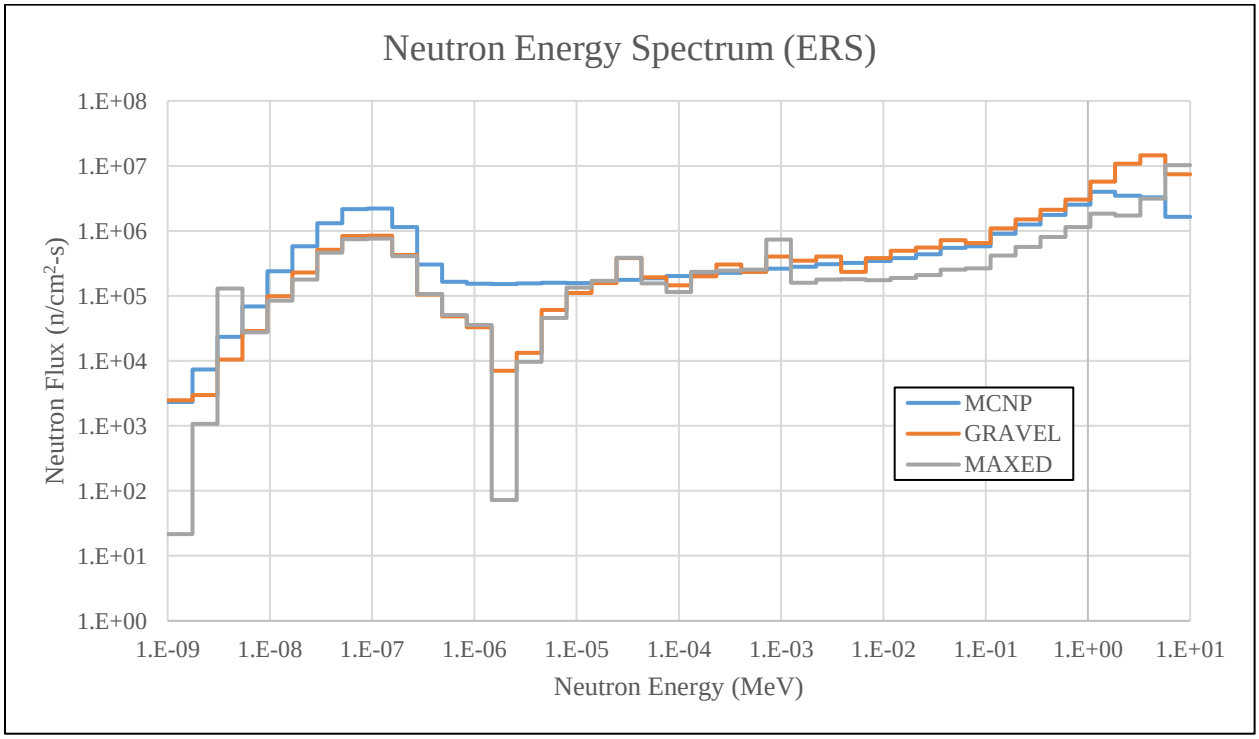

Figure 33. Raw neutron energy spectrum comparison (ERS - bare)

Most of the data in the lethargy-normalized plots cannot be seen due to the scale of the y-axis, for this reason further visual analysis was performed only on Figure 32 and Figure 33. The final chi-square PDF values for the GRAVEL and MAXED data were 1.085 and 1.173, respectively. GRAVEL performed 33 iterations before converging on its solution spectrum. Irregularities in the epithermal region of the unfolded spectra can be seen. There have been other studies performed using the UMG software to create energy spectra based on measured data [50] [51]. Irregularities in the epithermal region can be seen in these studies indicating this type of fluctuation is not uncommon.

4.5.2 Cadmium Covered Foil Results

It was assumed that the anomalies shown in the epithermal region of the GRAVEL and MAXED spectra were the results of insufficient data. A second set of foils were irradiated in the beam, only this time each foil was set inside cadmium casings. The measured responses for these foils can be seen in Table 14. Eleven foils were used, this was based on the foils that performed well in the bare foil analysis (e.g. low uncertainties and high count rates).

Table 14. Measured responses of the cadmium covered multi-foil array.

Foil	Reaction	Response {[n-b/cm^2-s]}	Error @ 2σ
Indium (In)	In-115(n,γ)In-116m	3.719E+08	3%
Manganese-Copper (8.7%Mn-Cu)	Mn-55(n,γ)Mn-56	1.497E+07	3%
Lutetium-Aluminum (5.2%Lu-Al)	Lu-175(n,γ)Lu-176m	4.586E+08	10%
Copper (Cu)	Cu-63(n,γ)Cu-64	6.280E+06	15%
Zinc (Zn)	Zn-64(n,p)Cu-64	2.649E+06	22%
Sodium Chloride (NaCl)	Na-23(n,γ)Na-24	3.175E+05	4%
Tungsten (W)	W-186(n,γ)W-187	1.869E+08	3%
Nickel (Ni)	Ni-58(n,p)Co-58	7.656E+06	4%
	Ni-58(n,2n)Ni-57	--	--
Gold (Au)	Au-197(n,γ)Au-198	4.168E+08	3%
Molybdenum (Mo)	Mo-98(n,γ)Mo-99	7.790E+06	4%
Cobalt (Co)	Co-59(n,γ)Co-60	5.369E+07	9%

An all-inclusive source particle rate term was defined for the MCNP model using the results from the bare and cadmium covered trials. The cadmium covered SPR results can be seen in Table 15 below and the new SPR term for the model is 3.363 x 10^{13} *sp/s*.

Table 15. SPR results from measured data and MCNP (cadmium covered).

Reaction of Interest	MCNP Activity (decays/sp)	Measured Activity (dps)	SPR (sp/s)
In-115(n,γ)In-116m	6.862E-09	2.398E+05	3.554E+13
Mn-55(n,γ)Mn-56	1.203E-10	6.142E+03	5.113E+13
Lu-175(n,γ)Lu-176m	8.505E-10	2.131E+03	2.314E+12
Cu-63(n,γ)Cu-64	5.326E-11	2.446E+03	4.584E+13
Zn-64(n,p)Cu-64	1.668E-11	1.180E+03	7.107E+13
Na-23(n,γ)Na-24	2.565E-11	5.772E+02	2.238E+13
W-186(n,γ)W-187	8.113E-10	1.362E+04	1.718E+13
Ni-58(n,p)Co-58	6.283E-13	5.994E+01	9.573E+13
Au-197(n,γ)Au-198	2.724E-10	1.602E+04	5.829E+13
Mo-98(n,γ)Mo-99	8.130E-12	1.095E+02	1.258E+13
Co-59(n,γ)Co-60	9.281E-14	5.328E+00	5.801E+13
		Average SPR	4.273E+13

The cadmium covered foils' response functions calculated by MCNP can be found in Appendix C. The new data obtained from the cadmium covered foils were added into the existing input files created from the bare foil data and used in UMG. The resulting spectra from MAXED and GRAVEL can be seen in Figure 34 and Figure 35.

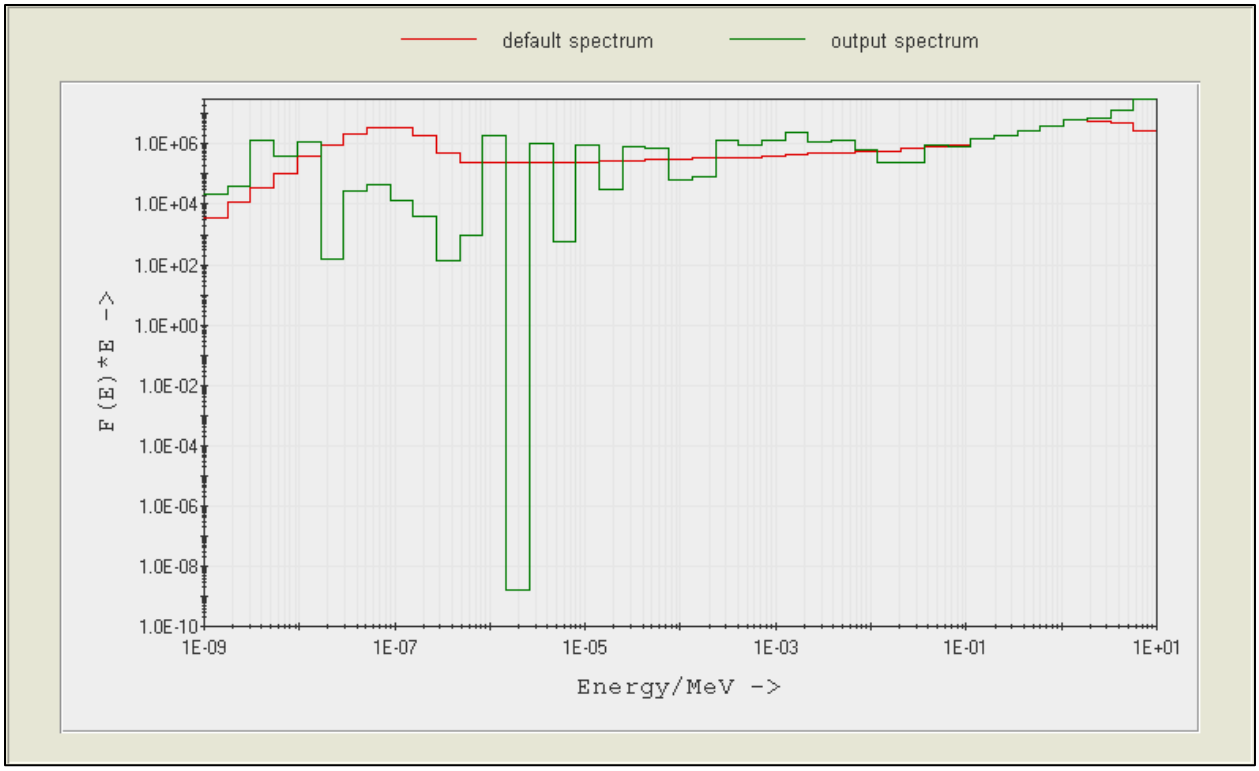

Figure 34. MAXED output spectrum based on cadmium covered and bare foil measurements.

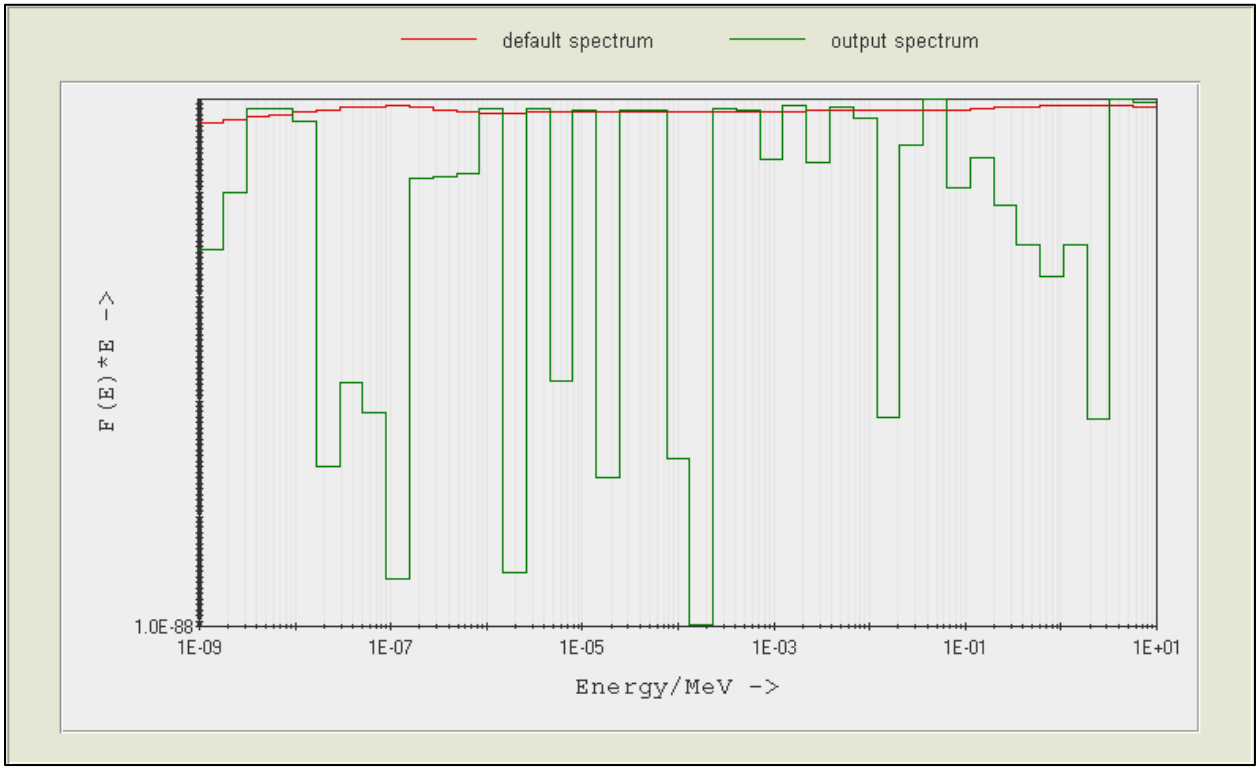

Figure 35. GRAVEL output spectrum based on cadmium covered and bare foil measurements.

The addition of the cadmium covered data added more anomalies to the neutron energy spectrum for both unfolding packages. The large uncertainties in the response functions calculated for the cadmium covered foils is believed to be the main contribution factor to the anomalies in the spectra. The two plots maintained a majority of these irregularities even after excluding the foils with large measurement uncertainties, zinc and copper. It was determined to use the unfolded spectra produced from the bare foil set for the remainder of the analysis. The cadmium covered data was used for comparison methods later on in the study.

The chi-squared values for the MAXED and GRAVEL spectra were compared to each other and the GRAVEL algorithm produced a better fit to the measured data than the MAXED algorithm based on GRAVEL's chi-square being closer to unity. The GRAVEL spectrum was then used to determine the best representation of the actual energy spectrum explained in the following sections.

4.5.3 Sensitivity Analysis of GRAVEL Spectrum

The results to the sensitivity analysis can be found in the table below. It is clear that the uncertainties in the foil responses are not large enough to have a noticeable effect on the chi-square value of the spectrum.

Table 16. Chi-square values of the GRAVEL spectrum as a function of perturbing the foil response.

Reaction	±	Response	Chi-squared
In-115(n,γ)In-116m	+	1.023E+09	1.0873
	-	9.630E+08	1.0869
Mn-55(n,γ)Mn-56	+	7.671E+07	1.0934
	-	7.225E+07	1.0887
Lu-175(n,γ)Lu-176m	+	5.789E+08	1.0990
	-	4.737E+08	1.0971
Cu-63(n,γ)Cu-64	+	2.868E+07	1.0952
	-	2.700E+07	1.0860
Zn-64(n,p)Cu-64	+	2.925E+06	1.0934
	-	2.755E+06	1.0895
Na-23(n,γ)Na-24	+	2.641E+06	1.0877
	-	2.487E+06	1.0882
W-186(n,γ)W-187	+	4.546E+08	1.0871
	-	4.282E+08	1.0996
Ni-58(n,p)Co-58	+	8.323E+06	1.0989
	-	7.839E+06	1.0948
Au-197(n,γ)Au-198	+	6.802E+08	1.0867
	-	6.406E+08	1.0993
Mo-98(n,γ)Mo-99	+	1.006E+07	1.0963
	-	9.471E+06	1.0881
Sc-45(n,γ)Sc-46	+	1.280E+08	1.0975
	-	1.182E+08	1.0969
Co-59(n,γ)Co-60	+	2.326E+08	1.0962
	-	2.104E+08	1.0855
Ti-47(n,p)Sc-47	+	1.705E+06	1.0953
	-	1.543E+06	1.0918

4.5.4 Comparison of MCNP and UMG Energy Spectra

The original MCNP source used for the ERS model and the corresponding neutron energy spectrum tallied at the image plane was used to calculate the attenuation factors for the model. The two spectra can be seen in Figure 36.

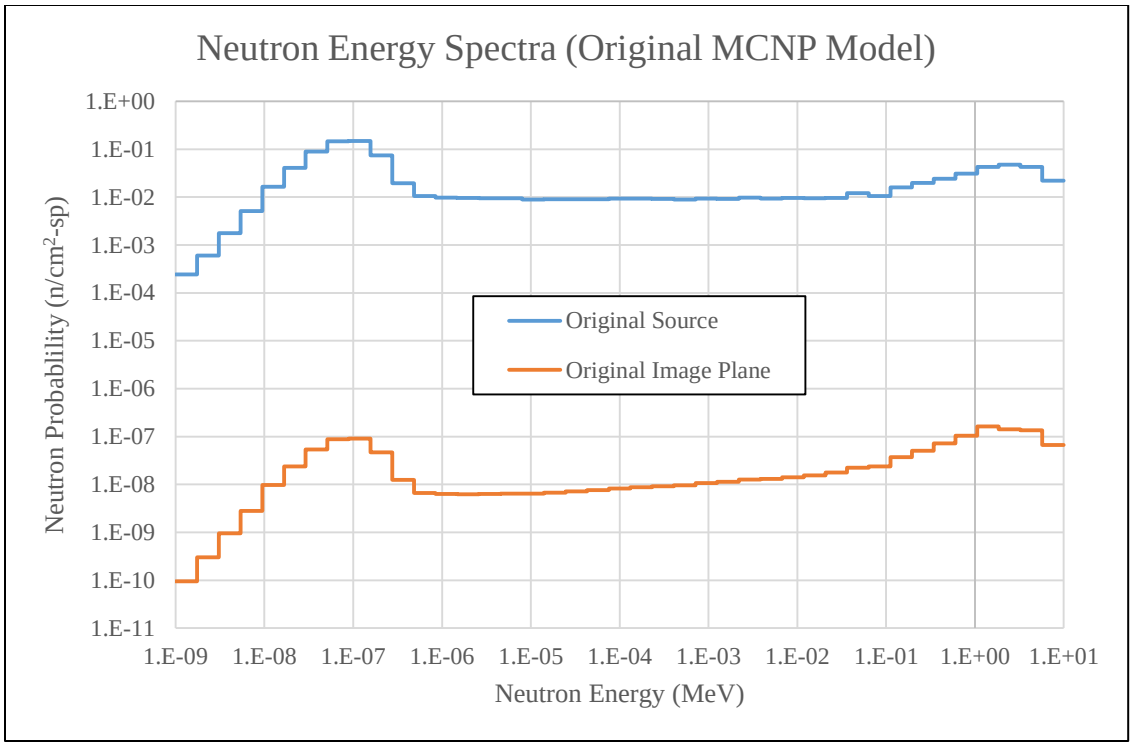

Figure 36. Source vs Image Plane comparison in the original MCNP model.

Figure 36 shows the fast region of the spectrum is attenuated less than the thermal region by the time the neutrons make it down the beamline to the image plane. The attenuation is a result of the material in the aperture and the air in the ERS that scatters a majority of the neutrons that make to the room. The slight differences in attenuation for each energy bin are accounted for by calculating the attenuation factors. These factors are shown in the Table 17 along with the resulting GRAVEL source definition.

Table 17. Attenuation factors and GRAVEL source definitions for the ERS beam line MCNP model.

Energy (Lower Bin Edge)	Attenuation Factor	GRV Source Probabilities	Energy (Lower Bin Edge)	Attenuation Factor	GRV Source Probabilities
1.00E-09	3.95E-07	2.04E-04	1.32E-04	9.42E-07	8.16E-03
1.75E-09	5.05E-07	2.26E-04	2.32E-04	1.01E-06	1.15E-02
3.07E-09	5.46E-07	7.84E-04	4.07E-04	1.08E-06	8.27E-03
5.39E-09	5.51E-07	1.98E-03	7.14E-04	1.16E-06	1.33E-02
9.45E-09	5.96E-07	7.02E-03	1.25E-03	1.24E-06	1.10E-02
1.66E-08	5.80E-07	1.56E-02	2.20E-03	1.30E-06	1.18E-02
2.91E-08	6.04E-07	3.49E-02	3.85E-03	1.41E-06	6.56E-03
5.10E-08	6.05E-07	5.59E-02	6.75E-03	1.47E-06	9.53E-03
8.94E-08	6.13E-07	5.55E-02	1.18E-02	1.64E-06	1.10E-02
1.57E-07	6.24E-07	2.72E-02	2.08E-02	1.86E-06	1.24E-02
2.75E-07	6.41E-07	6.72E-03	3.64E-02	1.84E-06	1.30E-02
4.82E-07	6.39E-07	3.05E-03	6.38E-02	2.27E-06	1.14E-02
8.45E-07	6.50E-07	2.07E-03	1.12E-01	2.34E-06	1.73E-02
1.48E-06	6.53E-07	4.32E-04	1.96E-01	2.59E-06	2.07E-02
2.60E-06	6.75E-07	7.90E-04	3.44E-01	2.97E-06	2.60E-02
4.56E-06	6.89E-07	3.50E-03	6.03E-01	3.35E-06	3.24E-02
7.99E-06	7.17E-07	6.05E-03	1.06E+00	3.84E-06	7.78E-02
1.40E-05	7.52E-07	8.19E-03	1.85E+00	3.01E-06	1.41E-01
2.46E-05	7.92E-07	1.86E-02	3.25E+00	3.17E-06	1.97E-01
4.31E-05	8.40E-07	8.95E-03	5.70E+00	3.03E-06	9.57E-02
7.55E-05	8.90E-07	6.32E-03	1.00E+01	3.19E-06	2.22E-02

After analyzing the foil responses determined by the MCNP model and the GRAVEL software, it becomes clear that a combined spectrum must be built that better represents the realistic parts of the solution spectra and correct for the irregularities shown. The Hybrid spectrum, which will be the name used for this combined spectrum, will be comprised of GRAVEL's thermal and fast regions and the original MCNP model's epithermal region. The thermal and fast regions of GRAVEL's neutron energy spectrum show clear shifts with minimal anomalies and GRAVEL's epithermal region shows nonphysical fluctuations. The derivation of the source definition for the Hybrid spectrum can be seen in Figure 37.

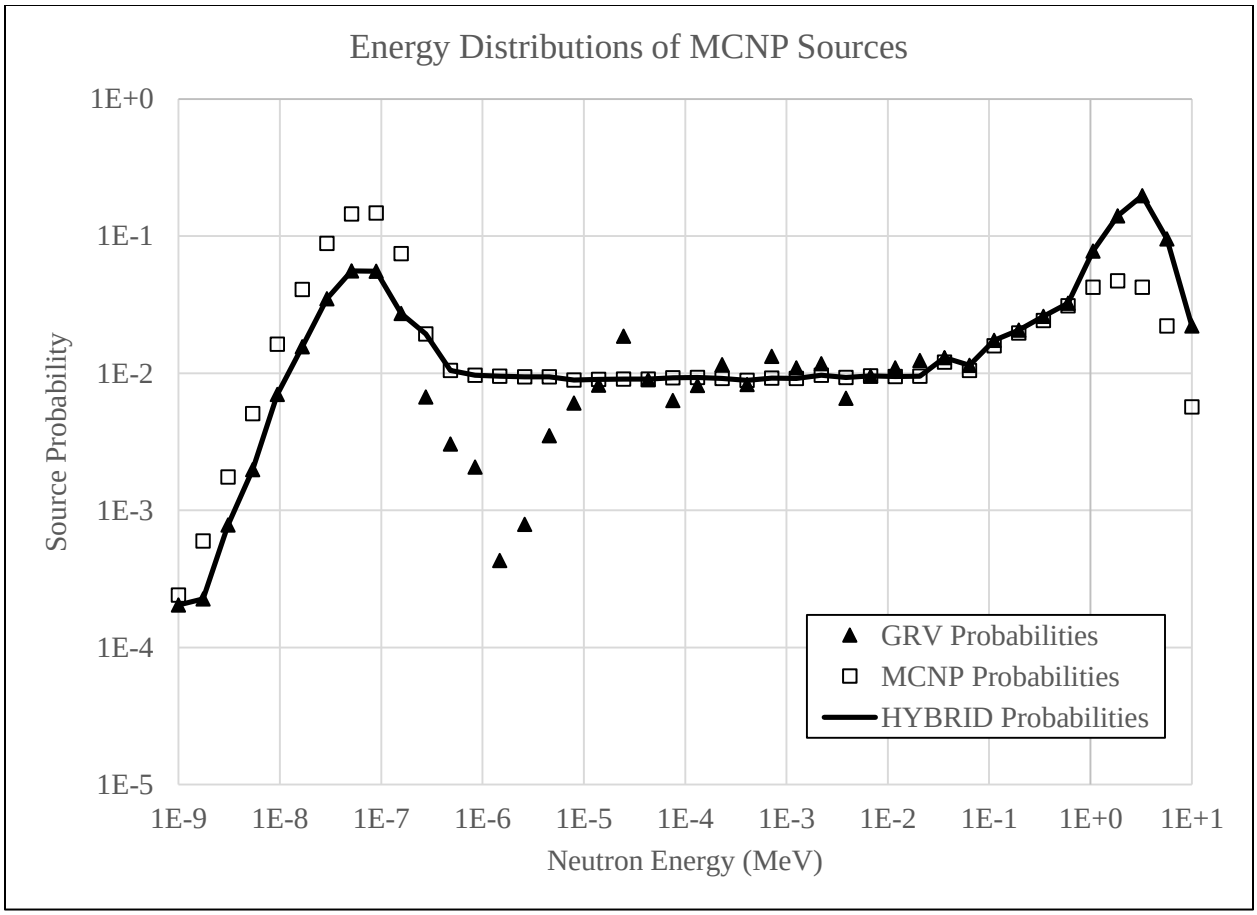

Figure 37. Visual derivation of the source definition for the hybrid spectrum.

The ERS MCNP6 model was simulated using the GRAVEL and Hybrid sources. There were three possible solution spectra at the ERS image plan: the original MCNP spectrum, the GRAVEL spectrum, and the Hybrid spectrum. Source particle rate terms were calculated for the GRAVEL and Hybrid spectra using the same process described for the original MCNP spectrum and these values can be found in Appendix E-1 and Appendix E-2. The resulting activities from the three spectra were compared to the measured activities of the bare and cadmium covered foils. A visual representation of how well the simulations match the measured data is shown in the Figure 38. The tabulated values for Figure 38 can found in Appendix E-3. Table 18 shows a numerical comparison of the data, the ratios closest to unity represent the best match to measured data.

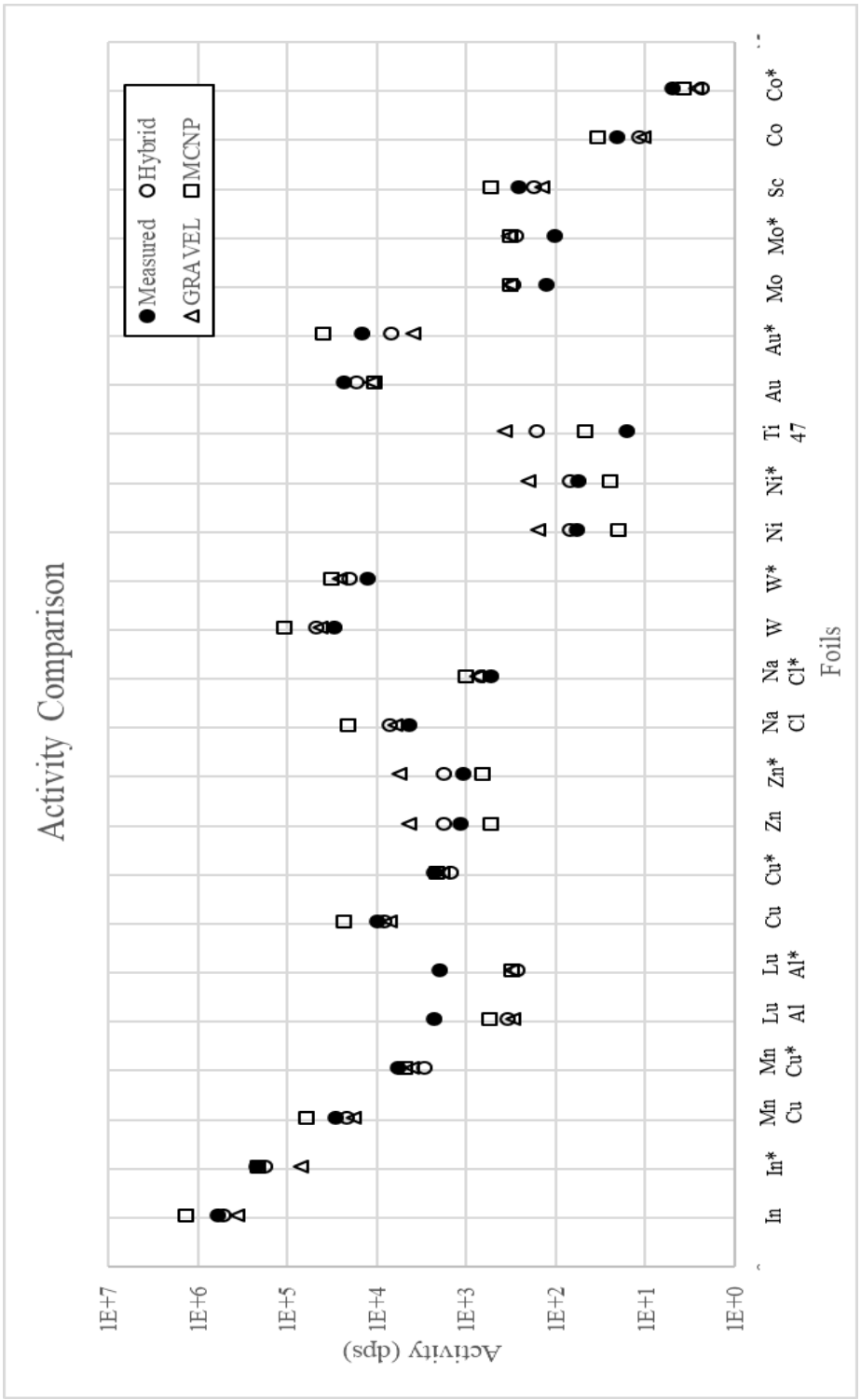

Figure 38. Activity comparison between three simulated spectrum and measured data.

Table 18. Ratio of measured data to GRAVEL and Hybrid spectra for the bare foil set.

Reaction	Ratio (Measured/ Hybrid)	Ratio (Measured/ GRAVEL)	Ratio (Measured/ MCNP)
In-115(n,γ)In-116m	1.13	1.64	0.44
Mn-55(n,γ)Mn-56	1.32	1.55	0.46
Lu-175(n,γ)Lu-176m	6.66	7.51	4.18
Cu-63(n,γ)Cu-64	1.19	1.40	0.44
Zn-64(n,p)Cu-64	0.65	0.27	2.23
Na-23(n,γ)Na-24	0.60	0.70	0.20
W-186(n,γ)W-187	0.64	0.70	0.27
Ni-58(n,p)Co-58	0.85	0.37	2.99
Ti-47(n,p)Sc-47	0.10	0.04	0.34
Au-197(n,γ)Au-198	1.38	2.04	0.59
Mo-98(n,γ)Mo-99	0.42	0.40	0.39
Sc-45(n,γ)Sc-46	1.45	1.81	0.48
Co-59(n,γ)Co-60	1.74	1.98	0.60
In-115(n,γ)In-116m*	1.24	3.21	1.04
Mn-55(n,γ)Mn-56*	1.93	1.39	1.52
Lu-175(n,γ)Lu-176m*	7.24	6.47	6.32
Cu-63(n,γ)Cu-64*	1.50	1.21	1.37
Zn-64(n,p)Cu-64*	0.60	0.19	2.11
Na-23(n,γ)Na-24*	0.78	0.71	0.67
W-186(n,γ)W-187*	0.64	0.48	0.50
Ni-58(n,p)Co-58*	0.81	0.27	2.84
Au-197(n,γ)Au-198*	2.18	3.77	1.75
Mo-98(n,γ)Mo-99*	0.36	0.30	0.40
Co-59(n,γ)Co-60*	2.10	1.81	1.71
# of Points Closest to Unity	**12**	**4**	**7**

It can be seen from Figure 38 and Table 18 that the Hybrid spectrum does predict the activities of the multi-foil array with a higher precision than the GRAVEL or original MCNP spectra. The last row in Table 18 is a quantitative measurement of how precise the simulations were compared to the measured data with the most accurate value being closest to 1. The Hybrid spectrum matched the closest for over half of the activities calculated. The Hybrid simulation was chosen as the best

representation of the neutron energy spectrum at the image plane when compared to the two other spectra. The chosen energy spectrum is shown in Figure 39 and Figure 40 plotted with an energy-normalized distribution and the raw neutron flux for each energy bin. The corresponding values for the spectrum can be found in Appendix E-4.

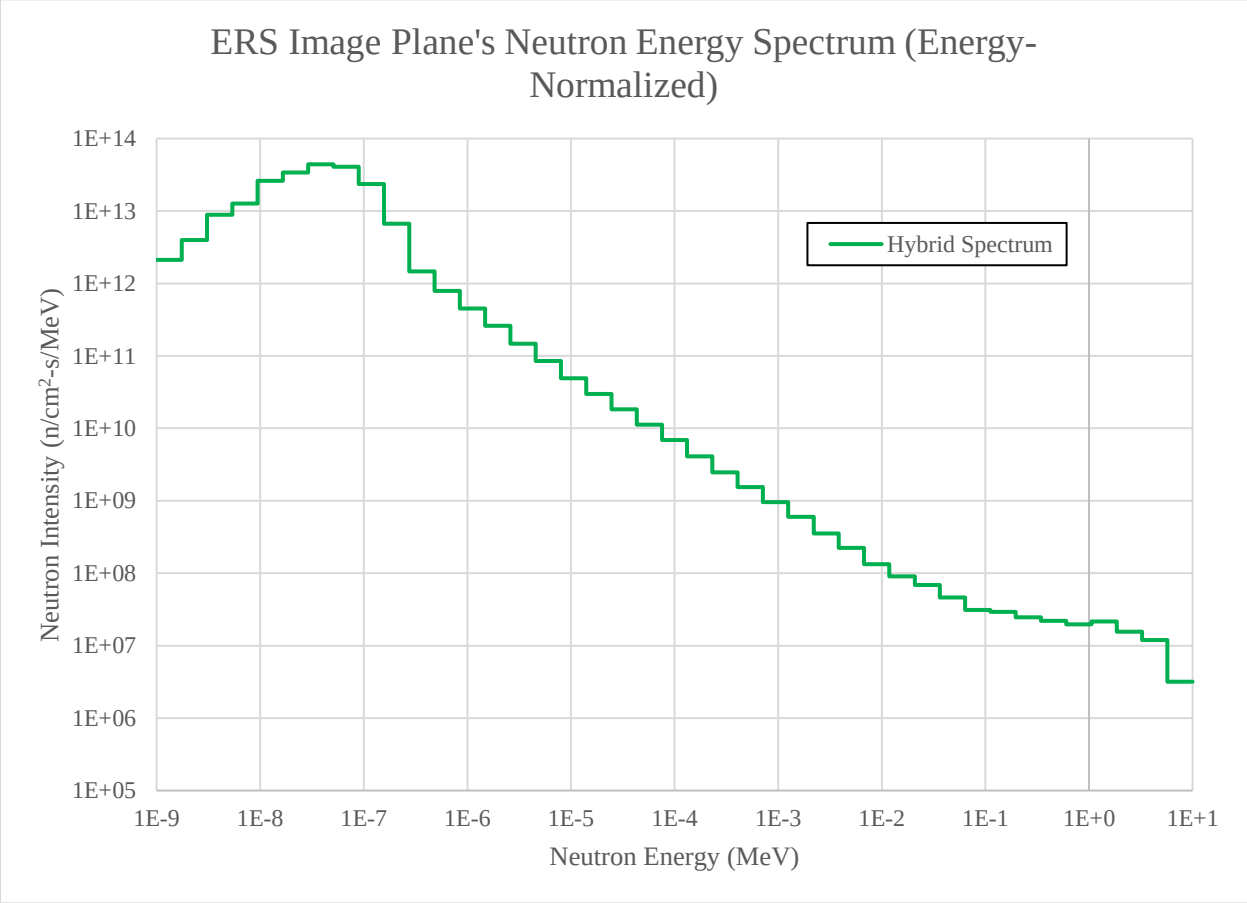

Figure 39. Neutron energy spectrum at the image plane of the ERS facility (energy-normalized).

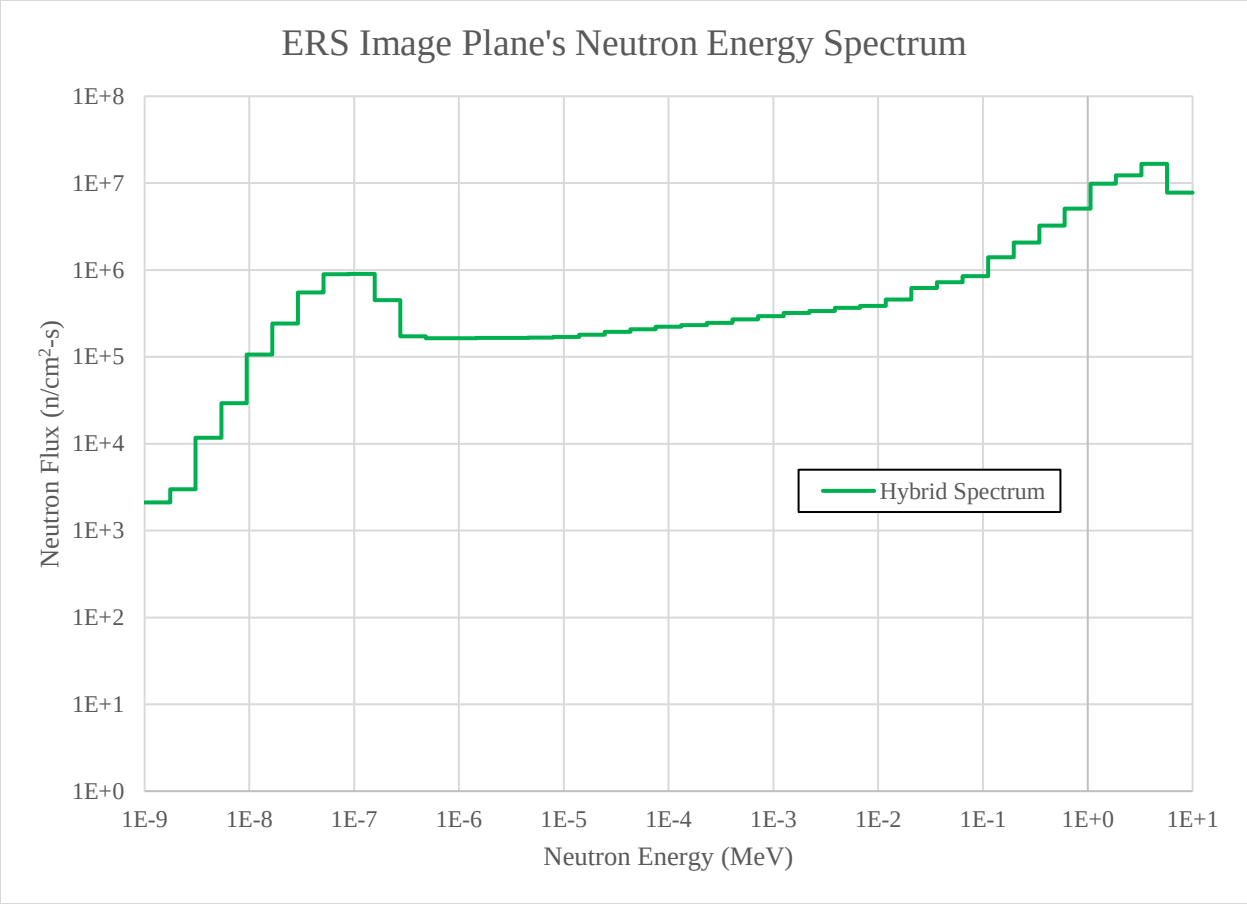

Figure 40. Neutron energy spectrum at the image plane of the ERS facility (raw neutron flux).

5 Summary and Conclusions

The neutron radiography capabilities at NRAD are very unique and in high demand. Used nuclear fuel is difficult to take neutron images of due to the density of the material and the high doses of gamma and neutron radiation being emitted. With the recent restart of the Transient Test Reactor (TREAT) at the Idaho National Laboratory, there will be an increase need for the abilities of the NRAD facility. It is essential that the neutron beams of the ERS and NRS are characterized to provide sufficient data to users of the facilities. The following characteristics were measured: Neutron flux, neutron beam profile, the cadmium ratio, image quality of the facility and the neutron energy spectrum. Two other neutron beam characteristics were studied and set up for future analysis: L/D ratio and the gamma energy spectrum.

The thermal neutron flux at the in the east radiography station was measured using a large array of gold foils spread across the entire area of the image plane. The flux was determined to be $9.61 \times 10^6 \pm 2.47 \times 10^5$ *n/cm*^{2}*-s*, which is 58% higher than the previous characterization performed in 2015. The increase in flux is due to the banking rods allowing more neutrons to make it to the image plane and not be absorbed by the material in the control rods. The beam profile was measured and defined as uniform across the image plane and the cadmium ratio using the gold foils was 2.05 ± 2.9%. The cadmium ratio indicated that the ERS neutron beam has a large epi-thermal and fast neutron component which is highly desired for nuclear fuel imaging capabilities. The image quality of the ERS was also measured using beam purity and sensitivity indicators. The facility was determined to fall into Category I which is the highest rank a neutron imaging station can have according to ASTM standards.

An MCNP model was created for the ERS facility to assist in determining the neutron energy spectrum at the image plane. The spectrum unfolding with MAXED and GRAVEL software was

used to calculate the energy spectrum based on measured responses of 18 different foils and the MCNP calculated data. The initial neutron energy spectrum was calculated in MCNP as well as the response function for each foil used in the measurements. The "best fit" solution spectrum produced by UMG was the GRAVEL spectrum which showed a chi-squared, "goodness of fit", to be 1.085 which was closer to unity than the MAXED spectrum could produce. Although the GRAVEL spectrum showed a better fit than MAXED, nonphysical anomalies were produced in the epithermal region. These irregularities were a result of the unfolding software. A hybrid spectrum was created in order to keep the real physical changes GRAVEL calculated but excluded the nonphysical anomalies. The Hybrid spectrum was built using the original MCNP spectrum's epithermal region and the GRAVEL spectrum's thermal and fast regions.

Source definitions were created for the GRAVEL and Hybrid spectra and subsequently simulated in the MCNP model of the ERS. Activities of the foils used in the measurements were predicted by the GRAVEL, Hybrid and original MCNP spectra and compared to the measured activities. The Hybrid spectrum was shown to produce the most accurate results compared to the other two spectra. It was concluded that the Hybrid spectrum will represent the neutron energy spectrum at the image plane in the east radiography station for the reactors most recent configuration.

6 Future Work

The gamma energy spectrum can provide important data that would assist in safely implementing future beam upgrades (i.e. CCD imaging systems). Shielding analysis has already been performed for the HPGe detector and an MCNP model has been built to give an estimate of the gamma energy spectrum expected in the beam. This work can be found in Appendix G.

The L/D ratio was the other characteristic not measured in the allotted time the project was given. Future work would involve analyzing the images of the wedges and determining if this is an appropriate method to measure the characteristic.

Improvements can also be made to the neutron energy spectrum. It was concluded in the previous section that the Hybrid spectrum produced the closest activities the ones measured but it did not match all of them which would be the ideal case when using this spectrum for modeling purposes. Some improvements that could be made involve selecting better foils to encompass the entire energy spectrum and irradiate foils closer to the aperture to compare those measured results to tallies taken closer to the reactor core. Another improvement would be using dosimetry cross-sections libraries when calculating activities in MCNP. These libraries have shown to give more accurate data than the standard libraries (i.e. ENDF/B-VIII or ENDF/B-VII).

The north beam ran into complications early in its reactivation process and was not included in this characterization effort. Characterization of the NRS should be done following the same procedures implemented in the ERS effort.

7 References

[1] S. W. Morgan, J. C. King and C. L. Pope, "Beam Characterization at the Neutron Radiography Reactor," *Nuclear Engineering and Design,* pp. 639-653, 2013.

[2] J. D. Bess, J. B. Briggs and R. M. Lell, "Neutron Radiography (NRAD) Reactor 64-Element Core Upgrade," Idaho National Laboratory , Idaho Falls, 2014.

[3] A. E. Craft, D. M. Wachs, M. A. Okuniewski, D. L. Chichester, W. J. Williams, G. C. Papaionannou and A. T. Smolinski, "Neutron Radiography of Irradiated Nuclear Fuel at Idaho National Laboratory," *Physics Procedia,* no. 69, pp. 483-490, 2015.

[4] G. R. Imel and T. Urbatsch, "Beam Characterization at the Neutron Radiography Facility (NRAD)," in *Fourth World Conference on Neutron Radiography*, Idaho Falls, 1992.

[5] H. Berger, "Neutron Radiography," *Annual Review of Nuclear Science,* no. 21, pp. 335-364, 1971.

[6] H. Berger and F. Iddings, "Neutron Radiography: A State-of-the-Art Report," Nondestructive Testing Information Analysis Center, Austin, 1998.

[7] ASTM International, "Standard Test Method for Determining the L/D Ratio of Neutron Radiography Beams," ASTM International, West Conshohocken, PA, 2008.

[8] B. Schillinger, "Estimation and Measurement of L/D on a Cold and Thermal Neutron Guide," *Nondestructive Testing Evaluation,* vol. 16, pp. 141-150, 2001.

[9] G. F. Knoll, Radiation Detection and Measurement, Hoboken: John Wiley & Sons, Inc., 2010.

[10] A. E. Craft, B. A. Hilton and G. C. Papaioannou, "Characterization of a Neutron Beam Following Reconfiguration of the Neutron Radiography Reactor (NRAD) Core and Addition of New Fuel Elements," *Nuclear Engineering Technology,* vol. 48, pp. 200-210, 2016.

[11] ASTM International, "Standard Test Method for Determining Thermal Neutron Reaction Rates and Thermal Neutron Fluence Rates by Radioactivation Techniques," ASTM International, West Conshohocken, PA, 2008.

[12] H. Kobayashi and R. H. Plaut, "Beam Formation and Characterization for Neutron Radiography," *Nondestructive Testing and Evaluation,* vol. 16, pp. 121-129, 2001.

[13] M. Shukla, S. S. Desai and T. Roy, "Neutron spatial flux profile measurement in compact subcritical system using miniature neutron detectors," *Nuclear Instruments and Methods in Physics Research A,* vol. 772, pp. 118-123, 2014.

[14] Korea Atomic Energy Research Institute, "Nuclear Data Center at KAERI," KAERI, [Online]. Available: http://atom.kaeri.re.kr/. [Accessed 20 September 2017].

[15] ASTM International, "Standard Test Method for Determining Image Quality in Direct Thermal Neutron Radiographic Examination," ASTM International, West Conshohocken, PA, 2010.

[16] J. K. Nimmagadda, "Analysis of Fast Reactor Filter Spectra in the Advanced Test Reactor and Neutron Spectral Measurement at Idaho Accelerator Center," Idaho State University, Pocatello, 2012.

[17] M. D. Horkely, "Neutron Spectral Measurements and Calculation Comparisons of Idaho State University ANG-201 Reactor," Idaho State University, Pocatello, 2013.

[18] S. Aghara, "Characterization and quantification of an in-core neutron irradiation facility at TRIGA II research reactor," *Nuclear Instruments and Methods in Physics Research,* vol. B, no. 248, pp. 181-190, 2006.

[19] H. Mazrou, T.Seguini and A. Nedjar, "Neutron Spectrum Measurements at a Radial Beam Port of the NUR Research Reactor using a Bonner Sphere Spectrometer," *Applied Radiation Isotopes,* 2016.

[20] H. Friedrich, V. Wagner and P. Wille, "A High Performance Neutron Velocity Selector," *Physica B,* no. 156 & 157, pp. 547-549, 1989.

[21] H. Friedrich, V. Wagner and P. Wille, "Performance of a High-Tech Neutron Velocity Selector," *Physica B,* no. 180 & 181, pp. 938-940, 1992.

[22] E. Mamontov, "Wide-angle Mechanical Velocity Selection for Scattered Neutrons in Inelastic Neutron Spectrometers," *Nuclear Instrumentation and Methods in Physics,* vol. A, pp. 83-91, 2014.

[23] T. Blosser and J. G.E. Thomas, "Neutron Flux and Neutron and Gamma-Ray Spectra Measurements at the HFIR," Oak Ridge National Laboratory , Oak Ridge, 1968.

[24] R. Arlt, V. Ivanov and K. Parnham, "Advantages and Use of CdZnTe Detectors in Safeguards Measurements," International Atomic Energy Agency, Vienna, 2015.

[25] W. Verbakel and F. Stecher-Rasmussen, "Determination of gamma-ray component of a neutron beam medical irradiation applications at the HFR in Petten," *Nuclear Instruments & Methods in Physics Research,* vol. A, no. 451, pp. 676-684, 2000.

[26] E. M. Baum, M. C. Ernesti, H. D. Knox, T. R. Miller and A. M. Watson, Nuclides and Isotopes: Chart of the Nuclides, Niskayuna, New York: Bechtel Marine Propulsion Corporation, 2009.

[27] A. Konefal, "ResearchGate," December 2014. [Online]. Available: https://www.researchgate.net/publication/269990703_InTech-Undesirable_radioisotopes_induced_by_therapeutic_beams_from_medical_linear_accelerators?enrichId=rgreq-f565356cf1166e66b5f813bc6effbe09-XXX&enrichSource=Y292ZXJQYWdlOzI2OTk5MDcwMztBUzoxNzgzOTU5MDg0. [Accessed 6 October 2017].

[28] N. R. Larson and B. J. Storms, Interviewees, *Email Correspondence.* [Interview]. 19 September 2017.

[29] J. R. Lamarsh and A. J. Baratta, Introduction to Nuclear Engineering, Upper Saddle River, New Jersey: Prentice Hall, 2001.

[30] R. Flemming, "Neutron Self-shielding Factors for Simple Geometries," *Applied Radiation Isotopes,* vol. 33, pp. 1263-1268, 1982.

[31] Reactor Experiments, Inc., Activation Foil Manual, Sunnyvale, CA: Reactor Experiments, Inc., 1965.

[32] I. Auterinen, T. Seren, K. Anttila, A. Kosunen and S. Salvolainen, "Measurement of free beam neutron spectra at eight BNCT facilities worldwide," *Applied Radiation and Isotopes,* vol. 61, pp. 1021-1026, 2004.

[33] ASTM International, "Standard Guide for Selection and Use of Neutron Sensors for Determining Neutron Spectra Employed in Radiation-Hardness Testing of Electronics," ASTM International, West Conshohocken.

[34] J. K. Shultis and R. E. Faw, Radiation Shielding, La Grange Park: American Nuclear Society, 2000.

[35] M. Reginatto, P. Goldhagen and S. Neumann, "Spectrum unfolding, sensitivty analysis and propagation of uncertainties with the maximum entropy deconvolution code MAXED," *Nuclear Intruments & Methods in Physics Research,* pp. 242-246, 2002.

[36] M. Regenatto, "Overview of spectral unfolding techniques and uncertainty estimation," *Radiation Measurements,* pp. 1323-1329, 2010.

[37] E. T. Jaynes, "Information Theory and Statistical Mechanics," *The Physical Review,* pp. 620-630, 1957.

[38] M. Reginatto and P. Goldhagen, "MAXED, A Computer Code for the Deconvolution of Multisphere Neutron Spectrometer Data Using the Maximum Entropy Method," Environmental Measurements Laboratory (Department of Energy), New York, 1998.

[39] M. Reginatto, "The "few-channel" unfolding programs in the UMG package: MXD_FC33, GRV_FC33 and IQU_FC33," Physikalisch-Technische Bundesanstalt (PTB), Braunshweig, 2004.

[40] R. Stiltskin, "Physics 133 Lab Manual," University of California Santa Cruz, Santa Cruz, 2015.

[41] X.-5. M. C. Team, "MCNP - A General Monte Carlo N-Particle Transport Code, Version 5," Los Alamos National Laboratory, Los Alamos, 2008.

[42] E. E. Lewis and J. W. F. Miller, Computational Methods of Neutron Transport, La Grange Park: American Nuclear Society , 1993.

[43] I. Shaaban and M. Albarhoum, "Design Calculation of na Epithermal Neutronic Beam for BNCT at the Syrian MNSR using the MCNP4C Code," *Progress in Nuclear Energy,* vol. 78, pp. 297-302, 2015.

[44] I. Kondo and K. Sakurai, "Experimental Evaluation of Reactor Neutron Spectrum in Irradiation Field," *Journal of Nuclear Science and Technology,* vol. 18, no. 6, pp. 461-472, 1981.

[45] V. Radulovic, Z. Stancar, L. Snoj and A. Trkov, "Validation of absolute axial neutron flux distribution calculations with MCNP with Au-197(n,gamma)Au-198 reaction rate distribution measurements at the JSI Mark II Reactor," *Applied Radiation and Isotopes,* vol. 84, pp. 57-65, 2014.

[46] J. D. Bess, "Neutron Radiography (NRAD) Reactor 64-Element Core Upgrade," Idaho National Laboratory, Idaho Falls, 2014.

[47] J. L. Conlin, D. K. Parsons, S. J. Gardiner, M. G. Gray, A. C. K. III, M. C. White and M. B. Lee, "Listing of Available ACE Data Tables," Los Alamos National Laboratory, Los Alamos, 2014.

[48] US Ink, "How Does a Densitometer Work?," Sun Chemical Corporation, [Online]. Available: http://www.sunchemical.com/product/technical-library/. [Accessed 29 September 2017].

[49] Los Alamos National Laboratory, "MCNP6 User's Manual," Los Alamos National Laboratory, Los Alamos, 2013.

[50] H. Mazrou, A. Nedjar and T. Seguini, "Neutron Spectrum Measurements at a radial beam port of the NUR research reactor using a Bonner speres spectrometer," *Applied Radiation and Isotopes,* vol. 114, pp. 63-70, 2016.

[51] M. R. Halstead, S. Lee, J. Petrosky, A. Bickley and P. Sokol, "Neutron energy spectrum characterization of TMR-1 at the Idiana University neutron source," *Physics Procedia*, vol. 26, pp. 188-195, 2012.

[52] E. Seabury, C. D. V. Siclen, J. McCabe, C. Wharton and A. Caffrey, "Neutron Damage iin Mechanically-Cooled High Purity Germanium Detectors for Field-Portable Prompt Gamma Neutron Activation Analysis Systems," IEEE, Idaho Falls, 2013.

[53] Ortec, "Integrated Cryocooling System," Ametek, Oak Ridge.

[54] B. Reynolds, Interviewee, *Ortec Northwest Account Manager.* [Interview]. 22 October 2017.

[55] Nuclear-Power, "Nuclear Power," WordPress, 2017. [Online]. Available: http://www.nuclear-power.net/glossary/boron-10/. [Accessed 20 October 2017].

[56] Bladewerx, "Shieldwerx," Bladewerx LLC, 2015. [Online]. Available: http://www.shieldwerx.com/. [Accessed 2017].

[57] ORTEC, "AN34 Experiments in Nuclear Science Laboratory Manual (4th Edition)," AMETEK Advanced Measurement Technology, Oak Ridge.

[58] V. Borrel, B. Kandel, F. Albernhe, P. Frabel, B. Cordier, G. Tauzin, S. Crespin, R. Coszach, J. Denis and P. Leleux, "Fast neutron-induced damage in INTEGRAL n-type HPGe detectors," *Nuclear Instruments & Methods in Physics Research,* vol. A, no. 430, pp. 348-362, 1999.

[59] M. Matzke, Unfolding of Pulse Height Spectra: The HEPRO Program System, Braunschweig: Physikalisch Technische Bundesanstalt, 1994.

[60] L. Snoh and M. Ravnik, "Calculation of Power Denisty with MCNP in TRIGA reactor," in *Nuclear Energy for New Europe* , Portoroz, Slovenia, 2006.

8 Appendices

Appendix A: Self-shielding and Scattering Correction Factors

Foil	MCNP Flux [φ] (n/cm^2-sp)	MCNP Reaction Rate [σ_a*φ] (n-b/cm^2-sp)	MCNP Reaction Rate [σ_t*φ] (n-b/cm^2-sp)	Σ_t (cm^{-1})	Σ_a (cm^{-1})	Σ_s (cm^{-1})	x (cm)	f_s
In-1	1.330E-06	6.164E-05	6.850E-05	2.066	1.858	0.207	0.0127	0.9883
Mn-Cu	1.351E-06	3.869E-06	1.991E-05	1.008	0.196	0.812	0.0051	0.9995
Fe-1	--	--	--	--	--	--	--	--
	1.376E-06	7.352E-07	9.496E-06	0.590	0.046	0.545	0.0127	0.9997
Lu-Al	1.372E-06	4.546E-05	5.714E-05	0.018	0.014	0.004	0.0102	0.9999
In-2	1.330E-06	6.164E-05	6.850E-05	2.066	1.858	0.207	0.0127	0.9883
Cu-1	--	--	--	--	--	--	--	--
	--	--	--	--	--	--	--	--
Cu-2	1.345E-06	1.112E-06	9.156E-06	0.392	0.048	0.344	0.0127	0.9997
Zn	1.362E-06	3.671E-07	7.548E-06	0.184	0.009	0.175	0.0254	0.9999
NaCl-1	1.365E-06	1.466E-07	6.777E-06	0.101	0.002	0.099	0.1905	0.9998
Al	1.373E-06	6.994E-08	3.724E-06	0.158	0.003	0.155	0.0127	1.0000
Mg	1.378E-06	2.397E-08	5.678E-06	0.164	0.001	0.163	0.0127	1.0000
W	1.377E-06	7.968E-06	2.528E-05	0.330	0.104	0.226	0.0127	0.9993
Ni	1.353E-06	1.295E-06	1.469E-05	0.660	0.058	0.602	0.0254	0.9993
	--	--	--	--	--	--	--	--
Ti	1.365E-06	1.722E-06	9.768E-06	0.029	0.005	0.024	0.0254	0.9999
V	--	--	--	--	--	--	--	--
Au	1.366E-06	3.405E-05	4.661E-05	2.005	1.465	0.540	0.0051	0.9963
Mo	1.384E-06	1.064E-06	1.056E-05	0.111	0.011	0.100	0.0076	1.0000
Zr	--	--	--	--	--	--	--	--
Fe-2	--	--	--	--	--	--	--	--
Sc	1.374E-06	7.649E-06	2.235E-05	0.662	0.227	0.436	0.0127	0.9986
Co	1.367E-06	1.100E-05	2.741E-05	2.061	0.827	1.234	0.0051	0.9979
NaCl	1.379E-06	4.546E-06	1.219E-05	0.097	0.036	0.061	0.1905	0.9966
S	1.367E-06	2.254E-07	3.119E-06	0.030	0.002	0.028	0.4737	0.9995

Appendix B: UMG input files

Appendix B-1. The default spectrum input file (defaultSpecF.flu)

```
MCNP6 Calculated Neutron Energy Spectrum for ERS (SPR Cd+B)
2           1
2          42          42   1.001E+01
1.000E-09   3.195E+03   0.000E+00       1
1.750E-09   1.013E+04   0.000E+00       2
3.070E-09   3.218E+04   0.000E+00       3
5.390E-09   9.409E+04   0.000E+00       4
9.450E-09   3.274E+05   0.000E+00       5
1.660E-08   7.963E+05   0.000E+00       6
2.910E-08   1.796E+06   0.000E+00       7
5.100E-08   2.950E+06   0.000E+00       8
8.940E-08   3.045E+06   0.000E+00       9
1.570E-07   1.568E+06   0.000E+00      10
2.750E-07   4.181E+05   0.000E+00      11
4.820E-07   2.247E+05   0.000E+00      12
8.450E-07   2.117E+05   0.000E+00      13
1.480E-06   2.092E+05   0.000E+00      14
2.600E-06   2.142E+05   0.000E+00      15
4.560E-06   2.176E+05   0.000E+00      16
7.990E-06   2.152E+05   0.000E+00      17
1.400E-05   2.280E+05   0.000E+00      18
2.460E-05   2.409E+05   0.000E+00      19
4.310E-05   2.560E+05   0.000E+00      20
7.550E-05   2.768E+05   0.000E+00      21
1.320E-04   2.947E+05   0.000E+00      22
2.320E-04   3.104E+05   0.000E+00      23
4.070E-04   3.239E+05   0.000E+00      24
7.140E-04   3.598E+05   0.000E+00      25
1.250E-03   3.839E+05   0.000E+00      26
2.200E-03   4.226E+05   0.000E+00      27
3.850E-03   4.392E+05   0.000E+00      28
6.750E-03   4.731E+05   0.000E+00      29
1.180E-02   5.198E+05   0.000E+00      30
2.080E-02   5.961E+05   0.000E+00      31
3.640E-02   7.471E+05   0.000E+00      32
6.380E-02   7.990E+05   0.000E+00      33
1.120E-01   1.243E+06   0.000E+00      34
1.960E-01   1.713E+06   0.000E+00      35
3.440E-01   2.419E+06   0.000E+00      36
6.030E-01   3.487E+06   0.000E+00      37
1.060E+00   5.475E+06   0.000E+00      38
1.850E+00   4.779E+06   0.000E+00      39
3.250E+00   4.526E+06   0.000E+00      40
5.700E+00   2.255E+06   0.000E+00      41
1.000E+01   6.093E+05   0.000E+00      42
```

Appendix B-2. Response function input file (RFdata_bareF.fmt)

```
Energy Bins and Cross Sections for the ERS Beam MCNP Model. Sam H. Giegel
Cross Sections derived from MCNP6 (1-23-2018)
       42  1
1.000E-09 1.750E-09 3.070E-09 5.390E-09 9.450E-09 1.660E-08 2.910E-08 5.100E-08
8.940E-08 1.570E-07 2.750E-07 4.820E-07 8.450E-07 1.480E-06 2.600E-06 4.560E-06
7.990E-06 1.400E-05 2.460E-05 4.310E-05 7.550E-05 1.320E-04 2.320E-04 4.070E-04
7.140E-04 1.250E-03 2.200E-03 3.850E-03 6.750E-03 1.180E-02 2.080E-02 3.640E-02
6.380E-02 1.120E-01 1.960E-01 3.440E-01 6.030E-01 1.060E+00 1.850E+00 3.250E+00
5.700E+00 1.000E+01
        0
       13
In NG TI  In   n,g  Th&Int
1.000E+00      cm^2         0         0    3    1    1    0
6.781E+02 5.681E+02 5.983E+02 4.412E+02 3.289E+02 2.698E+02 2.108E+02 1.625E+02
1.296E+02 1.063E+02 9.439E+01 9.930E+01 1.272E+02 1.009E+03 3.607E+02 9.676E+01
3.918E+00 4.589E+01 8.546E+00 7.268E+00 1.912E+00 1.127E+01 7.472E+00 5.875E+00
2.935E+00 2.544E+00 2.009E+00 2.361E+00 1.876E+00 1.396E+00 1.087E+00 8.299E-01
6.159E-01 4.547E-01 3.099E-01 2.361E-01 1.847E-01 2.257E-01 2.679E-01 1.952E-01
2.043E-01 1.599E-01
MC NG TI  Mg-Cu n,g Th&Int
1.000E+00      cm^2         0         0    3    1    1    0
6.688E+01 5.393E+01 4.421E+01 3.354E+01 2.765E+01 1.925E+01 1.493E+01 1.114E+01
8.480E+00 6.364E+00 4.496E+00 3.835E+00 2.636E+00 2.048E+00 1.522E+00 1.234E+00
8.646E-01 7.608E-01 5.652E-01 3.991E-01 3.672E-01 3.850E-01 5.302E-01 1.045E+01
1.325E+00 1.268E+00 6.032E-01 5.828E-01 1.562E-01 1.090E-01 4.809E-02 2.692E-02
1.980E-02 1.452E-02 1.009E-02 6.452E-03 4.390E-03 4.762E-03 4.942E-03 3.477E-03
6.561E-03 9.212E-03
LA NG TI  Lu-Al n,g Th&Int
1.000E+00      cm^2         0         0    3    1    1    0
1.890E+02 1.113E+02 7.572E+01 5.837E+01 4.501E+01 3.396E+01 2.549E+01 1.928E+01
1.458E+01 1.140E+01 8.680E+00 6.569E+00 5.142E+00 5.116E+00 9.467E+01 4.542E+01
1.798E+02 2.059E+02 2.359E+02 1.335E+02 4.585E+01 5.622E+01 3.373E+01 2.798E+01
1.860E+01 1.259E+01 8.921E+00 6.005E+00 3.906E+00 2.927E+00 1.946E+00 1.354E+00
8.815E-01 6.994E-01 5.495E-01 4.279E-01 2.579E-01 2.051E-01 2.055E-01 3.407E-01
2.671E-01 2.389E-01
Cu NG TH  Copper n,g    Th
1.000E+00      cm^2         0         0    3    1    1    0
3.466E+01 1.504E+01 1.617E+01 1.147E+01 8.760E+00 6.352E+00 5.133E+00 3.745E+00
2.862E+00 2.163E+00 1.630E+00 1.271E+00 9.037E-01 6.751E-01 5.238E-01 3.990E-01
3.040E-01 1.849E-01 1.463E-01 1.116E-01 7.243E-02 4.907E-02 3.060E-02 2.385E-02
2.869E+00 1.359E-01 2.984E-01 3.166E-01 1.967E-01 2.161E-01 1.026E-01 8.262E-02
4.055E-02 2.893E-02 2.389E-02 2.065E-02 1.404E-02 1.426E-02 1.336E-02 1.203E-02
1.313E-02 1.508E-02
Zn NP FA  Zinc n,prot Fast
1.000E+00      cm^2         0         0    3    1    1    0
0.000E+00 0.000E+00 0.000E+00 0.000E+00 0.000E+00 0.000E+00 0.000E+00 0.000E+00
0.000E+00 0.000E+00 0.000E+00 0.000E+00 0.000E+00 0.000E+00 0.000E+00 0.000E+00
0.000E+00 0.000E+00 0.000E+00 0.000E+00 0.000E+00 0.000E+00 0.000E+00 0.000E+00
0.000E+00 0.000E+00 0.000E+00 0.000E+00 0.000E+00 0.000E+00 0.000E+00 0.000E+00
0.000E+00 7.285E-09 7.108E-08 3.117E-07 9.355E-07 6.929E-06 6.375E-04 3.496E-02
1.473E-01 2.378E-01
NC NG TH  NaCl n,g Thermal
1.000E+00      cm^2         0         0    3    1    1    0
1.403E+00 1.548E+00 1.536E+00 1.183E+00 9.428E-01 7.125E-01 5.661E-01 4.359E-01
3.289E-01 2.547E-01 2.039E-01 1.551E-01 1.009E-01 9.031E-02 6.488E-02 4.760E-02
3.630E-02 2.747E-02 1.915E-02 1.563E-02 1.224E-02 9.796E-03 7.072E-03 6.325E-03
5.276E-03 6.278E-03 1.340E-02 1.010E-01 1.613E-02 4.122E-03 1.609E-03 4.362E-04
1.897E-03 2.698E-04 5.161E-04 7.539E-04 3.982E-04 3.201E-04 2.717E-04 3.484E-04
3.948E-04 4.016E-04
W  NG IN  W   n,g    Inter
1.000E+00      cm^2         0         0    3    1    1    0
```

```
1.814E+02 1.172E+02 1.318E+02 1.022E+02 7.648E+01 5.354E+01 4.102E+01 3.223E+01
2.461E+01 1.886E+01 1.440E+01 1.062E+01 8.462E+00 7.028E+00 5.614E+00 4.381E+00
5.185E+00 1.108E+01 3.445E+02 1.505E+01 1.225E+00 8.674E-02 1.122E+01 4.429E+00
4.312E+00 3.093E+00 1.010E+00 8.621E-01 5.179E-01 3.554E-01 2.488E-01 1.809E-01
2.257E-01 1.147E-01 7.745E-02 5.386E-02 4.209E-02 1.212E-01 4.577E-02 5.359E-02
3.663E-02 3.610E-02
Ni NP FA  Nickle n,prot FA
1.000E+00      cm^2         0         0    3    1    1    0
0.000E+00 0.000E+00 0.000E+00 0.000E+00 0.000E+00 0.000E+00 0.000E+00 0.000E+00
0.000E+00 0.000E+00 0.000E+00 0.000E+00 0.000E+00 0.000E+00 0.000E+00 0.000E+00
0.000E+00 0.000E+00 0.000E+00 0.000E+00 0.000E+00 0.000E+00 0.000E+00 0.000E+00
0.000E+00 0.000E+00 0.000E+00 0.000E+00 0.000E+00 0.000E+00 0.000E+00 0.000E+00
0.000E+00 0.000E+00 0.000E+00 0.000E+00 3.566E-05 8.433E-04 1.210E-02 1.128E-01
4.011E-01 6.258E-01
Au NG TI  Gold  n,g Th&Int
1.000E+00      cm^2         0         0    3    1    1    0
7.153E+02 3.020E+02 2.563E+02 2.257E+02 1.904E+02 1.412E+02 1.055E+02 8.177E+01
6.414E+01 4.858E+01 3.693E+01 3.015E+01 2.648E+01 2.641E+01 2.932E+01 1.928E+02
5.614E+02 5.936E+00 6.982E-01 4.685E-01 4.976E+01 8.186E+00 1.101E+01 1.892E+01
1.174E+01 7.806E+00 5.401E+00 2.281E+00 2.088E+00 1.412E+00 8.393E-01 6.397E-01
4.299E-01 3.397E-01 2.481E-01 2.031E-01 1.340E-01 1.052E-01 1.220E-01 9.439E-02
8.415E-02 1.122E-01
Mo NG IN  Mo    n,g  Inter
1.000E+00      cm^2         0         0    3    1    1    0
1.020E+00 5.365E-01 4.662E-01 3.230E-01 2.577E-01 1.887E-01 1.421E-01 1.098E-01
8.304E-02 6.495E-02 4.852E-02 3.581E-02 2.610E-02 2.138E-02 1.937E-02 1.651E-02
1.814E-02 3.964E+00 1.422E-01 6.125E-03 4.188E-03 3.005E-03 2.977E-03 1.185E-01
4.623E+00 1.185E+00 5.812E-01 3.264E-01 2.475E-01 2.371E-01 1.028E-01 8.608E-02
5.334E-02 5.172E-02 4.025E-02 3.592E-02 4.229E-02 4.199E-02 3.683E-02 3.029E-02
2.901E-02 2.441E-02
Sc NG IN  Sc   n,g   Inter
1.000E+00      cm^2         0         0    3    1    1    0
2.536E+02 1.098E+02 6.932E+01 6.801E+01 5.319E+01 3.848E+01 3.033E+01 2.280E+01
1.742E+01 1.303E+01 9.434E+00 7.437E+00 5.350E+00 4.079E+00 3.302E+00 2.461E+00
1.817E+00 1.313E+00 9.614E-01 7.661E-01 4.690E-01 3.067E-01 2.076E-01 1.209E-01
9.863E-02 4.185E-02 2.778E-02 2.683E-01 2.114E-01 1.787E-01 9.533E-02 6.905E-02
5.188E-02 3.143E-02 2.465E-02 1.465E-02 8.779E-03 7.802E-03 6.574E-03 6.379E-03
6.672E-03 6.709E-03
Co NG TI  Co   n,g  Th&Int
1.000E+00      cm^2         0         0    3    1    1    0
3.144E+02 1.665E+02 1.269E+02 1.042E+02 6.899E+01 5.187E+01 4.113E+01 3.130E+01
2.307E+01 1.741E+01 1.321E+01 9.945E+00 7.525E+00 5.619E+00 4.504E+00 3.520E+00
2.446E+00 2.890E+00 1.811E+00 1.692E+00 2.255E+00 3.704E+01 3.872E+01 1.715E+00
6.753E-01 6.138E-01 4.403E-02 5.581E-02 2.321E-01 8.132E-02 4.703E-02 5.391E-02
3.551E-02 1.637E-02 2.250E-02 1.168E-02 7.783E-03 7.622E-03 2.440E-02 7.399E-03
6.461E-02 8.116E-02
T-47 Fas  Ti  n,prot  Fast
1.000E+00      cm^2         0         0    3    1    1    0
0.000E+00 0.000E+00 0.000E+00 0.000E+00 0.000E+00 0.000E+00 0.000E+00 0.000E+00
0.000E+00 0.000E+00 0.000E+00 0.000E+00 0.000E+00 0.000E+00 0.000E+00 0.000E+00
0.000E+00 0.000E+00 0.000E+00 0.000E+00 0.000E+00 0.000E+00 0.000E+00 0.000E+00
0.000E+00 0.000E+00 0.000E+00 0.000E+00 0.000E+00 0.000E+00 0.000E+00 0.000E+00
0.000E+00 8.406E-09 2.559E-07 1.023E-06 1.147E-05 2.247E-04 3.677E-03 2.098E-02
7.013E-02 1.357E-01
```

Appendix B-3. Measured foil response input file (MeasureData_bareF.ibu).

```
Measured Responses for Multi-Foil Array (RR/atom)

   13    0
In NG TI   1.0      9.928E+08      0.000E+00    3.00    0.00     1
MC NG TI   2.0      7.448E+07      0.000E+00    3.00    0.00     2
LA NG TI   3.0      5.263E+08      0.000E+00   10.00    0.00     3
Cu NG TH   4.0      2.784E+07      0.000E+00    3.00    0.00     4
Zn NP FA   5.0      2.840E+06      0.000E+00    3.00    0.00     5
NC NG TH   6.0      2.564E+06      0.000E+00    3.00    0.00     6
W  NG IN   7.0      4.414E+08      0.000E+00    3.00    0.00     7
Ni NP FA   8.0      8.081E+06      0.000E+00    3.00    0.00     8
Au NG TI   9.0      6.604E+08      0.000E+00    3.00    0.00     9
Mo NG IN  10.0      9.764E+06      0.000E+00    3.00    0.00    10
Sc NG IN  11.0      1.231E+08      0.000E+00    4.00    0.00    11
Co NG TI  12.0      2.215E+08      0.000E+00    5.00    0.00    12
T-47 Fas  13.0      1.624E+06      0.000E+00    5.00    0.00    13

Foil       Diam    Activation     abs unc     Total     n/a     flag
Reaction   eter    Rate R           of R      % unc     % unc
```

Appendix B-4. MAXED control file (ers_MXD_bareF.inp).

```
MeasuredData_bareF.ibu                  File with measured data
RFdata_bareF.fmt                        File with response functions (RF)
ers_outputMXD                           Name of output file
defaultSpecF.flu                        File with default spectrum (DS)
10.01                                   Highest energy (units from "A")
1.1                                     requested final CHI^2 P.D.F.
1.0,0.85                                temperature, temp. reduction fact.
3,2                                     3 = RF energy bins, 2 = EdF/dE
1                                       1 = scale DS
0                                       0 = use the MAXED DS scale factor
```

Appendix B-5. GRAVEL control file (ers_GRV_bareF.inp).

```
MeasuredData_bareF.ibu                  File with measured data
RFdata_bareF.fmt                        File with response functions (RF)
ers_outputGRV                           Name of output file
defaultSpecF.flu                        File with default spectrum (DS)
10.01                                   Highest energy (units from "A")
1.1                                     requested final CHI^2 P.D.F.
200,10                                  max. # iter., freq. interim results
3,2                                     3 = RF energy bins, 2 = EdF/dE
1                                       1 = scale DS
0                                       0 = use the MAXED DS scale factor
```

Appendix C: Cadmium Covered Foil Response Functions

Appendix C-1. Response functions of foils 1, 2, 4, 7, and 9.

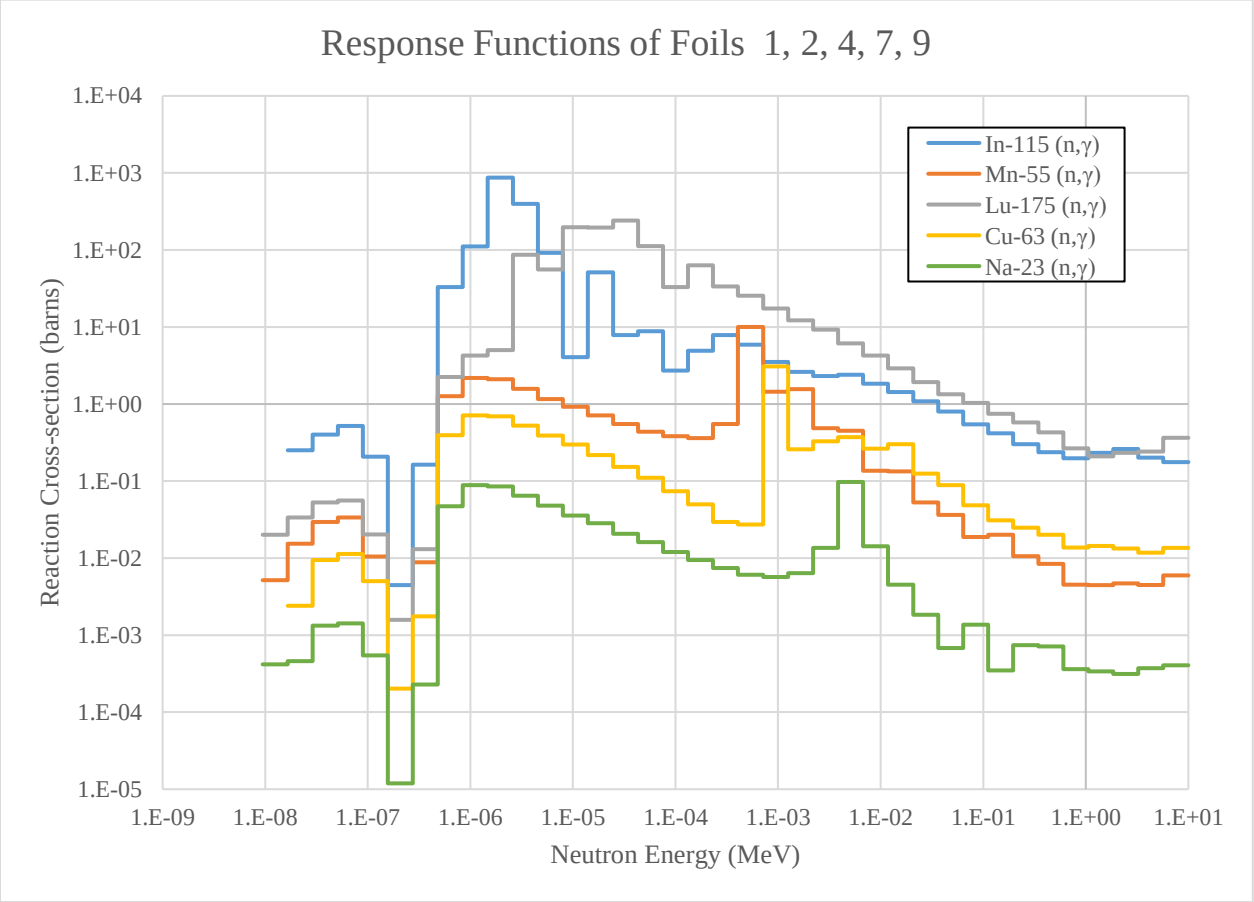

Appendix C-2. Response functions of foils 12, 16, 17, and 21.

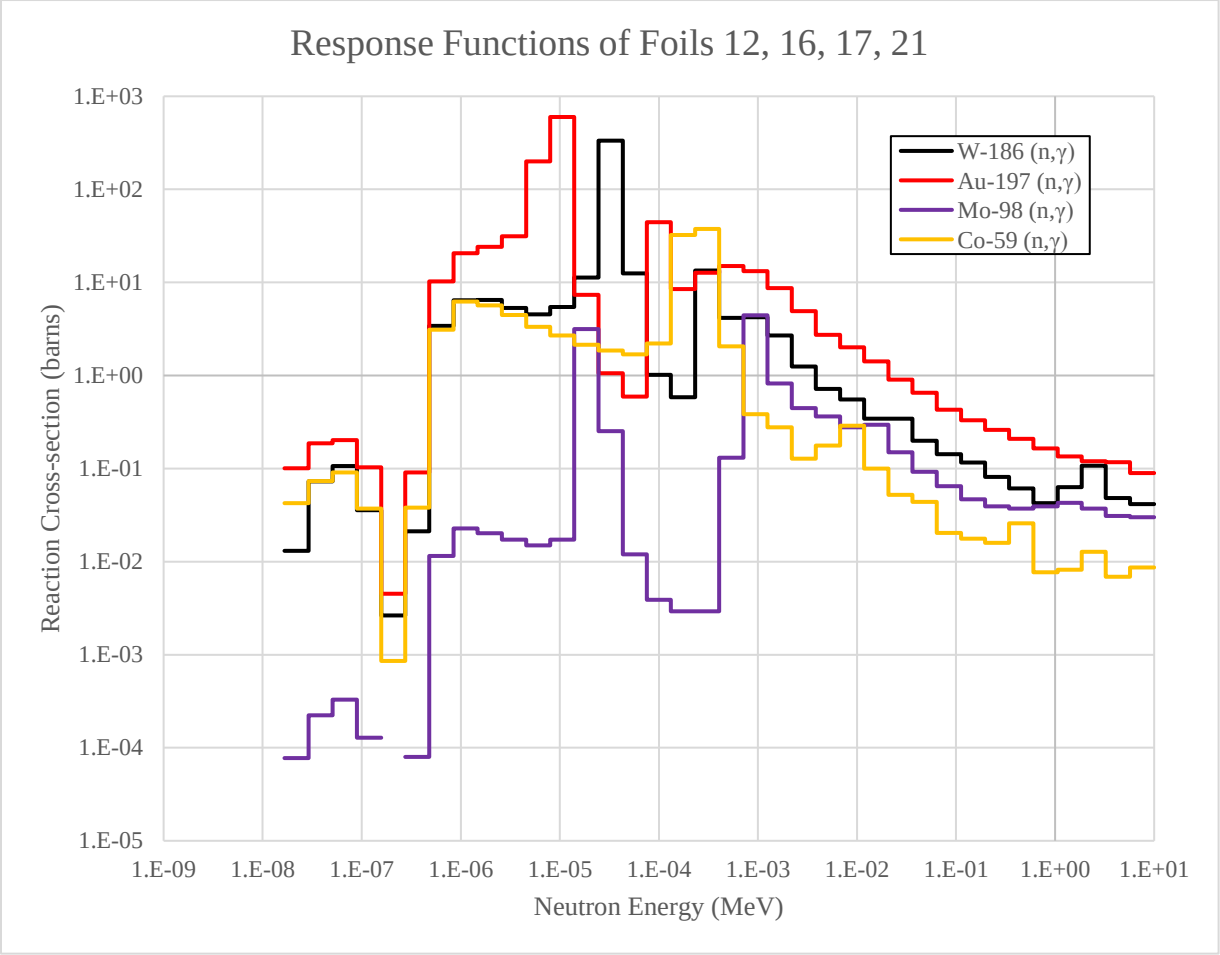

Appendix C-3. Response functions of foils 8 and 13.

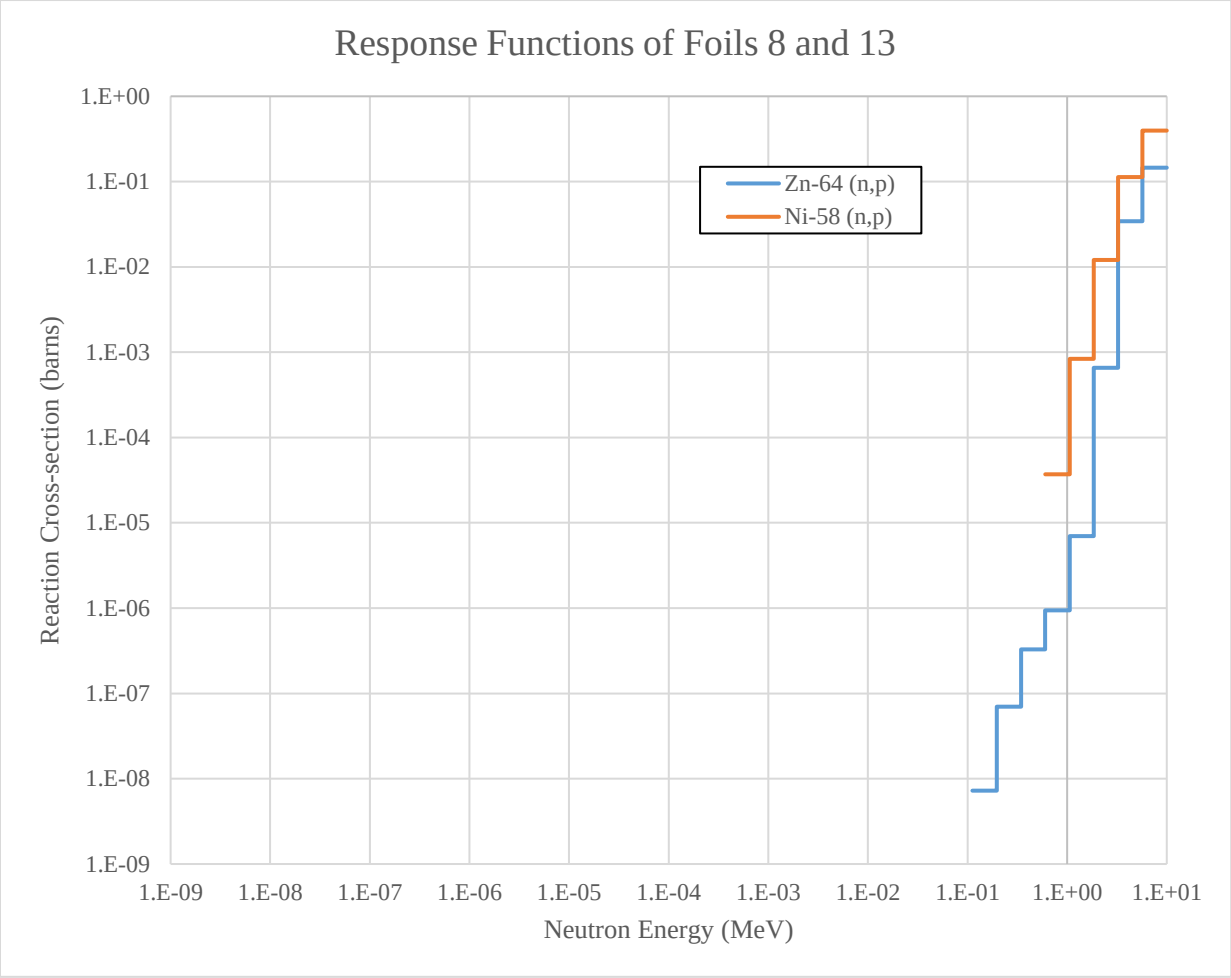

Appendix D: MCNP input file of ERS model

```
64-ELEMENT NRAD REACTOR EAST BEAM LINE
c
c Built by John Darrel Bess - Idaho National Laboratory
c Extended East Beam Line contributed by Sam H. Giegel
c June 1st, 2017
c
c Cell Cards ************************************************************
c ------ East Beam Line ------------------------------------------------
c
3701   2 5.0820E-05 (404 -405 436 -437 435 -434):(434 -442 -601) imp:n=1 $ Air in Beam Filter
Tube
3702  52 5.9939E-02 (-404:405:-436:437:-435) 402 -403 432 -433 431 -434 imp:n=1 $ Beam Filter
Tube
3703  52 5.9939E-02 (-402:403:-432:433:434) (438 -447 439 -440 406 -407)
                    (601:442) (-441:-445:446) imp:n=1 $ Beam Filter Tube Attachment Fixtures
3704  52 5.9939E-02 441 -444 445 -446 408 -13 (-447:448:-449:450:-409)
                    (601:-443:447) (602:-448:451) imp:n=1 $Beam Aperture Housing
3705  53 1.2258E-06 ((447 -448 449 -450 409 -13):(443 -447 -601):
                    (448 -451 -602)) (-410:413:-459:448:-455:456) imp:n=1 $ Helium in Aperture
Housing
3706  54 1.0026E-01 444 -452 631 -632 imp:n=1 $ Absorber Disc Aperture
3707  53 1.2258E-06 444 -452 -631 imp:n=1 $ Helium in Disc Aperture
3708  52 5.9939E-02 452 -454 -606 (603:-453) imp:n=1 $ Beam Stop
3709  53 1.2258E-06 -633 459 -448 imp:n=1 $ Helium in Bottom Aperture Hole
3710  53 1.2258E-06 -634 459 -448 imp:n=1 $ Helium in Top Aperture Hole
3711  54 1.0026E-01 460 -461 457 -458 411 -412 633 634 imp:n=1 $ Absorber Aperture Block
3712  52 5.9939E-02 (-460:461:-457:458:-411:412) 459 -448 455 -456 410 -413
                    633 634 imp:n=1 $ Absorber Assembly Housing
3713  210 0.019186  -604 613 454 -462 imp:n=1  $ Boral Liner
c
3770  52 5.9939E-02 (444 604 -605 -462):((444:-445:446) 448 -444 -605) imp:n=1    $ Beam Tube
3771  53 1.2258E-06 444 -613 -462 (-444:452:632) (-452:454:606):(453 -454 -603):
                    (-414 415 -465 466 462 -463) imp:n=1                          $ Helium in
Beam Tube
c
4021 66 5.9939E-02 1 -13 -72 (-2:71) #3770 #3771 #3713 imp:n=0 $ Reactor Tank
c
c --- East Beam Extension -------------------------------------------------
c
c --- Thru-Wall Collimator Assembly ---------------------------------------
c
5001  52 5.9939E-02  463 -499 -607 imp:n=1  $ Aluminum seal for inner beam window
5002 210 0.019186   -607 (414:-415:465:-466) 499 -464 imp:n=1    $ Boral Window (Inner)
5003  46 8.7653E-02  464 -467 -607 608 imp:n=1  $ Steel Sleeve
5004 265 -6.205      464 -498 -608 609 imp:n=1  $ Lead and Borated Polyethylene Mixture
5005  52 5.9939E-02  464 -467 -609 610 imp:n=1  $ Aluminum Sleeve
5006   2 5.0820E-05  464 -467 -610 611 imp:n=1  $ Air Filler around aluminum sleeve
5007 210 0.019186    464 -467 -611 612 imp:n=1  $ Boral Liner
5009 210 0.019186    467 -468 -607 (416:-417:469:-470) imp:n=1              $ Outer Beam Window
(Boral)
5010  52 5.9939E-02  468 -471 -607 imp:n=1                                  $ Aluminum seal for
outer beam window
5011  53 1.2258E-06  (464 -496 -612):(-465 466 495 -464 -414 415):
                     (496 -467 -612):(467 -497 -469 470 -416 417):
                     (497 -468 -469 470 -416 417):
                     (499 -495 -414 415 466 -465) imp:n=1                   $ Helium Filled
Through-wall collimator
5014   2 5.0820E-05  498 -467 -608 609 imp:n=1                              $ Air Filler between
Steel Sleeve and Aluminum Sleeve
5015  60 3.83405E-02 462 -463 -607 (414:-415:465:-466) imp:n=1              $ Indium Absorber
for inner beam window (Cut out to match shape of window)
c
c --- Gamma Shield/Neutron Shutter Assembly -------------------------------
c
5020  46 8.7653E-02 (-472:473:476:-477:-420) 750 -474 -475 478
                     419 -418 imp:n=1                          $ Steel Casing around LEAD
5021  58 0.0329854  -418 420 472 -473 -476 477 imp:n=1          $ Lead inside steel casing
```

```
5022  52 5.9939E-02 (-479:480:483:-484) 750 -481 485 -421 422
                    -482 imp:n=1                                        $ Neutron Shutter
Assembly
5023 210 0.019186    -421 422 ((479 -486):(494 -480)) -483 484 imp:n=1   $ Boral Sheets
5024  52 5.9939E-02  -421 422 ((486 -487):(493 -494)) -483 484 imp:n=1   $ Aluminum Spacers
5025 263 0.0590087   -421 422 ((489 -490):(492 -493)) -483 484 imp:n=1   $ Au Foils
5026  60 3.83405E-02 -421 422 ((488 -489):(491 -492)) -483 484 imp:n=1   $ In Foils
5027 264 0.0302577   -421 422 ((487 -488):(490 -491)) -483 484 imp:n=1   $ Gd Foils
5028 210 0.0590087   751 -750 478 -475 -418 419 imp:n=1                  $ Boral Plate in front
of GNA
c
c --- East Radiography Station Room ------------------------------------------
c
c ------- Elevator Shielding ---------------------------------------------------
c
5100 210 0.019186 423 -424 ((513 -515 514 -518):(517 521 -514 -518))
                  imp:n=1  $ Boral Lining infront of shielding surround elevator tube
5101  58 3.2988E-02 423 -424 ((513 -519 515 -516):(518 -519 521 -516))
                  imp:n=1  $ Lead Bricks that make up the shielding
5102  58 3.2988E-02 423 -425 519 -520 521 -516 imp:n=1  $ Second layer of shielding
5103  57 1.1978E-01 423 -425 522 -523
                  ((520 -524):(525 -526):(527 -528)) imp:n=1  $ Pure Polyethylene Layers of
Beam Stop
5104  59 1.183E-01  423 -425 522 -523
                  ((524 -525):(526 -527):(528 -529)) imp:n=1  $ 30% Borated Polyethylene Layers
of Beam Stop
c
c --- Image Plate & Multi-Foil Array ---------------------------------------
c
5105  52 5.9939E-02 -426 427 534 -533 535 -536 imp:n=1 vol=243.76  $ Aluminum Image Plate
5106  302 3.83405E-02   -534 713 -690  imp:n=1 vol=0.016087        $ Foil at Position #1  (In)
5107  320 1.872436E-02  -534 537 -691  imp:n=1 vol=0.006435        $ Foil at Position #2  (Mn-Cu)
5108  306 8.49104E-02   -534 713 -692  imp:n=1 vol=0.016087        $ Foil at Position #3  (Fe)
5109  319 1.4005369E-02 -534 719 -693  imp:n=1 vol=0.012870        $ Foil at Position #4  (Lu-Al)
5110  302 3.83405E-02   -534 713 -694  imp:n=1 vol=0.016087        $ Foil at Position #5  (In)
5111  305 8.49123E-02   -534 713 -695  imp:n=1 vol=0.016087        $ Foil at Position #6  (Cu)
5112  305 8.49123E-02   -534 713 -696  imp:n=1 vol=0.016087        $ Foil at Position #7  (Cu)
5113  315 6.57134E-02   -534 716 -697  imp:n=1 vol=0.032176        $ Foil at Position #8  (Zn)
5114  318 4.46204E-02   -534 718 -698  imp:n=1 vol=0.241319        $ Foil at Position #9  (NaCl)
5115  317 6.02381E-02   -534 713 -699  imp:n=1 vol=0.016087        $ Foil at Position #10 (Al)
5116  310 4.30630E-02   -534 713 -700  imp:n=1 vol=0.016087        $ Foil at Position #11 (Mg)
5117  309 6.32214E-02   -534 713 -701  imp:n=1 vol=0.016087        $ Foil at Position #12 (W)
5118  311 9.13376E-02   -534 716 -702  imp:n=1 vol=0.032176        $ Foil at Position #13 (Ni)
5119  313 5.67406E-02   -534 716 -703  imp:n=1 vol=0.032176        $ Foil at Position #14 (Ti)
5120  314 7.09301E-02   -534 537 -704  imp:n=1 vol=0.006435        $ Foil at Position #15 (V)
5121  263 0.0590087     -534 537 -705  imp:n=1 vol=0.006435        $ Foil at Position #16 (Au)
5122  307 6.41376E-02   -534 715 -706  imp:n=1 vol=0.009653        $ Foil at Position #17 (Mo)
5123  316 4.30419E-02   -534 713 -707  imp:n=1 vol=0.016087        $ Foil at Position #18 (Zr)
5124  306 8.49104E-02   -534 713 -708  imp:n=1 vol=0.016087        $ Foil at Position #19 (Fe)
5125  308 4.00396E-02   -534 713 -709  imp:n=1 vol=0.016087        $ Foil at Position #20 (Sc)
5126  304 9.09455E-02   -534 537 -710  imp:n=1 vol=0.006435        $ Foil at Position #21 (Co)
5127  318 4.46204E-02   -534 718 -711  imp:n=1 vol=0.241319        $ Foil at Position #22 (NaCl)
5128  312 3.8877E-02    -534 717 -712  imp:n=1 vol=0.600081        $ Foil at Position #23 (S)
c
c --- Multi-Foil Array (Unpeturbed) ----------------------------------------
c
c 5106  0   -534 537 -690  imp:n=1 vol=0.006435        $ Foil at Position #1  (In)
c 5107  0   -534 714 -691  imp:n=1 vol=0.016345        $ Foil at Position #2  (Mn-Cu)
c 5108  0   -534 537 -692  imp:n=1 vol=0.016345        $ Foil at Position #3  (Fe)
c 5109  0   -534 719 -693  imp:n=1 vol=0.012871        $ Foil at Position #4  (Lu-Al)
c 5110  0   -534 537 -694  imp:n=1 vol=0.006435        $ Foil at Position #5  (In)
c 5111  0   -534 537 -695  imp:n=1 vol=0.006435        $ Foil at Position #6  (Cu)
c 5112  0   -534 537 -696  imp:n=1 vol=0.006435        $ Foil at Position #7  (Cu)
c 5113  0   -534 716 -697  imp:n=1 vol=0.032177        $ Foil at Position #8  (Zn)
c 5114  0   -534 718 -698  imp:n=1 vol=0.241325        $ Foil at Position #9  (NaCl)
c 5115  0   -534 537 -699  imp:n=1 vol=0.006435        $ Foil at Position #10 (Al)
c 5116  0   -534 537 -700  imp:n=1 vol=0.006435        $ Foil at Position #11 (Mg)
c 5117  0   -534 537 -701  imp:n=1 vol=0.006435        $ Foil at Position #12 (W)
c 5118  0   -534 716 -702  imp:n=1 vol=0.032177        $ Foil at Position #13 (Ni)
c 5119  0   -534 716 -703  imp:n=1 vol=0.032177        $ Foil at Position #14 (Ti)
c 5120  0   -534 714 -704  imp:n=1 vol=0.016345        $ Foil at Position #15 (V)
```

```
c 5121  0   -534 537 -705  imp:n=1 vol=0.006435        $ Foil at Position #16 (Au)
c 5122  0   -534 715 -706  imp:n=1 vol=0.009653        $ Foil at Position #17 (Mo)
c 5123  0   -534 537 -707  imp:n=1 vol=0.006435        $ Foil at Position #18 (Zr)
c 5124  0   -534 537 -708  imp:n=1 vol=0.006435        $ Foil at Position #19 (Fe)
c 5125  0   -534 537 -709  imp:n=1 vol=0.006435        $ Foil at Position #20 (Sc)
c 5126  0   -534 714 -710  imp:n=1 vol=0.016345        $ Foil at Position #21 (Co)
c 5127  0   -534 718 -711  imp:n=1 vol=0.241325        $ Foil at Position #22 (NaCl)
c 5128  0   -534 717 -712  imp:n=1 vol=0.600096        $ Foil at Position #23 (S)
c --- Beam Scraper ------------------------------------------------------------
c
5151 210 0.019186   (540:-541:559:-560) -539 542 -567 568
                    558 -557 imp:n=1                          $ Boral Plate
5152  52 5.9939E-02 (544:-545:561:-562) -543 546 -569 570
                    557 -556 imp:n=1                          $ Aluminum Backing
5153 210 0.019186   ((-563 564):(-565 566)) -539 542 -555
                     556 imp:n=1                              $ Boral Shutters
c
c --- Elevator Specimen Tube --------------------------------------------------
c
5160 52 5.9939E-02 -571 572 -721 720 -574 imp:n=1                 $ Elevator Shell (Aluminum)
5161 52 5.9939E-02 (575:-577:579) -571 572 574 -573 -576
                    578 imp:n=1 vol=365.72
5162 52 5.9939E-02 -722 720 ((582 -580):(-583 581)) imp:n=1       $ Elevator Flanges
5163 52 5.9939E-02 -722 720 -574 ((-582 571):(-572 583)) imp:n=1
5164 52 5.9939E-02 (575:-577:579) ((-582 571):(-572 583)) 574 -576
                    578 -722 imp:n=1
5165 52 5.9939E-02 -721 720 ((580 -424):(-581 423)) imp:n=1
5166 330 0.0000269  (((-720 -574):(-579 -575 577 574)) -582 583):
                    -720 ((582 -424):(-583 423)) imp:n=1           $ Argon in Elevator Tube
c --- East Radiography Room ---------------------------------------------------
c
5200  2 5.0820E-05  -424 423 467 -530 531 -532 #5020
        #5021 #5022 #5023 #5024 #5025 #5026 #5027 #5028 #5100
        #5102 #5009 #5010 #5011 #5103 #5104
        #5101 #5105 #5106 #5107 #5108 #5109 #5110 #5111 #5112
        #5113 #5114 #5115 #5116 #5117 #5118 #5119 #5120 #5121
        #5122 #5123 #5124 #5125 #5126 #5127 #5128 #5151 #5152
        #5153 #5160 #5161 #5162 #5163 #5164 #5165 #5166 imp:n=1      $ East Radiography Room
(Filled w/ Air)
5201 331 9.95E-02   (502 -467 -512 503 -424 428):
                    (500 -467 607 -503 504 -424 428):
                    (467 -530 532 -512 -424 428):
                    (502 -467 -504 511 -424 428):
                    (467 -530 -532 531 428 -423):
                    (467 -530 -531 511 428 -424) imp:n=0             $ Concrete Surrounding ERS
5202 360 -3.595  -752 ((-500 462 607):(-462 52 72 605))
                   #3713 imp:n=0                                     $ Magnetite/Boron Frit
Grout surrounding NRAD Tank
c
c --- Model Boundary ----------------------------------------------------------
9998  0 (-1:13:72) (424:-423:-467:530:-531:532)
       #3713 #3771 #3770 #5001 #5002 #5003 #5004 #5005
       #5006 #5007 #5009 #5010 #5011
       #5014 #5015 #5020 #5021 #5022 #5023 #5024 #5025
       #5026 #5027 #5028 #5201 #5202 imp:n=0                          $ This defines
everything outside the beam extension
9999  1 9.9912E-02 2 -13 -71 #3771 #3770 #3708 #3706 #3707 #3705 #3709
                   #3711 #3712 #3704 #3703 #3702 #3701 #3710 #3713
                   imp:n=0                                            $ This defines the
boudary inside reactor tank
c

c Surface Cards ***************************************************************
c
c   **** = Sam Giegel addition to original model
c
c ------ Reference Points from Original Model -----------------------------------
1     pz    0        $ Tank Bottom Surface
2     pz    1.27     $ Tank/Mounting Pad Interface
13    pz  203.2      $ Tank Water Top Boundary
52    px    0        $ E/W Division of Tank
```

```
71    cz  99.06      $ Inner Tank Surface
72    cz  99.695     $ Outer Tank Surface
c
c ------ Horizontal Planes ------------------------------------------------------
c
402   pz   88.33993  $ Bottom Surface of Beam Filter Tubes
403   pz  104.84993  $ Top Surface of Beam Filter Tubes
404   pz   88.97493  $ Inside Bottom Surface of Beam Filter Tubes
405   pz  104.21493  $ Inside Top Surface of Beam Filter Tubes
406   pz   83.25993  $ Bottom Surface of Tube Attachment Fixtures
407   pz  109.92993  $ Top Surface of Tube Attachment Fixtures
408   pz   80.71993  $ Outside Bottom Surface of Aperture Housing
409   pz   81.98993  $ Inside Bottom Surface of Aperture Housing
410   pz   90.08618  $ Bottom of Absorber Assembly
411   pz   91.51493  $ Bottom of Absorber Block
412   pz  108.65993  $ Top of Absorber Block
413   pz  111.67618  $ Top of Absorber Assembly
414   pz  104.70815  $ Top of Inner Beam Window                                  ****
415   pz   88.48771  $ Bottom of Inner Beam Window                               ****
416   pz  110.25043  $ Top of Outer Beam Window                                  ****
417   pz   82.94543  $ Bottom of Outer Beam Window                               ****
418   pz  141.36243  $ Top of GNA                                               ****
419   pz   50.71918  $ Bottom of GNA                                            ****
420   pz   51.3542   $ Inside Bottom of GNA                                      ****
421   pz  111.12673  $ Top of NSA                                               ****
422   pz   82.06913  $ Bottom of NSA                                            ****
423   pz   43.255    $ Ground Level of East Radiography Station                 ****
424   pz  285.825    $ Ceiling of East Radiography Station                      ****
425   pz  164.54     $ Top of 2nd West Facing Wall of Shielding                 ****
426   pz  118.18493  $ Top of Image Plate                                       ****
427   pz   75.00493  $ Bottom of Image Plate                                    ****
428   pz   12.775    $ Bottom of Floor of ERS Room                              ****
c
c ------ Vertical Planes ----------------------------------------------------------
c --------- East Beam Assembly ---------
431   px   17.92069  $ Core Face of Beam Filter Tube
432   py   -6.985    $ South Surface of Beam Filter Tube
433   py    6.985    $ North Surface of Beam Filter Tube
434   px   51.57569  $ Back End of Beam Filter Tube
435   px   18.14929  $ Inside Core Face of Beam Filter Tube
436   py   -6.6675   $ Inside South Surface of Beam Filter Tube
437   py    6.6675   $ Inside North Surface of Beam Filter Tube
438   px   47.76569  $ Beam Filter Tube Attachment Fixtures
439   py  -10.4775   $ South Surface of Tube Attachment Fixtures
440   py   10.4775   $ North Surface of Tube Attachment Fixtures
441   px   52.84569  $ Core-Side Face of Beam Aperture Housing
442   px   52.52819  $ Beam Window Surface on Filter Tube
443   px   53.16319  $ Beam Window Surface on Aperture Housing
444   px   64.27569  $ Tank-Side Face of Beam Aperture Housing
445   py   -7.9375   $ South Surface of Aperture Housing
446   py    7.9375   $ North Surface of Aperture Housing
447   px   54.11569  $ Inside Core-Side Face of Aperture Housing
448   px   63.00569  $ Inside Tank-Side Face of Aperture Housing
449   py   -6.6675   $ Inside South Surface of Aperture Housing
450   py    6.6675   $ Inside North Surface of Aperture Housing
451   px   64.19949  $ Beam Window Surface on Aperture Housing
452   px   69.35569  $ Disc Absorber/Stop Interface
453   px   69.51317  $ Beam Window Surface in Absorber Stop
454   px   69.99069  $ Tank-Side Face of Absorber Stop
455   py   -6.62686  $ South Surface of Absorber Assembly
456   py    6.62686  $ North Surface of Absorber Assembly
457   py   -5.08     $ South Surface of Absorber Block
458   py    5.08     $ North Surface of Absorber Block
459   px   57.29069  $ Core-Side Face of Absorber Assembly
460   px   57.60819  $ Core-Side Face of Absorber Block
461   px   62.68819  $ Tank-Side Face of Absorber Block
c
c --- Thru-Wall Collimator
c
462   px   99.696    $ Core-Face of East Beam Extension                 ****
463   px   99.7458   $ East Face of Indium Sheet                        ****
```

```
464   px  100.54082  $ East Face of Inner Beam Window                  ****
465   py    6.764    $ North Side of Inner Beam Window                ****
466   py   -6.764    $ South Side of Inner Beam Window                ****
467   px  241.46     $ East Face of Thru-Wall Collimator              ****
468   px  242.095    $ East Face of Outer Beam Window                 ****
469   py    9.1948   $ North Side of Outer Beam Window                ****
470   py   -9.1948   $ South Side of Outer Beam Window                ****
471   px  242.2538   $ East Face of Aluminum Seal                     ****
c
c --- Gamma/Neutron Shutter Assembly
c
472   px   246.1641  $ West Face of GNA (Inner Wall)                  ****
473   px   271.8816  $ Inner East Face of GNA                         ****
474   px   274.4216  $ Outer East Face of GNA                         ****    In Front of Beam
Not In Front
475   py   -11.3375  $ North Outer Side of GNA                        ****        18.415
-11.3375
476   py   -11.9725  $ North Inner Side of GNA                        ****        17.78
-11.9725
477   py  -104.365   $ South Inner Side of GNA                        ****       -74.6125
-104.365
478   py  -105       $ South Outer Side of GNA                        ****       -75.2475
-105
479   px   244.1741  $ West Face Inside wall of Neutron Shutter Assembly  ****
480   px   246.2925  $ East Inner Wall of NSA                         ****
481   px   246.8425  $ East Outer Wall of NSA                         ****      In Front of Beam
Not In Front
482   py    43.095   $ North Outer Wall of NSA                        ****         12.08
43.095
483   py    42.545   $ North Inner Wall of NSA                        ****         11.53
42.545
484   py    20.235   $ South Inner Wall of NSA                        ****        -10.78
20.235
485   py    19.685   $ South Outer Wall of NSA                        ****        -11.33
19.685
486   px   244.8091  $ End of Boral Sheet #1                         ****
487   px   245.1266  $ End of Al Spacer#1                            ****
488   px   245.13168 $ End of Gd Foil#1                              ****
489   px   245.20788 $ End of In Foil#1                              ****
490   px   245.23328 $ End of Au Foil#1                              ****
491   px   245.23836 $ End of Gd Foil#2                              ****
492   px   245.31456 $ End of In Foil#2                              ****
493   px   245.33996 $ End of Au Foil#2                              ****
494   px   245.65746 $ End of Al Spacer#2                            ****
495   px   100.25    $ Surface Tally #2 Position                     ****
496   px   171.66    $ Surface Tally #3 Position                     ****
497   px   241.635   $ Surface Tally #4 Position                     ****
c
c --- Thru-Wall Collimator Add Ons ----------------------------------------
c
498   px   161.3408  $ End of Lead Shot                                    ****
499   px    99.90588 $ East Side of Aluminum Seal                         ****
500   px   119.54    $ Core Face of ERS Concrete Wall                     ****
501   px    52.635   $ End Of Air Boundary                                ****
502   px   210.98    $ Core facing side of concrete wall                  ****
503   py   101.6     $ Outer north side of concrete wall around collimator  ****
504   py  -101.6     $ Outer south side of concrete wall around collimator  ****
c
c --- East Radiography Station Layout -------------------------------------
c
511   py  -135.89    $ Outside Edge of South Wall (1 ft thick)        ****
512   py   229.87    $ Outside Edge of North Wall (1 ft thick)        ****
513   px   436.2463  $ 1st West Side of Shielding Surrounding Elevator ****
514   py    42.2275  $ South Face of Boral Liner                      ****
515   py    45.72    $ South Face of Lead Bricks                      ****
516   py    66.04    $ North Face of Shielding                        ****
517   px   535.3063  $ 2nd West Face of Boral Lining                   ****
518   px   539.1163  $ 2nd West Face of Shielding (Lead Portion)       ****
519   px   559.4363  $ Back Side of Taller Shielding                   ****
520   px   574.0413  $ Back Side of Shielding/Beginning of Beam Stop   ****
521   py   -62.23    $ 2nd South Face of Shielding                     ****
```

```
522   py   -59.69    $ South Face of Beam Stop                          ****
523   py    63.5     $ North Face of Beam Stop                          ****
524   px   579.7563  $ East Face of 1st Slab (poly)                     ****
525   px   584.8363  $ East Face of 2nd Slab (BP)                       ****
526   px   589.9163  $ East Face of 3rd Slab (poly)                     ****
527   px   594.9963  $ East Face of 4th Slab (BP)                       ****
528   px   600.0763  $ East Face of 5th Slab (poly)                     ****
529   px   605.1563  $ East Face of 6th Slab (BP) End of Beam Stop      ****
530   px   605.7913  $ East Wall of ERS                                 ****
531   py  -105.41    $ South Wall of ERS                                ****
532   py   199.39    $ North Wall of ERS                                ****
533   px   505.14763 $ East Side of Image Plate                         ****
534   px   504.83013 $ West Side of Image Plate (Facing Beam)           ****
535   py    -8.89    $ South Side of Image Plate                        ****
536   py     8.89    $ North Side of Image Plate                        ****
537   px   504.82505 $ Front of Foils on Image Plate (Facing Beam)      ****
c
c --- Beam Scraper -------------------------------------------------------
c
539   pz   142.95293 $ Top Outer Edge of Boral Plate                    ****
540   pz   117.55293 $ Top Inner Edge of Boral Plate                    ****
541   pz    74.37293 $ Bottom Inner Edge of Boral Plate                 ****
542   pz    50.24293 $ Bottom Outer Edge of Boral Plate                 ****
543   pz   135.33293 $ Top Outer Edge of Aluminum Backing               ****
544   pz   121.99793 $ Top Inner Edge of Aluminum Backing               ****
545   pz    71.19793 $ Bottom Inner Edge of Aluminum Backing            ****
546   pz    43.89293 $ Bottom Outer Edge of Aluminum Backing            ****
c
555   px   473.71005 $ East Face of Boral Shutter                       ****
556   px   473.03695 $ West Face of Boral Shutter/East Face of Aluminum Backing     ****
557   px   472.40195 $ West Face of Al Backing/East Face of Boral Plate             ****
558   px   471.72885 $ West Face of Boral Plate                         ****
559   py    12.7     $ Inner North Side of Boral Plate                  ****
560   py   -12.7     $ Inner South Side of Boral Plate                  ****
561   py    17.78    $ Inner North Side of Al Backing                   ****
562   py   -17.78    $ Inner South Side of Al Backing                   ****       In Front of
Beam      Not In Front of Beam
563   py    30.48    $ North Side of Boral Shutter                      ****             12.7
30.48
564   py    12.7     $ South Side of Boral Shutter                      ****              0.0
12.7
565   py   -12.7     $ North Side of Boral Shutter #2                   ****              0.0
-12.7
566   py   -30.48    $ South Side of Boral Shutter #2                   ****            -12.7
-30.48
567   py    38.1     $ Outer North Side of Boral Plate                  ****
568   py   -38.1     $ Outer South Side of Boral Plate                  ****
569   py    40.05    $ Outer North Side of Al Backing                   ****
570   py   -40.05    $ Outer South Side of Al Backing                   ****
c
c --- Elevator Specimen Tube ---------------------------------------------
c
571   pz   131.20543 $ Top of Elevator Tube                             ****
572   pz    61.99043 $ Bottom of Elevator Tube                          ****
573   px   504.19005 $ Back Face of Elevator Tube                       ****
574   px   498.79255 $ Beginning of Rectangular Portion of E-Tube       ****
575   py    15.875   $ North Inside Wall of E-Tube                      ****
576   py    16.51    $ North Outside Wall of E-Tube                     ****
577   py   -15.875   $ South Inside Wall of E-Tube                      ****
578   py   -16.51    $ South Outside Wall of E-Tube                     ****
579   px   504.03003 $ Inner East Wall of E-Tube                        ****
580   pz   138.82543 $ Top of Top Flange of E-Tube                      ****
581   pz   54.37043  $ Bottom of Bottom Flange on E-Tube                ****
582   pz  131.84043
583   pz   61.35543
c
c ------ Radii ------
c --------- East Beam Assembly ---------
601   c/x   0  96.59493   5.3975   $ Beam Filter Window
602   c/x   0  96.59493   4.52374  $ Beam Tube Window
603   c/x   0  96.59493   5.715    $ Beam Tube Window
```

```
604   c/x   0  96.59493  10.16     $ Beam Tube Inner Surface
605   c/x   0  96.59493  11.43     $ Beam Tube Outer Surface
606   c/x   0  96.59493  10.11936  $ Beam Tube Absorber Stop
607   c/x   0  96.59793  30.48     $ O.R. of Al sheet, Boral sheet and Steel Sleeve ****
608   c/x   0  96.59793  29.5275   $ I.R. of Steel Sleeve/O.R of Lead-Boral Filler  ****
609   c/x   0  96.59793  20.32     $ I.R. of Lead-Boral Filler/O.R. of Al Sleeve    ****
610   c/x   0  96.59793  19.05     $ I.R. of Al Sleeve/O.R. of Air Filled Space     ****
611   c/x   0  96.59793  17.78     $ I.R. of Air Filled Space/O.R. Boral Liner      ****
612   c/x   0  96.59793  17.145    $ I.R. of Boral Liner                            ****
613   c/x   0  96.59493   9.4869   $ I.R. of Boral Liner before thru-wall           ****
c
631   c/x   0  96.59793  4.445    $ Disc Absorber Inner Hole
632   c/x   0  96.59793 10.1346   $ Disc Absorber Outer Surface
633   k/x  28.74579 0  96.59793 0.003741 1  $ Bottom Hole in Block Absorber
634   k/x  46.42537 0 103.57993 0.0044895 1   $ Top Hole in Block Absorber
c
c ---- Multi-Foil Array ------------------------------------------------------
c
690   c/x  -6.35  102.31  0.635  $ Foil Position #1             (Upper Most Right Corner of
Array)
691   c/x  -3.81  102.31  0.635  $ Foil Position #2
692   c/x  -1.27  102.31  0.635  $ Foil Position #3
693   c/x   1.27  102.31  0.635  $ Foil Position #4
694   c/x   3.81  102.31  0.635  $ Foil Position #5
695   c/x   6.35  102.31  0.635  $ Foil Position #6
696   c/x  -6.35   99.77  0.635  $ Foil Position #7
697   c/x  -3.81   99.77  0.635  $ Foil Position #8
698   c/x  -1.27   99.77  0.635  $ Foil Position #9
699   c/x   1.27   99.77  0.635  $ Foil Position #10
700   c/x   3.81   99.77  0.635  $ Foil Position #11
701   c/x   6.35   99.77  0.635  $ Foil Position #12
702   c/x  -6.35   97.23  0.635  $ Foil Position #13
703   c/x  -3.81   97.23  0.635  $ Foil Position #14
704   c/x  -1.27   97.23  0.635  $ Foil Position #15
705   c/x   1.27   97.23  0.635  $ Foil Position #16
706   c/x   3.81   97.23  0.635  $ Foil Position #17
707   c/x   6.35   97.23  0.635  $ Foil Position #18
708   c/x  -3.81   94.69  0.635  $ Foil Position #19             (Last Row Far Right Corner)
709   c/x  -1.27   94.69  0.635  $ Foil Position #20
710   c/x   1.27   94.69  0.635  $ Foil Position #21
711   c/x   3.81   94.69  0.635  $ Foil Position #22
712   c/x   6.35   94.69  0.635  $ Foil Position #23             (Bottom Most Left Corner of
Array)
713   px  504.81743              $ 0.005"  (0.0127 cm)
715   px  504.82251              $ 0.003"  (0.00762 cm)
716   px  504.80473              $ 0.010"  (0.0254 cm)
717   px  504.35642              $ 0.1865" (0.47371 cm)
718   px  504.63963              $ 0.075"  (0.1905 cm)
719   px  504.81997              $ 0.004"  (0.01016 cm)
c
c ---- E-Tube Cylinders ------------------------------------------------------
c
720   c/z  498.15755 0 15.875     $ Inside Shell of E-Tube                        ****
721   c/z  498.15755 0 16.51      $ Outside Shell of E-Tube                       ****
722   c/z  498.15755 0 23.495     $ Outside of E-Tube Top/Bottom Flange           ****
c
c ---- Extra Surfaces --------------------------------------------------------
c
750   px  242.9891                $ West Face of Outer Wall of GS                ****
751   px  242.3541                $ West Face of Boral sheet of GS               ****
752   c/x   0 96.59793 91.44      $ Cylinder of Magnetite Grout (3 ft radius)    ****
c

c Data Cards ****************************************************************
c --- Water -------------------------------------------------------------------
m1     1001.70c 6.6600E-02   1002.70c 7.6599E-06   8016.70c 3.3291E-02
       8017.70c 1.2655E-05
c     Total     9.9912E-02
mt1    lwtr.10t hwtr.10t
c
c --- Air ---------------------------------------------------------------------
```

```
m2     1001.70c  5.0303E-07   1002.70c 5.7856E-11   7014.70c 3.9123E-05
       7015.70c  1.4451E-07   8016.70c 1.0800E-05   8017.70c 4.1056E-09
       18036.70c 7.9027E-10  18038.70c 1.4843E-10  18040.70c 2.3391E-07
        6000.70c 9.5977E-09   2003.70c 1.8051E-16   2004.70c 1.3176E-10
       36078.70c 1.0033E-13  36080.70c 6.5356E-13  36082.70c 3.3194E-12
       36083.70c 3.2936E-12  36084.70c 1.6339E-11  36086.70c 4.9590E-12
c      Total     5.0820E-05
c
c ------ SS 304 Beam Extensions ------
m46    26054.70c 3.5004E-03  26056.70c 5.4949E-02  26057.70c 1.2690E-03
       26058.70c 1.6888E-04  24050.70c 7.6491E-04  24052.70c 1.4751E-02
       24053.70c 1.6726E-03  24054.70c 4.1634E-04  28058.70c 5.5882E-03
       28060.70c 2.1526E-03  28061.70c 9.3571E-05  28062.70c 2.9834E-04
       28064.70c 7.5980E-05  25055.70c 8.7693E-04  14028.70c 7.9104E-04
       14029.70c 4.0167E-05  14030.70c 2.6478E-05   6000.70c 1.6044E-04
       15031.70c 3.4997E-05  16032.70c 2.1391E-05  16033.70c 1.7126E-07
       16034.70c 9.6669E-07  16036.70c 4.5067E-09
c      Total     8.7653E-02
mt46   fe56.12t
c
c ------ Al 6061 Beam Tubes ------
m52    13027.70c 5.8593E-02  24050.70c 2.6495E-06  24052.70c 5.1093E-05
       24053.70c 5.7936E-06  24054.70c 1.4421E-06  29063.70c 4.8671E-05
       29065.70c 2.1694E-05  12024.70c 5.2843E-04  12025.70c 6.6898E-05
       12026.70c 7.3655E-05  25055.70c 2.2197E-05  14028.70c 3.2037E-04
       14029.70c 1.6268E-05  14030.70c 1.0724E-05  26054.70c 5.9561E-06
       26056.70c 9.3499E-05  26057.70c 2.1593E-06  26058.70c 2.8736E-07
       30000.70c 3.1082E-05  22046.70c 2.1012E-06  22047.70c 1.8949E-06
       22048.70c 1.8776E-05  22049.70c 1.3779E-06  22050.70c 1.3193E-06
       27059.70c 6.8975E-06  28058.70c 4.7151E-06  28060.70c 1.8162E-06
       28061.70c 7.8950E-08  28062.70c 2.5173E-07  28064.70c 6.4108E-08
       50112.70c 3.3215E-08  50114.70c 2.2600E-08  50115.70c 1.1642E-08
       50116.70c 4.9788E-07  50117.70c 2.6298E-07  50118.70c 8.2935E-07
       50119.70c 2.9414E-07  50120.70c 1.1156E-06  50122.70c 1.5854E-07
       50124.70c 1.9826E-07
c      Total     5.9939E-02
mt52   al27.12t
c
c ------ Helium ------
m53    2003.70c 1.6794E-12   2004.70c 1.2258E-06
c      Total     1.2258E-06
c
c ------ Boron Nitride ------
m54    5010.70c 9.6267E-03    5011.70c 3.8749E-02   7014.70c 4.8197E-02
       7015.70c 1.7802E-04   13027.70c 6.8105E-07  79197.70c 6.3900E-09
       4009.70c 1.3966E-07   20040.70c 1.8899E-05  20042.70c 1.2614E-07
       20043.70c 2.6319E-08  20044.70c 4.0668E-07  20046.70c 7.7983E-10
       20048.70c 3.6457E-08  24050.70c 2.3980E-08  24052.70c 4.6243E-07
       24053.70c 5.2436E-08  24054.70c 1.3052E-08  29063.70c 1.3700E-08
       29065.70c 6.1063E-09  26054.70c 1.3173E-09  26056.70c 2.0679E-08
       26057.70c 4.7756E-10  26058.70c 6.3554E-11  19039.70c 6.9048E-07
       19040.70c 8.6626E-11  19041.70c 4.9830E-08  12024.70c 4.0904E-08
       12025.70c 5.1784E-09  12026.70c 5.7015E-09  25055.70c 3.2074E-08
       42092.70c 1.9468E-09  42094.70c 1.2135E-09  42095.70c 2.0885E-09
       42096.70c 2.1882E-09  42097.70c 1.2528E-09  42098.70c 3.1656E-09
       42100.70c 1.2633E-09  11023.70c 1.0949E-06  28058.70c 1.4599E-08
       28060.70c 5.6236E-09  28061.70c 2.4445E-10  28062.70c 7.7943E-10
       28064.70c 1.9850E-10  82204.70c 8.5042E-11  82206.70c 1.4639E-09
       82207.70c 1.3424E-09  82208.70c 3.1830E-09  14028.70c 9.9634E-05
       14029.70c 5.0592E-06  14030.70c 3.3350E-06  50112.70c 1.0284E-10
       50114.70c 6.9976E-11  50115.70c 3.6048E-11  50116.70c 1.5416E-09
       50117.70c 8.1427E-10  50118.70c 2.5679E-09  50119.70c 9.1075E-10
       50120.70c 3.4543E-09  50122.70c 4.9089E-10  50124.70c 6.1388E-10
       22046.70c 2.1687E-09  22047.70c 1.9557E-09  22048.70c 1.9379E-08
       22049.70c 1.4221E-09  22050.70c 1.3617E-09  23000.70c 2.4707E-08
       74182.70c 1.8142E-09  74183.70c 9.7965E-10  74184.70c 2.0976E-09
       74186.70c 1.9545E-09  30000.70c 1.9248E-08  40090.70c 7.0986E-09
       40091.70c 1.5480E-09  40092.70c 2.3662E-09  40094.70c 2.3979E-09
       40096.70c 3.8632E-10   8016.70c 3.3814E-03   8017.70c 1.2854E-06
c      Total     1.0026E-01
c
```

```
c ---- Polyethlyene --------------------------------
m57    1001.70c 7.9855E-02  6000.70c 3.9929E-02
c      Total    1.19784E-01
mt57   poly.10t
c
c ---- Lead ----------------------------------------
m58    82204.70c 0.0004618  82206.70c 0.0079495 82207.70c 0.0072898
       82208.70c 0.0172843
c      Total     0.0329854
c
c ---- 30% Borated Polyethylene --------------------
m59    6000.70c 3.6000E-02  5010.70c 4.0198E-03  5011.70c 1.618E-02
       1001.70c 6.1900E-02  8016.70c 8.0667E-05  8017.70c 3.200E-08
       26054.70c 1.3340E-06 26056.70c 2.116E-05 26057.70c 5.06E-07
       7014.70c 8.8500E-05  7015.70c 3.560E-07 14028.70c 1.023E-05
       14029.70c 5.2200E-07  14030.70c 3.440E-07
c      Total     1.183E-01
mt59   poly.10t
c
c ---- Indium --------------------------------------
m60    49113.70c 1.6448E-03  49115.70c 3.66957E-02
c      Total     3.83405E-02
c
c ------ Al 6061 Mounting Pad and Tank ------
m66   13027.70c 5.8593E-02  24050.70c 2.6495E-06  24052.70c 5.1093E-05
      24053.70c 5.7936E-06  24054.70c 1.4421E-06  29063.70c 4.8671E-05
      29065.70c 2.1694E-05  12024.70c 5.2843E-04  12025.70c 6.6898E-05
      12026.70c 7.3655E-05  25055.70c 2.2197E-05  14028.70c 3.2037E-04
      14029.70c 1.6268E-05  14030.70c 1.0724E-05  26054.70c 5.9561E-06
      26056.70c 9.3499E-05  26057.70c 2.1593E-06  26058.70c 2.8736E-07
      30000.70c 3.1082E-05  22046.70c 2.1012E-06  22047.70c 1.8949E-06
      22048.70c 1.8776E-05  22049.70c 1.3779E-06  22050.70c 1.3193E-06
      27059.70c 6.8975E-06  28058.70c 4.7151E-06  28060.70c 1.8162E-06
      28061.70c 7.8950E-08  28062.70c 2.5173E-07  28064.70c 6.4108E-08
      50112.70c 3.3215E-08  50114.70c 2.2600E-08  50115.70c 1.1642E-08
      50116.70c 4.9788E-07  50117.70c 2.6298E-07  50118.70c 8.2935E-07
      50119.70c 2.9414E-07  50120.70c 1.1156E-06  50122.70c 1.5854E-07
      50124.70c 1.9826E-07
c     Total     5.9939E-02
mt66   al27.12t
c
c ----- Boral -------------------------------------------------------
m210    5010.70c 9.6195E-04   5011.70c 3.8720E-03   6000.70c 1.2080E-03
        13027.70c 1.3144E-02
c       Total     0.019186
c
c ---- Cadmium ----------------------------------
m261    48106.70c 0.0005819  48108.70c 0.0004143  48110.70c 0.0058146
        48111.70c 0.0059589  48112.70c 0.0112336  48113.70c 0.0056889
        48114.70c 0.0133750  48116.70c 0.0034869
c       Total     0.0465543
c
c ---- Gold ------------------------------------------------------------
m263    79197.70c 0.0590087
c
c ---- Gadolinium ------------------------------------------------------
m264   64152.80c 0.0000605  64154.80c 0.0006596  64155.80c 0.0044781
       64156.80c 0.0061938  64157.80c 0.0047353  64158.80c 0.0075160
       64160.80c 0.0066143
c      Total     0.0302577
c
c ---- Mixture of Borated Polyethylene and Lead -----------------------
m265   82204.70c 0.01393    82206.70c 0.2398      82207.70c 0.2199
       82208.70c 0.5214     05010.70c 4.8755E-05  05011.70c 1.960E-04
       01001.70c 5.074E-05  01002.70c 6E-09       06000.70c 0.4565
c      Total     6.205  (Mass Density)
c
c ---- Foil Materials -------------------------------------------------
c
c ---- Indium ----------------------------------------------------------  $ 0.005" (x2)
m302   49113.70c 1.6448E-03  49115.70c 3.66957E-02
```

```
c      Total     3.83405E-02
c
c ---- Dysprosium -------------------------------
m303   66156.70c 0.0000177  66158.70c 0.0000301  66160.70c 0.0007380
       66161.70c 0.0059858  66162.70c 0.0080729  66163.70c 0.0078894
       66164.70c 0.0089555
c      Total     0.0316895
c
c ---- Cobalt ------------------------------------------------------------  $ 0.002"
m304   27059.70c 0.0909455
c
c ---- Copper ------------------------------------------------------------  $ 0.005" (x2)
m305   29063.70c 0.0587168  29065.70c 0.0261954
c      Total     0.0849123
c
c ---- Iron --------------------------------------------------------------  $ 0.005" (x2)
m306   26054.70c 0.0049630  26056.70c 0.0779087  26057.70c 0.0017993
       26058.70c 0.0002394
c      Total     0.0849104
mt306 fe56.12t
c
c ---- Molybdenum --------------------------------------------------------  $ 0.003"
m307   42092.70c 0.0093192  42094.70c 0.0058686  42095.70c 0.0101594
       42096.70c 0.0106917  42097.70c 0.0061572  42098.70c 0.0156432
       42100.70c 0.0062983
c      Total     0.0641376
c
c ---- Scandium ----------------------------------------------------------  $ 0.005"
m308   21045.70c 0.0400396
c
c ---- Tungsten ----------------------------------------------------------  $ 0.005"
m309   74180.80c 0.0000759  74182.80c 0.0167537  74183.80c 0.0090470
       74184.80c 0.0193710  74186.80c 0.0179738
c      Total     0.0632214
c
c ---- Mangnesium --------------------------------------------------------  $ 0.005"
m310   12024.70c 0.0340155  12025.70c 0.0043063  12026.70c 0.0047412
c      Total     0.0430630
c
c ---- Nickle ------------------------------------------------------------  $ 0.010"
m311   28058.70c 0.0621799  28060.70c 0.0239515  28061.70c 0.0010412
       28062.70c 0.0033198  28064.70c 0.0008453
c      Total     0.0913376
c
c ---- Sulfur ------------------------------------------------------------  $ 0.1865"
m312   16032.70c 0.0369293  16033.70c 0.0002916  16034.70c 0.0016523
       16036.70c 0.0000039
c      Total     0.0388770
c
c ---- Titanium ----------------------------------------------------------  $ 0.010"
m313   22046.70c 0.0046811  22047.70c 0.0042215  22048.70c 0.0418291
       22049.70c 0.0030697  22050.70c 0.0029392
c      Total     0.0567406
c
c ---- Vanadium ----------------------------------------------------------  $ 0.002"
m314   23050.80c 0.0001773  23051.80c 0.0707528
c      Total     0.0709301
c
c ---- Zinc --------------------------------------------------------------  $ 0.010"
m315   30064.80c 0.0323113  30066.80c 0.0182223  30067.80c 0.0026548
       30068.80c 0.0121241  30070.80c 0.0004009
c      Total     0.0657134
c
c ---- Zirconium ---------------------------------------------------------  $ 0.005"
m316   40090.70c 0.0221450  40091.70c 0.0048293  40092.70c 0.0073817
       40094.70c 0.0074807  40096.70c 0.0012052
c      Total     0.0430419
c
c ---- Aluminum ----------------------------------------------------------   $ 0.005"
m317   13027.70c 0.0602381
c
```

```
c ---- Sodium Chloride (NaCl) ------------------------------------------   $ 0.075" (x2)
m318   11023.70c 0.02233102  17035.70c 0.0166711  17037.70c 0.00563877
c      Total     0.0446204
c
c ---- 4.9% Lu-Al ------------------------------------------------------   $ 0.004"
m319   71175.70c 1.0753E-04  71176.70c 2.8693E-06  13027.70c 0.013894968
c      Total 0.014005369
mt319 al27.12t
c
c ---- Mn-Cu 81.3% -----------------------------------------------------   $ 0.002"
m320   29063.70c 2.3518E-03  29065.70c 1.0492E-03  25055.70c 1.71033E-02
c      Total 0.018720436
c
c ---- Argon Gas -------------------------------------------------------
m330   18036.70c 0.0000001 18040.70c 0.0000268

c      Total 0.0000269
c
c ---- Concrete --------------------------------------------------------
m331    1001.70c 0.030369     6000.70c 0.000286     8016.70c 0.049773
       11023.70c 0.000916    12024.70c 5.6873E-05  12025.70c 7.2000E-06
       12026.70c 7.9270E-06  13027.70c 0.001024    14028.70c 1.3855E-02
       14029.70c 7.0383E-04  14030.70c 4.6451E-04  19039.70c 3.3319E-03
       19040.70c 4.2000E-08  19041.70c 2.3960E-05  20040.70c 1.4395E-03
       20042.70c 9.6080E-06  20043.70c 2.0050E-06  20044.70c 3.1036E-05
       20046.70c 5.9000E-08  20048.70c 2.7770E-06  26054.70c 9.3520E-06
       26056.70c 1.4681E-04  26057.70c 3.3900E-06  26058.70c 4.5100E-07
c      Total     9.95E-02
c
c ---- 30% Borated Poly Neutron Shielding ----------------------------------
m332    6000.70c 3.6000E-02   5010.70c 4.0198E-03   5011.70c 1.6180E-02
        1001.70c 6.1900E-02   8016.70c 8.0669E-05   8017.70c 3.1000E-08
       26054.70c 1.3440E-06  26056.70c 2.1103E-05  26057.70c 4.8700E-07
       26058.70c 6.5000E-08   7014.70c 8.8576E-05   7015.70c 3.2400E-07
       14028.70c 1.0237E-05  14029.70c 5.2000E-07  14030.70c 3.4300E-07
c      Total     0.1183037
c
c ---- Tally Materials -------------------------------------------------
c
m333    22047.80c 1 $ Ti-47
m334    22048.80c 1 $ Ti-48
m335    49115.80c 1 $ In-115
m336    74186.80c 1 $ W-186
m337    25055.80c 1 $ Mn-55
m338    29063.80c 1 $ Cu-63
m342    28058.80c 1 $ Ni-58
m343    26056.80c 1 $ Fe-56
m344    71175.70c 1 $ Lu-175
m345    30064.80c 1 $ Zn-64
m346    11023.70c 1 $ Na-23
m347    12024.70c 1 $ Mg-24
m348    42098.70c 1 $ Mo-98
m349    49115.26y 1 $ In-115 Dosimetry Data
c
c ---- Boron Frit/Mangnetite -------------------------------------------
c      (w %)
m360    1001.70c -3.16E-03   5010.70c -4.12E-05   5011.70c -1.66E-04
        8016.70c -3.31E-01   9019.70c -4.58E-05  11023.70c -2.41E-04
       12000.60c -9.20E-03  13027.70c -2.31E-02  14000.60c -2.59E-02
       16000.60c -3.21E-03  19000.60c -1.99E-05  20000.60c -7.09E-02
       25055.70c -1.95E-03  26000.50c -4.65E-01  30000.70c -1.31E-04
       56130.70c -8.46E-06  56132.70c -8.06E-06  56134.70c -1.93E-04
       56135.70c -5.26E-04  56136.70c -6.27E-04  56137.70c -8.97E-04
       56138.70c -5.72E-03  22000.60c -5.33E-02  23000.70c -3.05E-03
       24000.50c -1.66E-03
c      Density = -3.595
c ---- Source Cards ----------------------------------------------------
c
sdef erg=d3 pos 53.16369 0 96.59493 rad=d2 ext 0 axs 1 0 0
     vec 1 0 0 dir=d1                                                    $ Beam origin
located at beam filter window inlet
```

```
si1 h 0  0.64279  0.86603  0.90631  0.92799  0.94693  0.96305  0.97629
         0.98664  0.99406  0.99851  1                                          $ Angular
direction range (90 deg to 0 deg) split into 11 Weighted bins (New Rod Height)
sp1   0  3.08E-01  2.19E-01  6.54E-02  4.70E-02  5.51E-02  6.40E-02
         6.90E-02  6.72E-02  5.59E-02  3.66E-02  1.26E-02                     $ Bin
probability
si2   0 5.3975                                                                $ Beam radius
range
sp2  -21 1                                                                    $ Power law
uniform area sampling
si3  h 0.00E+00  1.00E-09  1.75E-09  3.07E-09  5.39E-09  9.45E-09
       1.66E-08  2.91E-08  5.10E-08  8.94E-08  1.57E-07  2.75E-07
       4.82E-07  8.45E-07  1.48E-06  2.60E-06  4.56E-06  7.99E-06
       1.40E-05  2.46E-05  4.31E-05  7.55E-05  1.32E-04  2.32E-04
       4.07E-04  7.14E-04  1.25E-03  2.20E-03  3.85E-03  6.75E-03
       1.18E-02  2.08E-02  3.64E-02  6.38E-02  1.12E-01  1.96E-01
       3.44E-01  6.03E-01  1.06E+00  1.85E+00  3.25E+00  5.70E+00
       1.00E+01                                                               $ Energy
spectrum 42 equal logarithmic bins (43 bin edges)
sp3    0.000E+00  2.407E-04  5.964E-04  1.753E-03  5.082E-03  1.633E-02
       4.080E-02  8.847E-02  1.449E-01  1.476E-01  7.468E-02  1.940E-02
       1.046E-02  9.684E-03  9.533E-03  9.436E-03  9.394E-03  8.929E-03
       9.021E-03  9.050E-03  9.064E-03  9.250E-03  9.302E-03  9.178E-03
       8.887E-03  9.224E-03  9.189E-03  9.670E-03  9.298E-03  9.568E-03
       9.450E-03  9.529E-03  1.208E-02  1.049E-02  1.582E-02  1.965E-02
       2.419E-02  3.098E-02  4.235E-02  4.721E-02  4.243E-02  2.215E-02
       5.686E-03                                                              $ Energy
Spectrum Bin Probability (Beam Filter Window Source, New Rod Height)
c
c ---- Number of Particles to Simulate -------------------------------------
c
mode n
nps 8E+10
c ---- Tallies -------------------------------------------------------------
c
F14:n 5106
FM14 1 335 102
FC14 "(n,gamma) Reaction Rate of In Foil"
FT14 scx 3
c
F24:n 5107
FM24 1 337 102
FC24 "(n,gamma) Reaction Rate of Mn-Cu Foil"
FT24 scx 3
c
F34:n 5108
FM34 1 343 103
FC34 "(n,proton) Reaction Rate of Fe Foil"
FT34 scx 3
c
F44:n 5109
FM44 1 344 102
FC44 "(n,gamma) Reaction Rate of Lu-Al Foil"
FT44 scx 3
c
F54:n 5110
FM54 1 335 51                                          $ 51 = (n,n') to first excited state
FC54 "(n,n') Reaction Rate of In Foil"                 $ This is the reaction that has been
giving you results
FT54 scx 3
c
F254:n 5110
FM254  1 335 4                                         $  4 = Total Inelastic cross-section
FC254  "(n,n') Reaction Rate of In Foil"
FT254  scx 3
c
F354:n 5110
FM354  1 349 4                                         $  4 = Total Inelastic cross-section.
This is using Dosimetry Data for the material
FC354  "(n,n') Reaction Rate of In Foil"
FT354  scx 3
```

```
c
F74:n 5112
FM74 1 338 102
FC74 "(n,gamma) Reaction Rate of Cu Foil"
FT74 scx 3
c
F84:n 5113
FM84 1 345 103
FC84 "(n,proton) Reaction Rate of Zn Foil"
FT84 scx 3
c
F94:n 5114
FM94 1 346 102
FC94 "(n,gamma) Reaction Rate of NaCl Foil"
FT94 scx 3
c
c F104:n 5115                                          $ Even though these reactions were
detected by the
c FM104 1 317 107                                      $ gamma counter, the statistics were
too high.
c FC104 "(n,alpha) Reaction Rate of Al Foil"           $ 14% and 13%. They will be excluded
in future measurements
c FT104 scx 3
c
c F114:n 5116
c FM114 1 347 103
c FC114 "(n,proton) Reaction Rate of Mg Foil"
c FT114 scx 3
c
F124:n 5117
FM124 1 336 102
FC124 "(n,gamma) Reaction Rate of W Foil"
FT124 scx 3
c
F134:n 5118
FM134 1 342 103
FC134 "(n,proton) Reaction Rate of Ni Foil"
FT134 scx 3
c
F144:n 5119
FM144 1 333 103
FC144 "(n,proton) Reaction Rate of Ti-47 Foil"
FT144 scx 3
c
F2144:n 5119
FM2144 1 334 103
FC2144 "(n,proton) Reaction Rate of Ti-48 Foil"
FT2144 scx 3
c
F164:n 5121
FM164 1 263 102
FC164 "(n,gamma) Reaction Rate of Gold Foil"
FT164 scx 3
c
F174:n 5122
FM174 1 348 102
FC174 "(n,gamma) Reaction Rate of Mo Foil"
FT174 scx 3
c
F204:n 5125
FM204 1 308 102
FC204 "(n,gamma) Reaction Rate of Sc Foil"
FT204 scx 3
c

F214:n 5126
FM214 1 304 102
FC214 "(n,gamma) Reaction Rate of Co Foil"
FT214 scx 3
c
```

```
c F224:n 5127                                                    $ These two reactions were not
accurately counted when
c FM224 1 318 107                                                $ measurements were taken. They
will be left out for now.
c FC224 "(n,alpha) Reaction Rate of NaCl Foil"
c FT224 scx 3
c
c F234:n 5128
c FM234 1 312 103
 FC234 "(n,proton) Reaction Rate of S Foil"
 FT234 scx 3
c
print


F12:n 534  $ Front Face of Aluminum Plate behind foils
SD12  767.74
c
```

Appendix E: MCNP vs UMG Analysis.

Appendix E-1. SPR values for Hybrid spectrum.

Reaction of Interest	Bare SPR	Cd Covered SPR	
In-115(n,γ)In-116m	3.228E+13	3.561E+13	
Mn-55(n,γ)Mn-56	3.783E+13	5.533E+13	
Lu-175(n,γ)Lu-176m	2.252E+12	2.447E+12	
Cu-63(n,γ)Cu-64	3.425E+13	4.297E+13	
Zn-64(n,p)Cu-64	1.867E+13	1.733E+13	
Na-23(n,γ)Na-24	1.720E+13	2.236E+13	
W-186(n,γ)W-187	1.830E+13	1.822E+13	
Ni-58(n,p)Co-58	2.436E+13	2.324E+13	
Ti-47(n,p)Sc-47	2.864E+12	--	
Au-197(n,γ)Au-198	3.969E+13	6.241E+13	
Mo-98(n,γ)Mo-99	1.215E+13	1.044E+13	
Sc-45(n,γ)Sc-46	4.170E+13	--	
Co-59(n,γ)Co-60	4.981E+13	6.020E+13	**Overall**
Average	2.549E+13	3.187E+13	2.868E+13

Appendix E-2. SPR values for GRAVEL spectrum.

Reaction of Interest	Bare SPR	Cd Covered SPR	
In-115(n,γ)In-116m	4.973E+13	1.250E+14	
Mn-55(n,γ)Mn-56	4.701E+13	5.429E+13	
Lu-175(n,γ)Lu-176m	2.682E+12	2.968E+12	
Cu-63(n,γ)Cu-64	4.255E+13	4.698E+13	
Zn-64(n,p)Cu-64	8.062E+12	7.535E+12	
Na-23(n,γ)Na-24	2.135E+13	2.783E+13	
W-186(n,γ)W-187	2.135E+13	1.866E+13	
Ni-58(n,p)Co-58	1.124E+13	1.069E+13	
Ti-47(n,p)Sc-47	1.302E+12	--	
Au-197(n,γ)Au-198	6.170E+13	1.466E+14	
Mo-98(n,γ)Mo-99	1.207E+13	1.171E+13	
Sc-45(n,γ)Sc-46	5.499E+13	--	
Co-59(n,γ)Co-60	5.994E+13	7.060E+13	**Overall**
Average	3.031E+13	4.753E+13	3.892E+13

Appendix E-3. Simulated vs actual activities: MCNP, GRAVEL, and Hybrid spectra.

Reaction	Measured	±%	GRAVEL	±%	Hybrid	±%	MCNP	±%
In-115(n,γ)In-116m	6.401E+05	3.00%	3.901E+05	1.71%	5.687E+05	2.12%	1.445E+06	0.92%
In-115(n,γ)In-116m*	2.398E+05	3.00%	7.463E+04	3.76%	1.931E+05	2.72%	2.306E+05	2.72%
Mn-55(n,γ)Mn-56	3.056E+04	3.00%	1.970E+04	1.74%	2.317E+04	1.63%	6.618E+04	0.77%
Mn-55(n,γ)Mn-56*	6.142E+03	3.00%	4.403E+03	2.52%	3.183E+03	2.15%	5.136E+03	2.73%
Lu-175(n,γ)Lu-176m	2.446E+03	10.00%	2.763E+04	5.09%	3.115E+04	4.66%	4.957E+04	2.79%
Lu-175(n,γ)Lu-176m*	2.131E+03	10.00%	2.795E+04	3.27%	2.498E+04	9.24%	3.631E+04	6.32%
Cu-63(n,γ)Cu-64	1.084E+04	3.00%	7.722E+03	2.57%	9.077E+03	2.87%	2.491E+04	1.01%
Cu-63(n,γ)Cu-64*	2.446E+03	15.00%	2.026E+03	5.78%	1.632E+03	5.58%	2.273E+03	6.32%
Zn-64(n,p)Cu-64	1.265E+03	3.00%	4.757E+03	0.50%	1.944E+03	0.66%	5.672E+02	0.97%
Zn-64(n,p)Cu-64*	1.180E+03	22.00%	6.097E+03	0.22%	1.953E+03	0.31%	7.119E+02	0.62%
Na-23(n,γ)Na-24	4.662E+03	3.00%	6.618E+03	1.38%	7.775E+03	1.39%	2.285E+04	0.62%
Na-23(n,γ)Na-24*	5.772E+02	4.00%	8.073E+02	1.18%	7.402E+02	1.09%	1.095E+03	1.04%
W-186(n,γ)W-187	3.215E+04	3.00%	4.564E+04	4.82%	5.040E+04	4.28%	1.183E+05	1.67%
W-186(n,γ)W-187*	1.362E+04	3.00%	2.840E+04	4.67%	2.144E+04	4.37%	3.464E+04	4.41%
Ni-58(n,p)Co-58	6.327E+01	3.00%	1.706E+02	0.48%	7.449E+01	0.66%	2.118E+01	0.89%
Ni-58(n,p)Co-58*	5.994E+01	4.00%	2.183E+02	0.21%	7.398E+01	0.29%	2.682E+01	0.55%
Ti-47(n,p)Sc-47	1.735E+01	5.00%	4.039E+02	0.47%	1.737E+02	0.63%	5.047E+01	0.91%
Au-197(n,γ)Au-198	2.538E+04	3.00%	1.247E+04	2.97%	1.834E+04	3.41%	1.163E+04	3.66%
Au-197(n,γ)Au-198*	1.602E+04	3.00%	4.254E+03	5.41%	7.362E+03	3.68%	4.313E+04	1.20%
Mo-98(n,γ)Mo-99	1.373E+02	3.00%	3.446E+02	9.49%	3.240E+02	10.84%	3.471E+02	5.72%
Mo-98(n,γ)Mo-99*	1.095E+02	4.00%	3.641E+02	4.56%	3.008E+02	4.53%	3.494E+02	7.03%
Sc-45(n,γ)Sc-46	2.775E+02	4.00%	1.529E+02	1.64%	1.908E+02	1.92%	5.762E+02	0.73%
Co-59(n,γ)Co-60	2.198E+01	5.00%	1.111E+01	2.20%	1.265E+01	1.96%	3.684E+01	0.80%
Co-59(n,γ)Co-60*	5.328E+00	9.00%	2.937E+00	3.85%	2.538E+00	3.26%	3.962E+00	3.24%

**Cadmium covered foil.*

Appendix E-4. Neutron energy spectrum at the ERS Image Plane.

Lower Energy Bin Edge (MeV)	F2 Tally at ERS Image Plane	±%	Neutron Flux (n/cm^2-s/MeV)	Neutron Flux (n/cm^2-s)
1.00E-09	7.355E-11	5.21%	2.109E+12	2.109E+03
1.75E-09	1.042E-10	4.39%	3.986E+12	2.990E+03
3.07E-09	4.097E-10	2.37%	8.900E+12	1.175E+04
5.39E-09	1.023E-09	1.66%	1.265E+13	2.934E+04
9.45E-09	3.693E-09	0.84%	2.608E+13	1.059E+05
1.66E-08	8.461E-09	0.54%	3.394E+13	2.427E+05
2.91E-08	1.923E-08	0.37%	4.412E+13	5.515E+05
5.10E-08	3.123E-08	0.28%	4.089E+13	8.956E+05
8.94E-08	3.152E-08	0.29%	2.354E+13	9.040E+05
1.57E-07	1.567E-08	0.42%	6.646E+12	4.493E+05
2.75E-07	6.019E-09	0.63%	1.463E+12	1.726E+05
4.82E-07	5.703E-09	0.69%	7.901E+11	1.635E+05
8.45E-07	5.689E-09	0.68%	4.494E+11	1.632E+05
1.48E-06	5.745E-09	0.68%	2.595E+11	1.648E+05
2.60E-06	5.751E-09	0.69%	1.473E+11	1.649E+05
4.56E-06	5.785E-09	0.73%	8.465E+10	1.659E+05
7.99E-06	5.893E-09	0.69%	4.928E+10	1.690E+05
1.40E-05	6.252E-09	0.68%	2.983E+10	1.793E+05
2.46E-05	6.759E-09	0.68%	1.829E+10	1.938E+05
4.31E-05	7.257E-09	0.64%	1.125E+10	2.081E+05
7.55E-05	7.755E-09	0.66%	6.865E+09	2.224E+05
1.32E-04	8.117E-09	0.63%	4.120E+09	2.328E+05
2.32E-04	8.605E-09	0.63%	2.468E+09	2.468E+05
4.07E-04	9.448E-09	0.63%	1.548E+09	2.709E+05
7.14E-04	1.025E-08	0.59%	9.572E+08	2.939E+05
1.25E-03	1.119E-08	0.58%	5.985E+08	3.208E+05
2.20E-03	1.171E-08	0.57%	3.534E+08	3.357E+05
3.85E-03	1.282E-08	0.55%	2.229E+08	3.678E+05
6.75E-03	1.347E-08	0.51%	1.332E+08	3.863E+05
1.18E-02	1.593E-08	0.49%	9.047E+07	4.569E+05
2.08E-02	2.163E-08	0.42%	6.894E+07	6.205E+05
3.64E-02	2.512E-08	0.43%	4.618E+07	7.204E+05
6.38E-02	2.972E-08	0.38%	3.111E+07	8.525E+05
1.12E-01	4.897E-08	0.33%	2.914E+07	1.404E+06
1.96E-01	7.245E-08	0.27%	2.474E+07	2.078E+06
3.44E-01	1.131E-07	0.21%	2.191E+07	3.243E+06
6.03E-01	1.775E-07	0.17%	1.965E+07	5.090E+06
1.06E+00	3.442E-07	0.11%	2.160E+07	9.872E+06
1.85E+00	4.277E-07	0.09%	1.553E+07	1.227E+07
3.25E+00	5.815E-07	0.07%	1.191E+07	1.668E+07
5.70E+00	2.715E-07	0.10%	3.178E+06	7.785E+06
1.00E+01	6.697E-08	0.18%	4.466E+05	1.921E+06

Appendix F: Experimental Validation of the MCNP6 East Beam Line Model

Gold Foil Measurements vs MCNP6

The calculations performed by MCNP6 throughout this thesis project must be verified against real data to ensure that the model is simulating the physics correctly. The method used in this section involves comparison of the gold foil measurements, bare and cadmium covered, to an identical set created in the MCNP environment. Cadmium and bare foil sets were used to determine if the model is accurately simulating not only the thermal energy region of neutrons but also the epi-thermal. The epi-thermal region is important in this particular case because the ERS neutron beam has a very low cadmium ratio indicating that there is a rather large contribution of epi-thermal neutrons to the image plane flux.

There were four separate measurements taken of the 21 foil array, two sets of bare foils and two sets of cadmium covered resulting in a total of 84 measurements. The measured results for each set can be found in sections 4.1 and 4.3. The 21 foil array was built in MCNP6 using the model that determined the initial neutron energy spectrum and the response functions of the multi-foil array. As mentioned earlier in the thesis there must be a de-normalization factor involved in MCNP calculations convert the tally output from per source particle (n/cm2-sp) to units of neutron flux (n/cm^2-s). A factor can be determined based on reactor power level using the following two equations:

$$DF_{NRAD} = \frac{P * \eta}{E_f * 1.6 \times 10^{13}} \tag{26}$$

$$DF_{ERS} = DF_{NRAD} * F2\ Tally\ Result * A_x \tag{27}$$

The number of source particles (neutrons) passing through a surface can be found by correlating the reactor power level (P), the energy released per fission (E_f) and the number of neutrons produced per fission (η) in the reactor core [1]. The equations above show the correlation and how a de-normalization factor (DF_{NRAD}) was first calculated for the NRAD reactor MCNP model and then a new de-normalization factor (DF_{ERS}) was calculated from combining the NRAD factor with the F2 tally, where A_x is the cross-sectional area of the surface the tally was placed on and the number, 1.6x10^{13}, is a conversion term from MeV to joules. The de-normalized factor equations result in a value with units of *sp/s*, which when multiplied by the F2 and F4 tally results, produce a neutron flux with units of *n/cm^2-s*. The following assumptions were made when calculating the two de-normalization factors for the model:

P	=	250 kWth
E_f	=	200 MeV/fission
η	=	2.44 neutrons/fission

The area was taken at the beam filter window in the NRAD model and was determined to be 91.524 cm^2. The location of the beam filter window relative to the core taken can be seen in Figure *19*. The reactor power dependent, de-normalized factor for the ERS was determined to be 3.945x10^{13} sp/s.

Two tallies were taken of each foil, an unmodified volume averaged tally (F14) and a modified volume averaged tally (F24). The F24 tally was used to determine the reaction rate of

each foil and the corresponding units can be seen in the FC24 card. The tally set up and results can be seen below.

```
F14:n 5106 5107 5108 5109 5110 5111 5112 5113 5114 5115 5116 5117
      5118 5119 5120 5121 5122 5123 5124 5125 5126
c
F24:n 5106 5107 5108 5109 5110 5111 5112 5113 5114 5115 5116 5117
      5118 5119 5120 5121 5122 5123 5124 5125 5126
FM24  1 263 102
FC24  "(n,gamma) Reaction Rate of Gold Foil (n-b/cm^2-sp)"
```

Figure 2. Reaction rate determination of the 21 gold foil array.

Table 1. F14 and F24 tally results of bare 21 gold foil array.

F14 Tally (n/cm^2-sp)	Error	F24 Tally Result (n-b/cm^2-sp)	Error
1.402E-06	1.63%	3.340E-05	4.14%
1.379E-06	1.56%	3.244E-05	3.91%
1.334E-06	1.58%	3.157E-05	3.40%
1.424E-06	1.88%	3.694E-05	8.03%
1.392E-06	1.62%	3.411E-05	4.94%
1.374E-06	1.78%	3.366E-05	5.79%
1.412E-06	1.90%	3.501E-05	6.21%
1.389E-06	1.58%	3.335E-05	3.48%
1.323E-06	1.57%	3.237E-05	4.06%
1.380E-06	2.18%	3.469E-05	5.46%
1.416E-06	1.63%	3.168E-05	3.83%
1.351E-06	1.76%	3.323E-05	5.04%
1.398E-06	1.61%	3.349E-05	3.75%
1.403E-06	1.81%	3.424E-05	4.36%
1.370E-06	2.59%	3.253E-05	4.31%
1.404E-06	2.11%	3.294E-05	3.92%
1.394E-06	2.46%	3.424E-05	6.20%
1.340E-06	1.46%	3.156E-05	4.35%
1.357E-06	1.99%	3.615E-05	7.53%
1.378E-06	1.87%	3.213E-05	3.19%
1.328E-06	1.48%	3.097E-05	3.79%

The activities can be calculated from these tallies by using Equation 24. The parameters for this equation can be found in the table directly below.

$$A_{MCNP} = F24 * DF_{ERS} * N * V * (1 - \exp(-\lambda t)) \quad (28)$$

Table 2. Equation 3 parameters.

Parameter	Value	Units
De-normalization Factor (DF_{ERS})	$3.945x10^{13}$	*sp/s*
Atom Density (N)	$5.663x10^{-2}$	*atoms/cm*^{3}
Volume (V)	$6.435x10^{-3}$	*cm*^{3}
Decay Constant (λ)	$2.980x10^{-6}$	*s*$^{-1}$
Time of Irradiation (t)	$1.800x10^{4}$	*s*

The MCNP calculated activities were compared to the averaged measured activities in the beam. The results show a large discrepancy between the two sets of data.

Table 3. MCNP vs measured bare gold foil activities.

	MCNP Activity (dps)	Measured Activity (dps)	Ratio
	2.530E+04	1.795E+04	1.41
	2.464E+04	1.765E+04	1.40
	2.350E+04	1.743E+04	1.35
	2.755E+04	1.769E+04	1.56
	2.575E+04	1.813E+04	1.42
	2.516E+04	1.736E+04	1.45
	2.608E+04	1.788E+04	1.46
	2.509E+04	1.806E+04	1.39
	2.432E+04	1.799E+04	1.35
	2.584E+04	1.784E+04	1.45
	2.384E+04	1.802E+04	1.32
	2.475E+04	1.780E+04	1.39
	2.501E+04	1.784E+04	1.40
	2.574E+04	1.839E+04	1.40
	2.418E+04	1.806E+04	1.34
	2.444E+04	1.780E+04	1.37
	2.559E+04	1.765E+04	1.45
	2.353E+04	1.780E+04	1.32
	2.707E+04	1.758E+04	1.54
	2.440E+04	1.795E+04	1.36
	2.418E+04	1.825E+04	1.33
Average	2.505E+04	1.786E+04	1.40

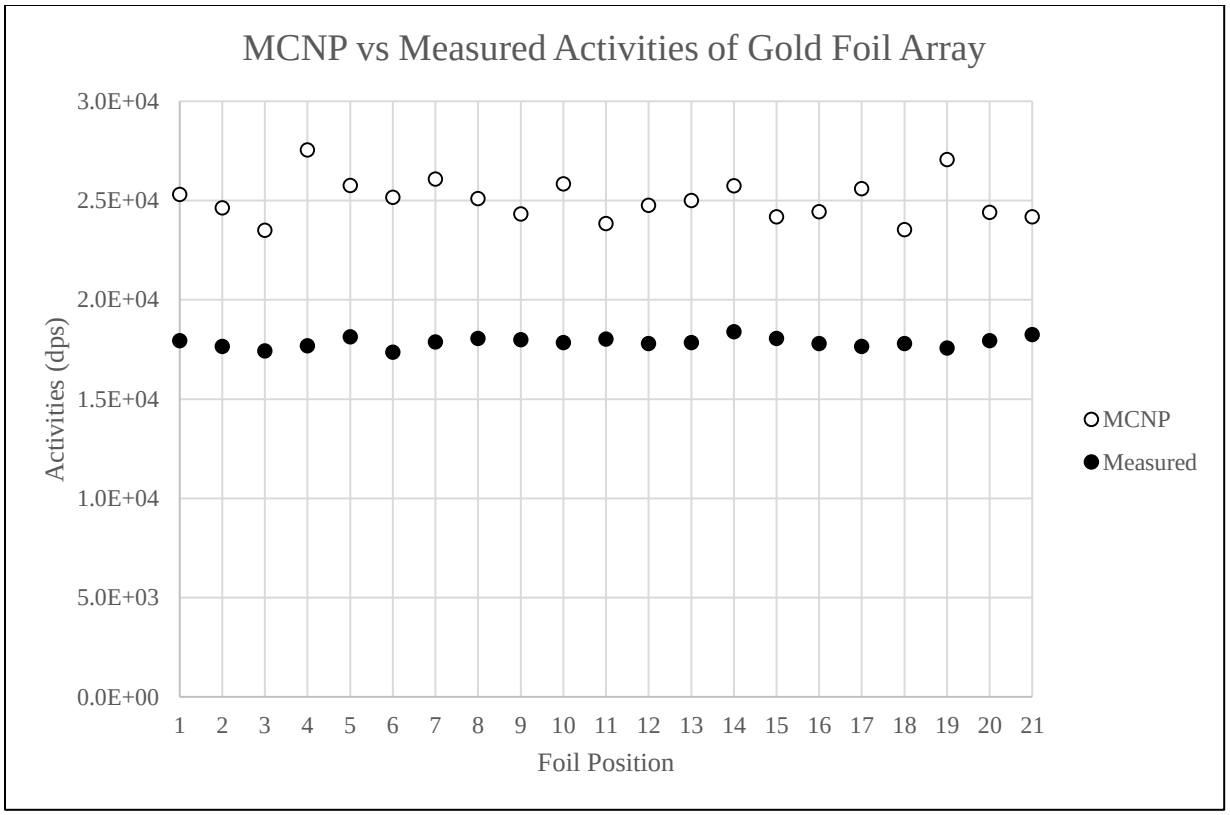

Figure 1. MCNP vs measured activities for the bare 21-gold foil array.

MCNP calculates an average of 40% higher activity values than what was measured in the ERS beam. It should be noted that the beam profile is still relatively uniform across the image plane based on the MCNP model. To fully understand how and why the model is simulating more neutrons, the same measurements were simulated for the cadmium covered 21-gold foil array. These simulated results for the F14 and F24 tallies can be seen below along with the comparison between the MCNP calculated activities and the measured activities.

Table 4. MCNP vs measured cadmium covered gold foil activities.

F14 Tally (n/cm^2-sp)	Error	F24 Tally Result ($n\text{-}b/cm^2$-sp)	Error	MCNP Activity (dps)	Measured Activity (dps)	Ratio
1.068E-06	1.92%	6.962E-06	8.10%	5.222E+03	8.327E+03	0.63
1.067E-06	2.01%	6.892E-06	8.58%	5.160E+03	8.475E+03	0.61
1.036E-06	1.86%	6.270E-06	7.15%	4.711E+03	8.438E+03	0.56
1.082E-06	2.01%	7.253E-06	7.59%	5.449E+03	8.290E+03	0.66
1.037E-06	1.76%	7.425E-06	8.62%	5.536E+03	8.549E+03	0.65
1.060E-06	2.17%	6.102E-06	7.38%	4.565E+03	8.623E+03	0.53
1.096E-06	2.07%	7.857E-06	8.50%	5.878E+03	8.327E+03	0.71
1.065E-06	1.86%	6.380E-06	7.88%	4.813E+03	8.475E+03	0.57
1.067E-06	2.61%	6.122E-06	7.38%	4.588E+03	8.623E+03	0.53
1.086E-06	1.91%	7.176E-06	7.90%	5.364E+03	8.623E+03	0.62
1.077E-06	2.08%	6.913E-06	8.69%	5.193E+03	8.808E+03	0.59
1.058E-06	2.20%	6.828E-06	10.00%	5.104E+03	8.660E+03	0.59
1.084E-06	1.82%	6.481E-06	9.22%	4.849E+03	8.475E+03	0.57
1.074E-06	2.42%	7.679E-06	8.15%	5.721E+03	8.438E+03	0.68
1.027E-06	1.86%	6.624E-06	8.84%	4.922E+03	8.623E+03	0.57
1.041E-06	1.74%	7.404E-06	8.65%	5.562E+03	8.771E+03	0.63
1.070E-06	2.04%	7.286E-06	8.49%	5.464E+03	8.845E+03	0.62
1.037E-06	1.74%	5.758E-06	7.51%	4.293E+03	8.512E+03	0.50
1.043E-06	1.75%	6.418E-06	8.04%	4.778E+03	8.623E+03	0.55
1.060E-06	2.18%	6.042E-06	7.96%	4.509E+03	8.586E+03	0.53
1.023E-06	1.75%	6.786E-06	8.29%	5.157E+03	8.697E+03	0.59
			Average	5.088E+03	8.562E+03	0.59

The cadmium covered foils simulate a lower activity than what was measured. The activities are 40% lower which is the same difference the bare foil measurements had. The cadmium ratio of the gold foils was compared next. The experimentally measured ratio was roughly 2 and the average cadmium ratio calculated by MCNP was about 5. It can be concluded from the data presented that the thermal region in the model is 40% larger than experimental measurements suggest. Based on this conclusion the source particle rate (SPR) technique was used in the neutron energy spectrum modeling portion of the thesis. This technique fits the MCNP data to the activities measured in the beam but can only be useful for the particular environment the foils were exposed to experimentally. The draw back here is that each time the reactor power changes, new measurements must be taken to confirm MCNP can match the data.

Appendix G: Shielding Analysis in ERS for an HPGe Detector

Introduction

A HPGe detector will be set up in the east radiography station (ERS) to measure the gamma energy spectrum of the neutron beam from the Neutron Radiography (NRAD) reactor. An external, electrical cooling system will be mounted to the detector and is composed of electronic and mechanical parts that help keep the detector at a steady operational temperature. These pieces must be shielded from the majority of neutrons and gammas that can cause damage if not properly attenuated.

The entire East Radiography Station has a high neutron flux background outside the neutron beam line. This indicates that the neutrons are scattering as soon as they leave the through-wall collimator and are dispersing throughout the room. The dispersion leads to activation of materials and objects that are out of the direct line of the neutron beam. Due to this recently discovered problem a more careful approach must be taken when considering shielding configurations for the HPGe detector.

It would be prudent to talk briefly about the effects neutrons have on HPGe detectors and why it is desired to have as little neutron interaction as possible with the semiconductor crystal in the detector.

Issues with Neutron Damage on HPGe Detector Crystals

An experiment was performed on n-type HPGe detectors that used a ^{252}Cf source to determine the amount of neutron fluence required to distort the read out of the detector [52]. The source was emitting $1x10^7$ n/s with a flux of 1300 n/cm^2-s impinging on the detector face. They determined that the full-width half-maxed (FWHM) of a ^{60}Co 1.33 MeV gamma peak, from a separate source, started to expand when the detector was exposed to about $4x10^8$ n/cm^2. This study was used as a guide line to set the limits for the maximum allowable neutron flux incident on the HPGe detector for the ERS experiments.

The required time to allow the detector to accumulate the amount of counts necessary to obtain reasonable statistics may be at least five minutes. Using five minutes as the maximum allowable time for the detector to be exposed it can be assumed that enough data will be collected if the neutron flux incident on the crystal is $1.3x10^6$ n/cm^2-s.

The assumption above is only valid for the detector crystal. The main electronics that compose the multi-channel analyzer, the pre-amplifier, and the high-voltage supply among others, will all be safely outside of the ERS and insulated cords will connect the detector crystal and cooling system. The integrated cryo-cooling system (ICS) will be attached to the detector and placed inside the ERS. The ICS is mechanically cooled so a majority of the parts inside the box do not need attention [53]. According to an Ortec representative, there is no reason to suspect that the ICS will be effected by neutron damage [54].

MCNP Assistance

The same MCNP6 model used in the neutron energy spectrum determination was used to obtain an approximation of the magnitude of neutron dose. MCNP was used to analyze an evolving shielding arrangement that could offer adequate protection against the neutrons and photons

emitted from the NRAD reactor core. Shielding materials must first be studied to determine which ones will work best for this specific scenario. The effectiveness of a shielding material depends highly on the type and energy of the particle that is to be attenuated. In these circumstances, photons and neutrons are the particles of interest and the type of energy spectra that can be expected are that of a thermal neutron reactor.

MCNP6 was used to calculate a source definition for both photons and neutrons, this source was used in the ERS model to calculate neutron flux and photon dose rate at various positions in the room. The neutron and photon sources were derived from the NRAD reactor model using the same process described in section 3.6.3 of the thesis with a few minor differences. A separate F2 tally was created for the photon source and can be seen in the figure below. This tally has an equal logarithmic energy distribution from 0.01 MeV to 20 MeV that only tracks the photons passing from the reactor to the ERS. A picture of the ERS MCNP model can be seen in Figure 2.

```
F32:p   677
*C32    90.000   50.000   30.000 25.000 21.875  18.75  15.625
        12.5     9.375    6.25   3.125   0
F42:p   677
*C42    90  0
E42     0.01 48ilog 20
```

Figure 1. F2 tally used to create NRAD photon source.

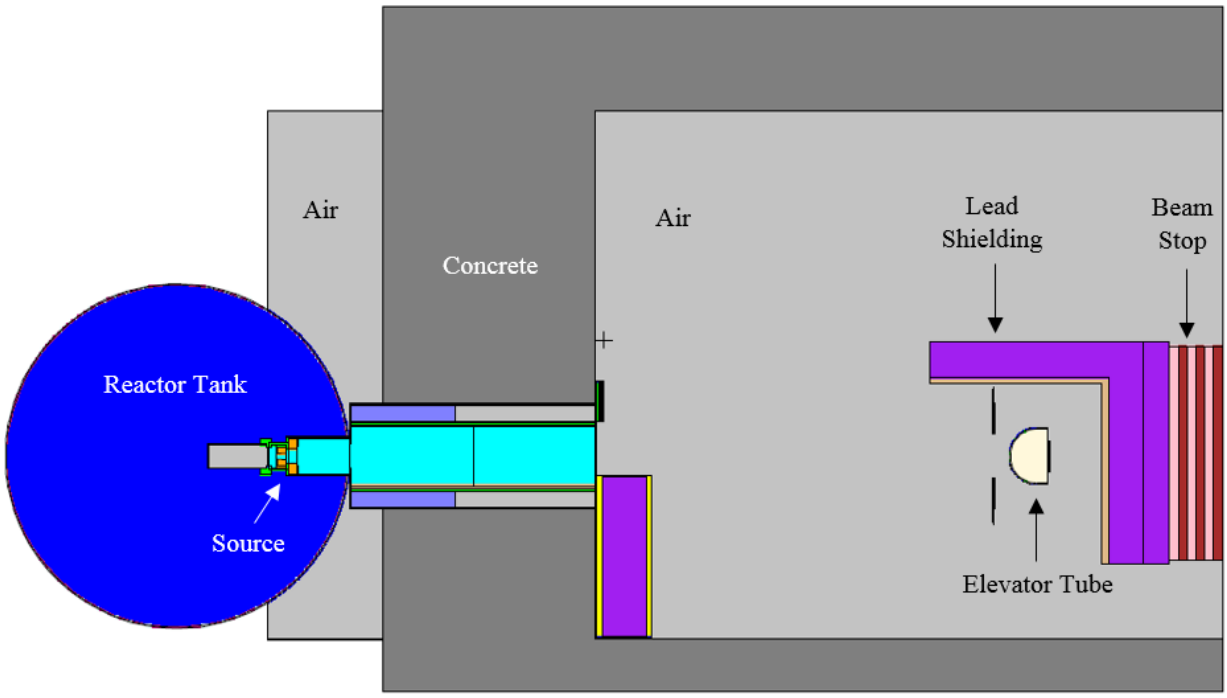

Figure 2. MCNP6 Model of the East Radiography Station.

The first stage of the analysis will consider primary neutrons from the reactor core and secondary photons created by neutron interactions with the surrounds. An F4 tally was placed in the model where the detector system will be. This tally will calculate the neutron flux magnitude

in that region with no shielding and will be compared to similar tallies taken behind shielding. This will allow the effectiveness of each shielding arrangement to be measured. An initial FMESH of the model was also added to the input file. Simulating 100 million neutrons emitted from the source the FMESH will be plotted over the entire area of the ERS room. An FMESH uses the same principles as the F4 volume tally. It is a track-length tally that calculates the average flux through a specified mesh volume. The FMESH can then be plotted as a function of F4 intensity along the desired area [41]. The top view of the FMESH performed over the entire ERS model can be seen in Figure 3 with the neutron flux values as a function of color printed on the right-hand side. The side view of the FMESH is shown in Figure 4. It should be noted that all MCNP runs were scaled to a reactor power of 5 Watts, this is the desired operating power when using the HPGe detector in the ERS. The scaling factor calculated uses the same equation and parameters discussed in section 0 (Appendix C) with the reactor power being the only value changing.

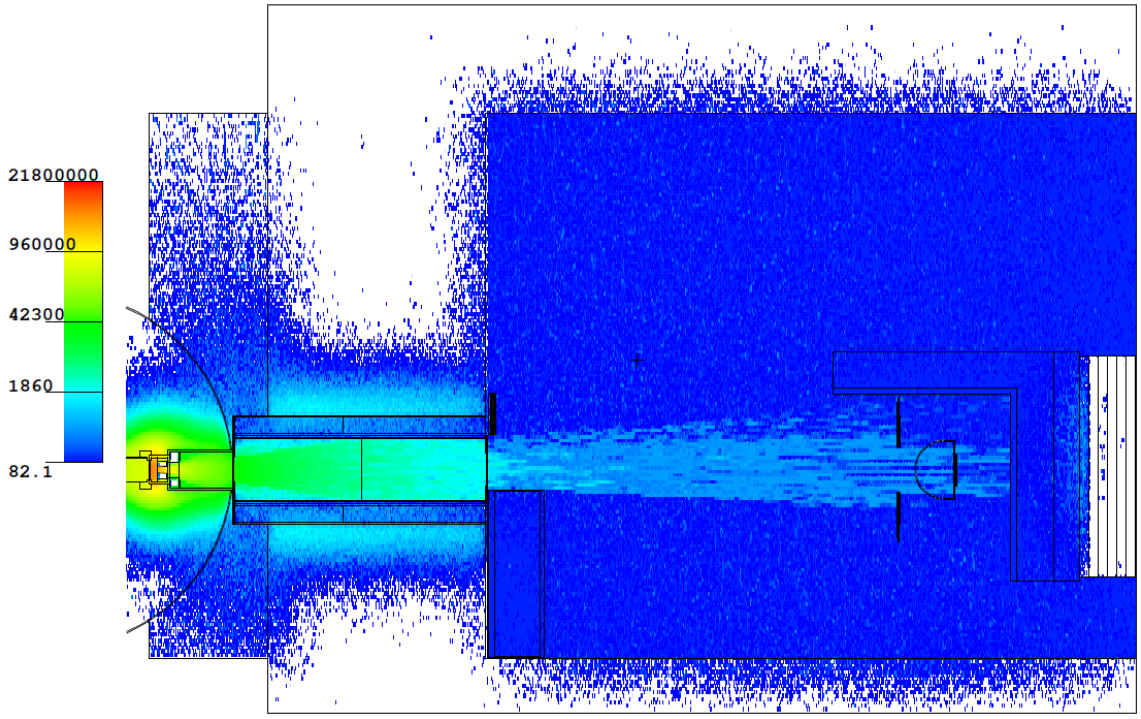

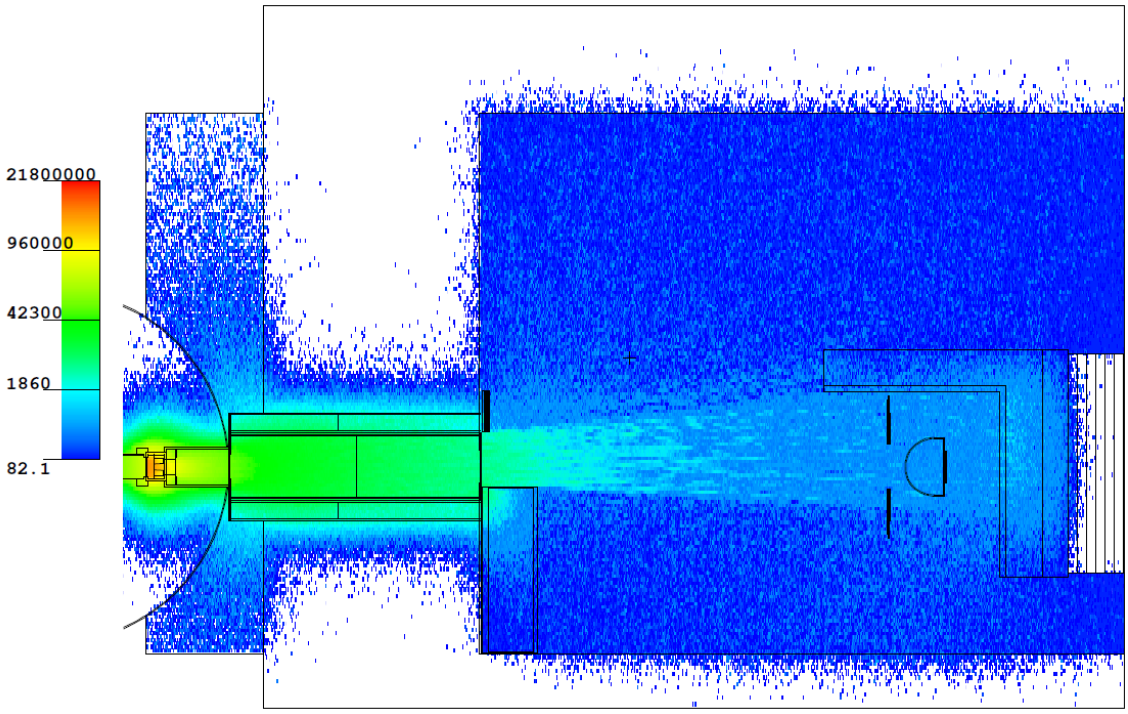

Figure 3. Plan Views of Neutron Flux FMESHs for Energy Bin 1 (Top) and 2 (Bottom) in the ERS Model.

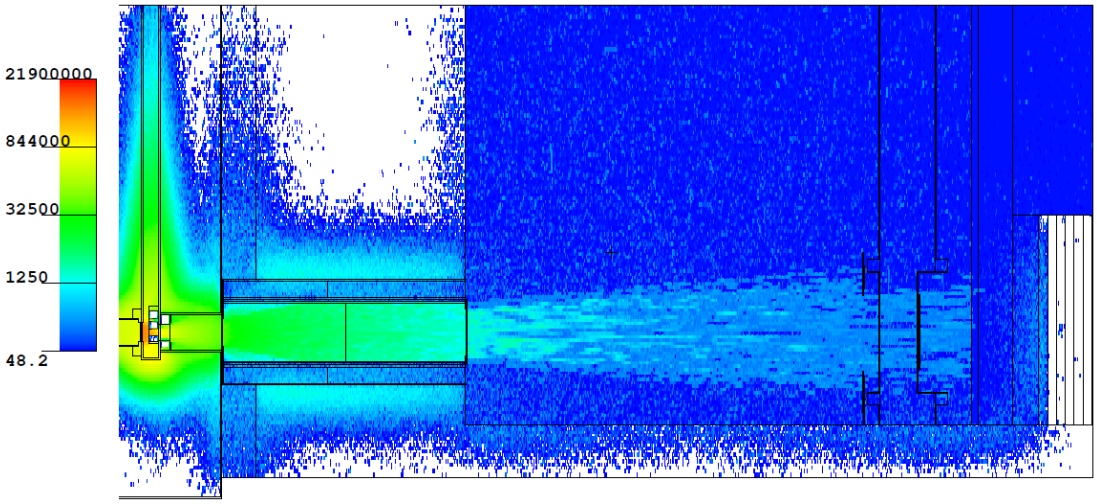

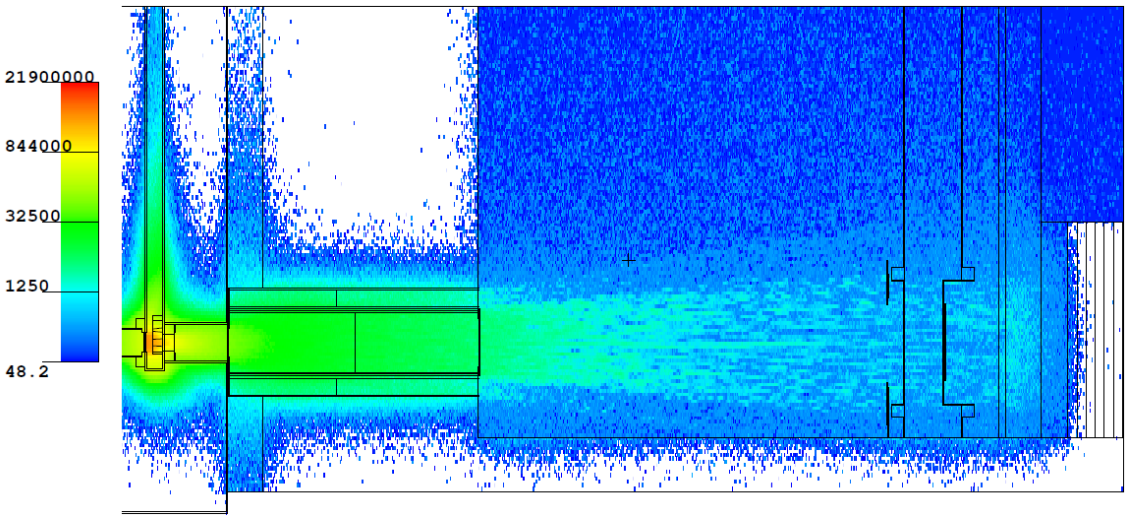

Figure 4. Side Views of Neutron Flux FMESHs for Energy Bin 1 (Top) and 2 (Bottom) in the ERS Model.

The average neutron flux incident on the F4 tally volume was roughly 440 n/cm2-s at a reactor power level of 5 watts. Neutrons with energies greater than thermal (0.5 eV) are found to have the greatest affect in the ERS room after studying the two figures above. This conclusion will be used to choose materials that are suited to shield and absorb high energy neutrons. It should be noted that after the discussion in section 0(Appendix C), the values shown in this section should be interpreted as conservative estimates. The current MCNP model of the ERS is simulating a larger thermal neutron contribution than what was measured.

Shielding Arrangement #1

The crystal in the detector is to be centered in the middle of the neutron beam with a direct line-of-sight to the reactor core. The detector sub-systems must then be shielded adequately to account for the neutrons scattered by the air in the ERS. The initial shielding arrangement involved a 4-inch thick, 30% borated-polyethylene (BP-30) wall followed by an 8-inch thick wall of lead bricks with the detector placed directly behind it. A second 4-inch thick wall of lead was placed to the south of the detector as well. This configuration can be seen in Figure 5. Each wall in front of the beam had a 1-inch diameter hole cut out to ensure that the crystal would be exposed to the unperturbed flux of the neutron beam.

Boron-10 is a great neutron absorber with a thermal microscopic absorption cross-section of about 3840 barns [4]. The polyethylene that is mixed in the boron is used to slow the fast neutrons down by inelastic collisions of nuclei so that the ^{10}B atom can absorb them at lower energies. Polyethylene is made of carbon and hydrogen which are both known to be good neutron moderators [55]. It should be noted that boron also produces a 0.42 MeV photon when it interacts with neutrons making it necessary to place a photon absorber behind this material. Lead, a classic gamma shielding material, is placed behind the borated-polyethylene to attenuate the secondary photons emitted from neutron activation and the reactor core. The combination of these three materials should attenuate any undesired particles from reaching the HPGe detector.

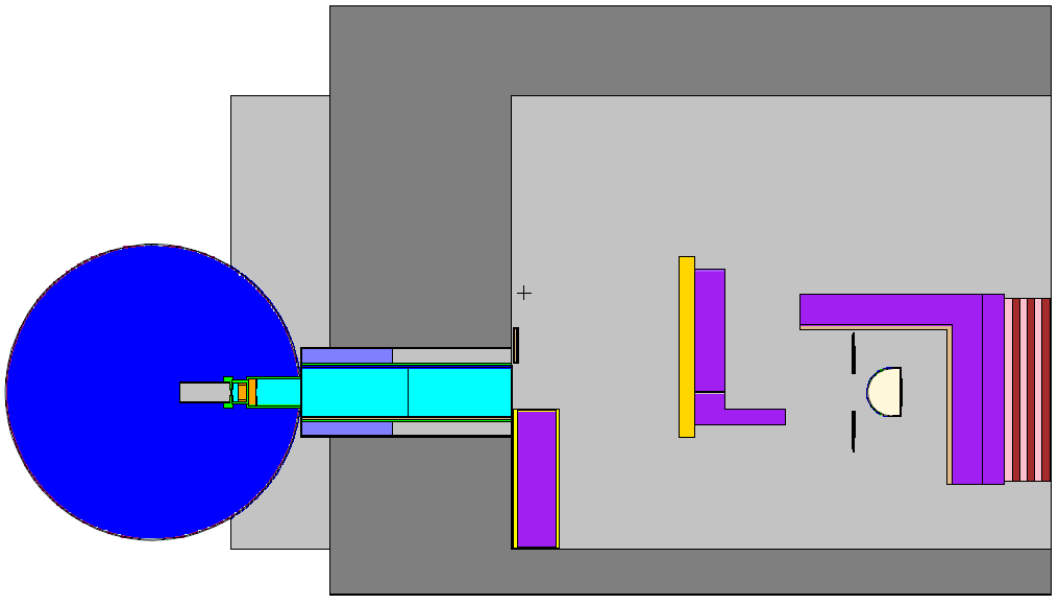

Figure 5. MCNP6 Model of Shielding Arrangement #1.

The first MCNP run was conducted to calculate the magnitude and energy spectrum of the neutron flux in the beamline and the ERS room. An FMESH of the MCNP model with Shielding Arrangement #1 was performed with the results scaled to a reactor power level of 5 watts. The FMESH called on two separate plots: particle flux of neutrons less than or equal to 0.5 eV and particle flux of neutrons with energies above 0.5 eV. The two FMESH plots can be seen below with the values color coded on the right-hand side of the pictures. The contribution of photons will be analyzed later in this report.

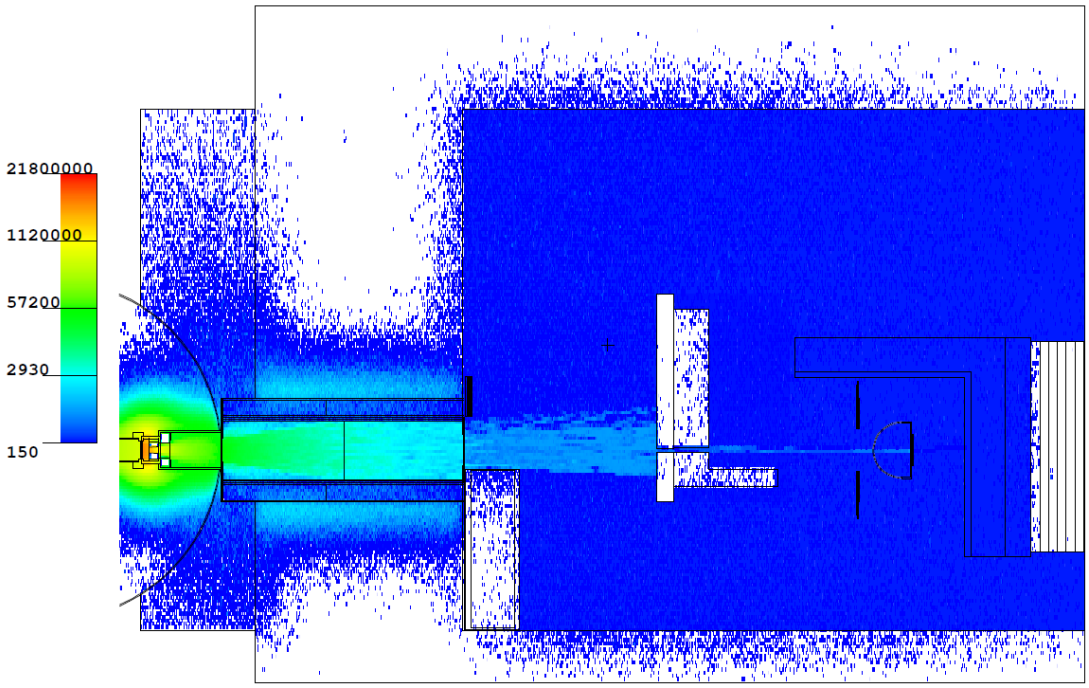

Figure 6. Neutron FMESH with Shielding Arrangement #1 (Energy Bin 1).

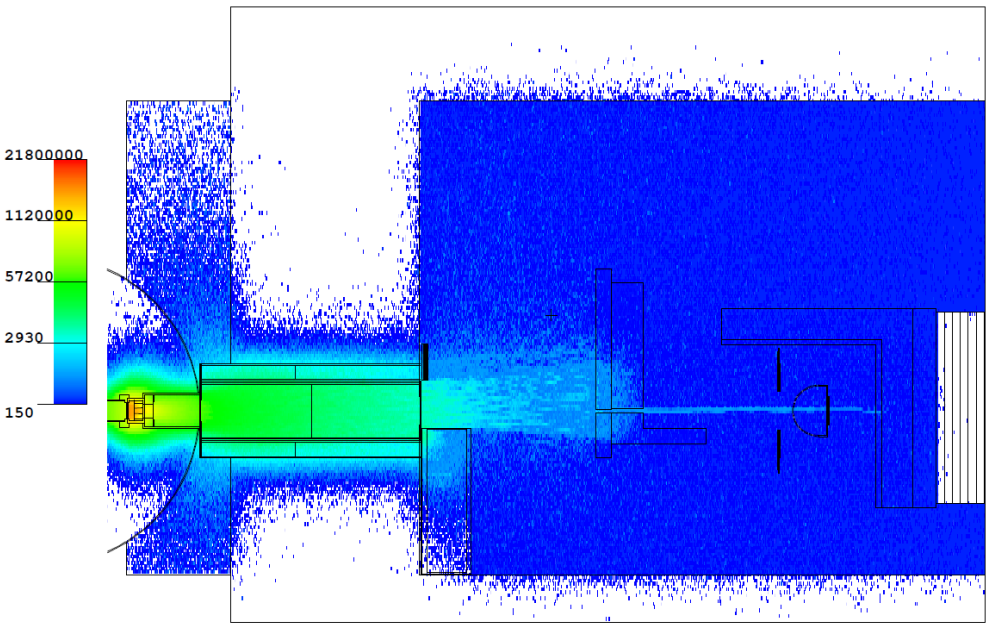

Figure 7. Neutron FMESH with Shielding Arrangement #1 (Energy Bin 2).

The input file for the ERS MCNP model can be found in the appendix of this report along with specific tally set up and geometry arrangement for all shielding configurations. It can be seen from the FMESH plots that the neutron flux in most of the room is between 102 and 103 *n/cm*^{2}-s, this same flux is relatively consistent throughout which means neutrons will be approaching the detector from all directions. It was determined from this analysis that a more elaborate shielding configuration must be designed for the second attempt.

Shielding Arrangement #2

A polyethylene layered BP-5 wall will be placed in front of the beam as it enters the room for the second shielding configuration. The wall will have 1 inch of BP-5 followed by an inch of polyethylene an inch of BP-5 behind that and finally the wall ending with an inch of polyethylene. The shielding surrounding the area where the detector will be placed has not changed geometrically but two new materials will replace the 4 inches of BP-30 so see what type of shielding material will work best for this arrangement. The first addition will be 7.5% lithium-enriched polyethylene (LiP) sheets that can be used to shield both fast and thermal neutrons. Lithium is advantageous over boron because it does not produce a high energy gamma ray when exposed to neutrons. Unfortunately, lithium falls behind boron when microscopic absorption cross-sections are discussed. ^{6}Li has a microscopic absorption cross-section of about 941 barns for thermal neutrons [56]. The polyethylene uses the same principles in the BP-30 sheets to slow the neutrons down from fast energies, allowing the lithium to absorb them.

The second material used in this shielding arrangement is simply a less enriched version of the borated polyethylene used in Shielding Arrangement #1. The sheets will consist of 5% boron enriched polyethylene (BP-5). The analysis of the first shielding arrangement suggests that the fast

neutrons from the beam are not slowing down to thermal energies quick enough before they pass through the BP-30 shielding and the lead does very little to stop the remaining neutrons from reaching the HPGe detector. The much higher hydrogen content in the BP-5 will cause more inelastic collisions and the remaining 10B will absorb these slower neutrons.

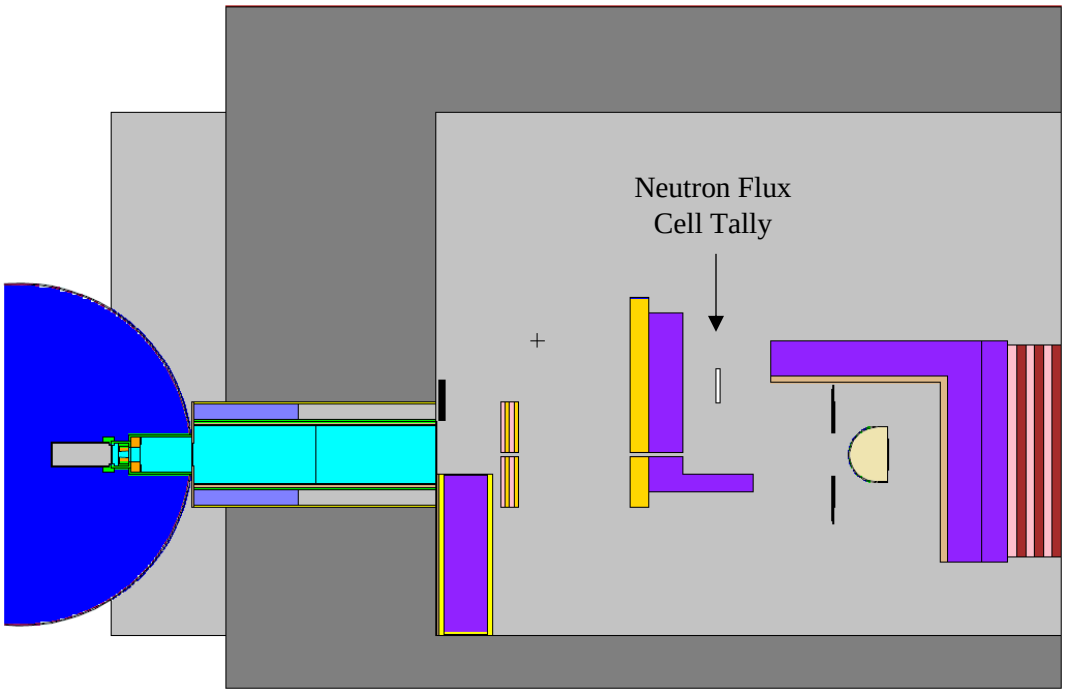

Figure 8. MCNP6 Model of Shielding Arrangement #2.

The shielding arrangement described above was run in MCNP6, first using the BP-30 and then replacing it with BP-5 and finally LiP, three separate runs were conducted. Figure 8 also shows the position of the F4 volume tally used in all shielding arrangements to compare the magnitude of the neutrons incident on the shielded area. The neutron flux values tallied in the cell can be seen in Table 1. The flux behind Shielding Arrangement #1 was also compared to the configurations described above to determine how much the shielding has improved.

Table 1. Neutron Flux behind Shielding Arrangement #2.

Shielding Material	F4 Tally Results (n/cm^2-sp)	Error	5 Watt Neutron Flux (n/cm^2-s)
No Shielding	5.56E-07	1.98%	438.42
BP-30 (SA#1)	8.00E-08	5.88%	62.95
BP-30	3.24E-08	8.66%	25.49
BP-5	3.32E-08	8.55%	26.15
LiP	3.54E-08	8.22%	27.84

The polyethylene layered BP-5 wall has almost equalized the effectiveness of the shielding materials. The wall cuts the neutron flux down by almost a factor of 3 when comparing it to

Shielding Arrangement #1 value for BP-30 and reduces the overall intensity with no shielding by a factor of 17.

Shielding Arrangement #3

The third shielding arrangement will include all the same shielding materials but in a slightly different setup. The detector was completely surrounded with shielding which required the design and construction of a box made out of BP-30, BP-5, LiP, and lead. The MCNP model for this arrangement can be seen in the figure below.

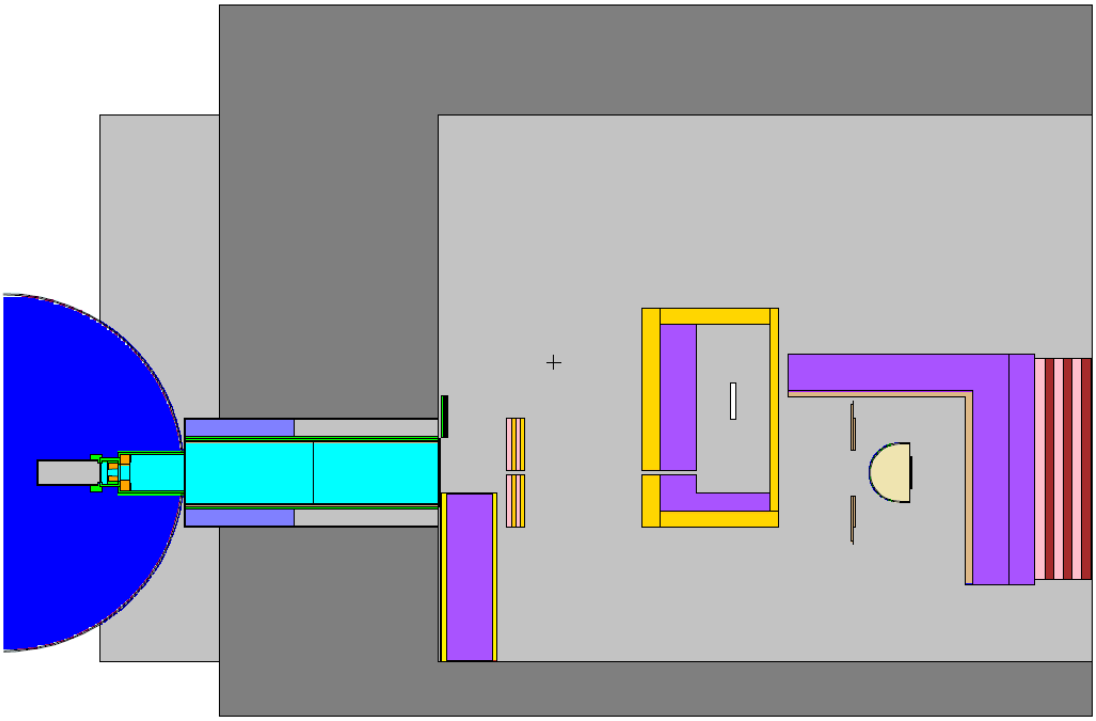

(Plan View)

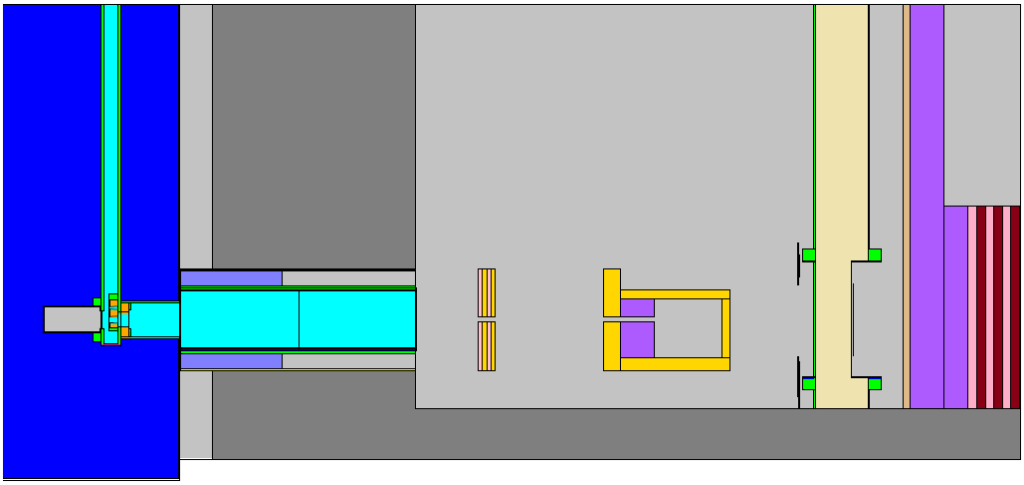

(Side View)

Figure 9. MCNP6 Model of Shielding Arrangement #3.

The detector will be completely incased in neutron and gamma shielding material. Based on the results from Shielding Arrangement #2 it was decided to place the BP-30 directly in front of the beam. The LiP will be used as the lid and back wall of the box while BP-5 will be used to shield the sides. There is a 3.5-inch slab of BP-30 placed on the bottom of the box as well.

Four trials will be tested in MCNP to determine how sensitive the arrangement is to changes in different geometries and thicknesses. Trial #1 will use 3.5-inch BP-5 side walls, 2-inch LiP lid and back wall, and a 3.5-inch BP-30 bottom cover. The two parameters that will stay constant in all four trials will be the 4-inch thick BP-30 wall and 8-inch thick lead wall directly in front of the beam. A picture of Trail #1 can be seen below for both the plan and side views of the arrangement.

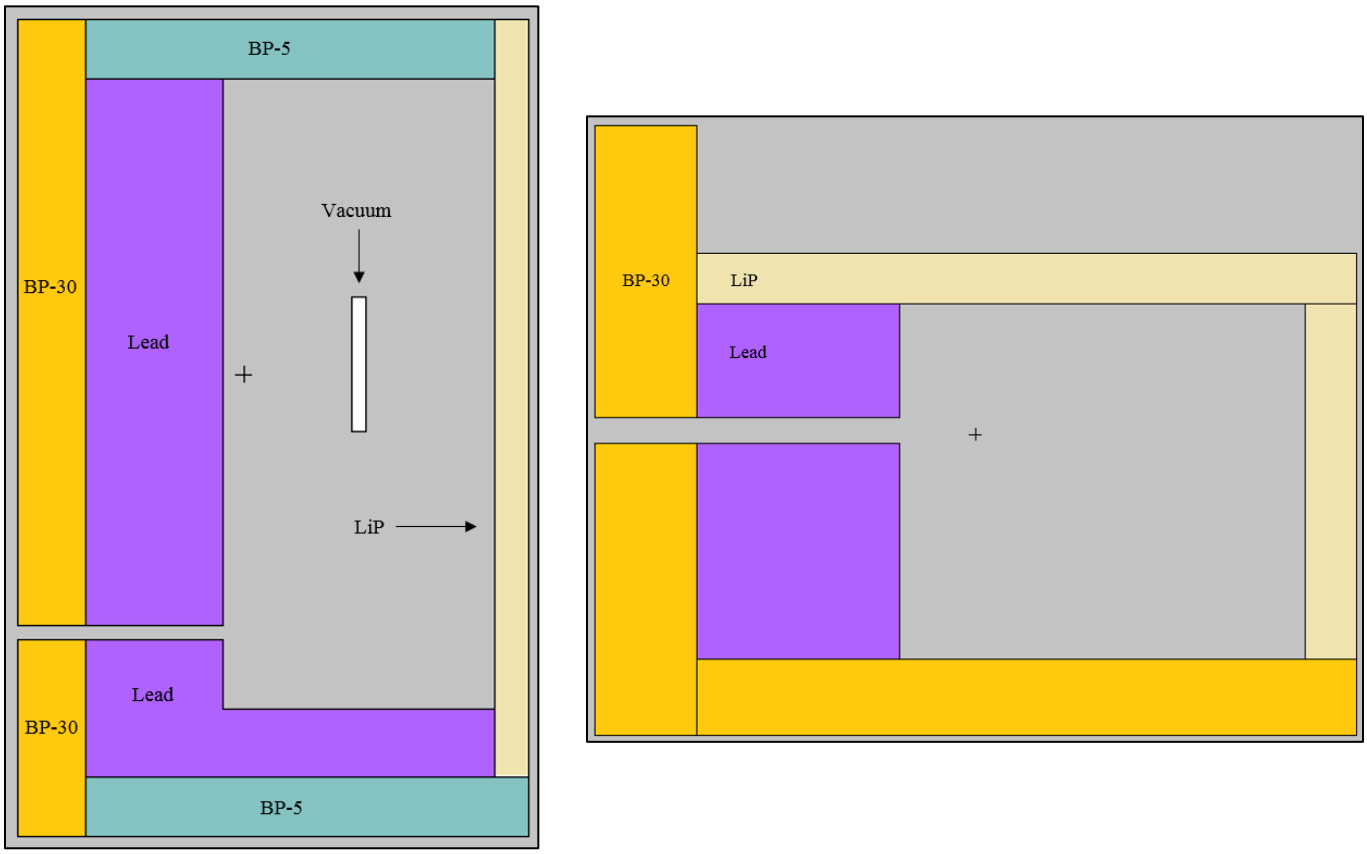

(Plan) (Side)

Figure 10. Plan and Side View of Trial #1 for Shielding Arrangement #3.

Trial #2 will simulate the shielding arrangement of Trial #1 with the exception of the bottom layer of BP-30. This trial will help us determine how much of an effect the neutrons scattering from the floor and the air underneath the detector have on the detector area. The two side walls of BP-5 will be trimmed down to 2-inch thick slabs for the Trial #3 while reinserting the 3-inch slab of BP-30 back underneath the detector area. This will test the sensitivity to the BP-5 thickness and determine how much we will need to build an effective shield. The last and final

trial will involve another layer of shielding taken away. The two side walls, the top of the shielding box and the back side of the box will each have a thickness of 1 inch. The results for trials one through four can be seen in the table below along with their uncertainties.

Table 2. Neutron Flux Results for Shielding Arrangement #3 (Trials 1 - 4).

Trial	F4 Tally Results (n/cm^2-sp)	Error	5 Watt Neutron Flux (n/cm^2-s)
No Shielding	5.56E-07	1.98%	438.42
#1	8.93E-09	7.39%	7.05
#2	2.47E-08	5.75%	19.51
#3	8.83E-09	7.37%	6.97
#4	1.11E-08	8.80%	8.79

The MCNP results for trials 1 through 4 show that removing the bottom layer of BP-30 from the arrangement has a large effect on the system. The calculations also show that reducing the thickness of the walls and lid of the box have very little effect. Based on these results two more trials were run but this time the bottom layer's thickness was first cut down to 2 inches in Trial #5 using the same geometry as Trial #3. Trial #6 uses a thickness of 1 inch for the bottom layer and matches all other dimensions of Trial #4. Table 3 shows the results calculated from these two trials.

Table 3. Neutron Flux Results for Shielding Arrangement #3 (Trials 5 & 6).

Trial	F4 Tally Results (n/cm^2-sp)	Error	5 Watt Neutron Flux (n/cm^2-s)
#5	1.00E-08	9.20%	7.92
#6	1.69E-08	7.17%	13.35

Final Analysis

The shielding arrangement of Trial #1 has the maximum amount of material allowing it to have the best shielding capabilities, permitting only 7.05 n/cm^2-s ± 0.7013 n/cm^2-s. Trial #4 allows about two more neutrons per second with considerably less material than Trial #1. Trial #4 is comprised of 1-inch thick pieces of BP-5 for the side walls, 1-inch thick pieces of LiP for the top and back walls and a 3-inch thick piece of BP-30 for the bottom. The neutron flux in the detector area for Trial #4 is 8.79 n/cm^2-s ± 0.7735 n/cm^2-s.

Results from section 0 (Appendix C) suggests that the model simulates a higher thermal neutron flux resulting in a lower fast neutron flux. It is unclear how large of an impact this discrepancy will have on how the data should be interpreted from the model. Further measurements and characterization efforts of both the neutron energy spectrum and gamma energy spectrum should assist in validating the MCNP model's capabilities in the future with regard to the ERS.

The shielding arrangement used for Trial #4 was chosen based on the combination of materials and how well it attenuated the neutrons compared to all other configurations. AutoCAD drawings can be found below that show a detailed plan for the shielding set up in the ERS room.

Neutron Shielding Materials:

- 8 Slabs of BP-30 (24” x 24” x 1”)
- 12 Slabs of BP-5 (24” x 24” x 1”)
- 4 Slabs of LiP (24” x 24” x 1”)

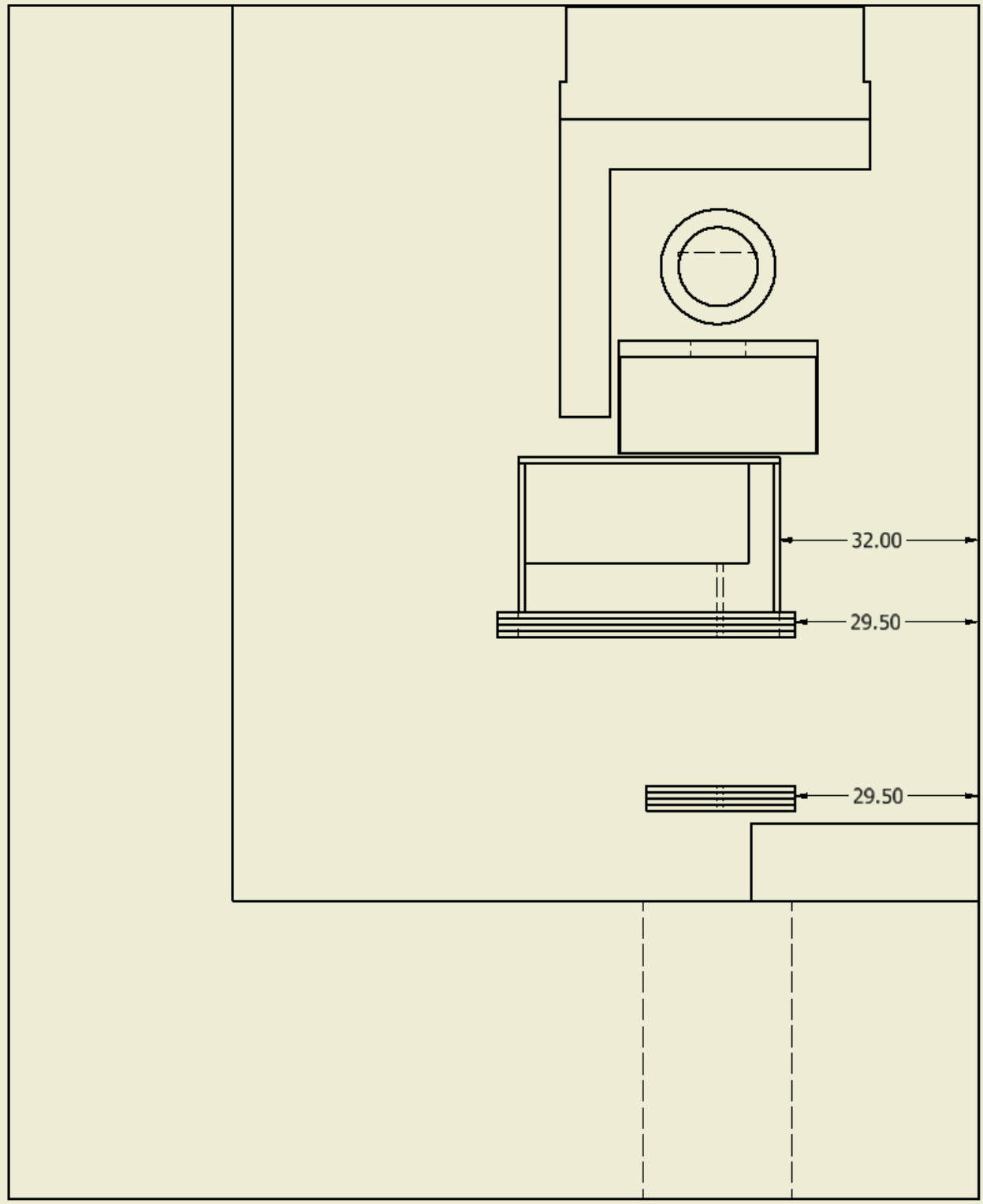

Figure 11. Plan View of shielding arrangement in ERS.

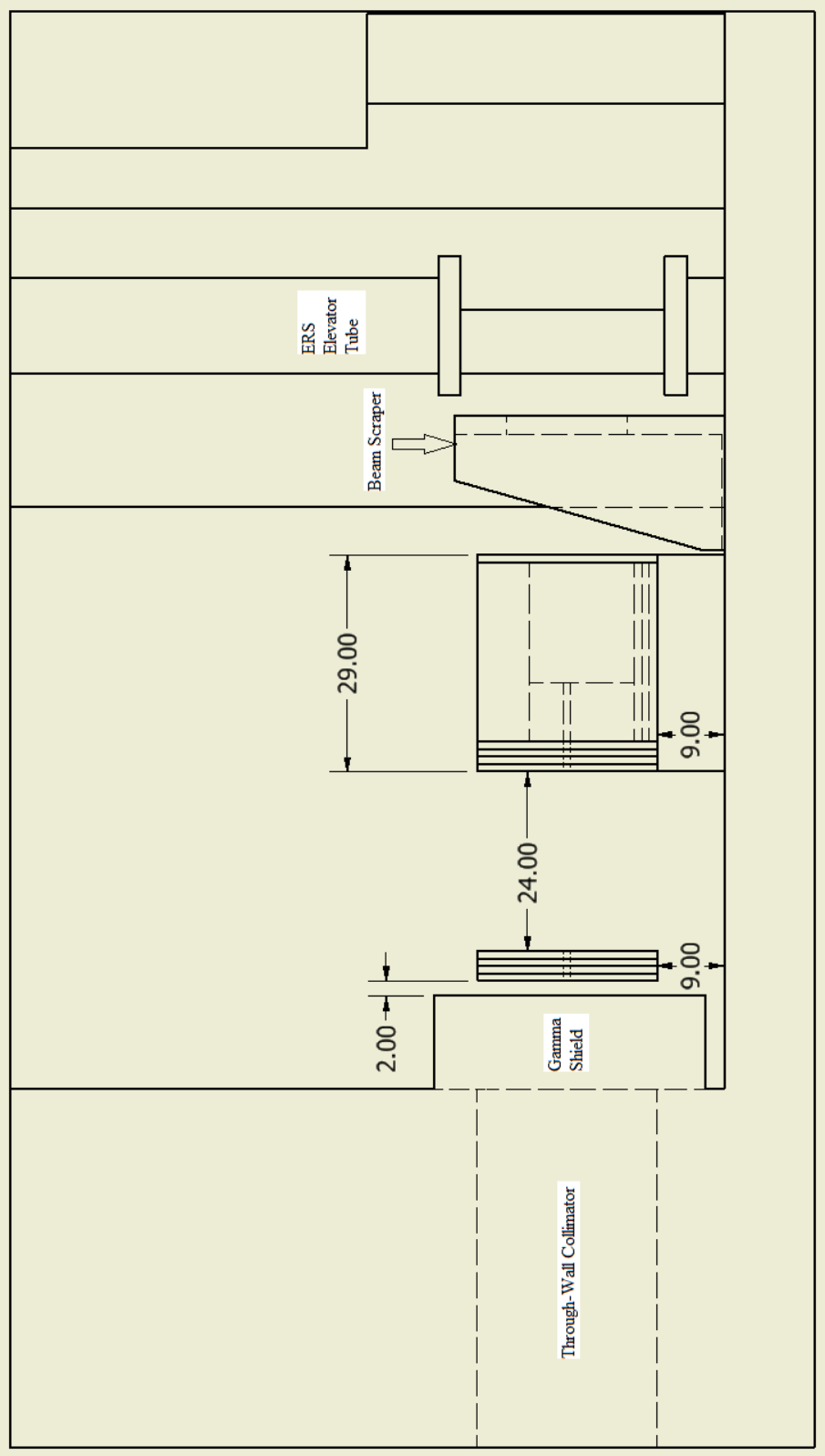

Figure 12. Side View of shielding arrangement in ERS.

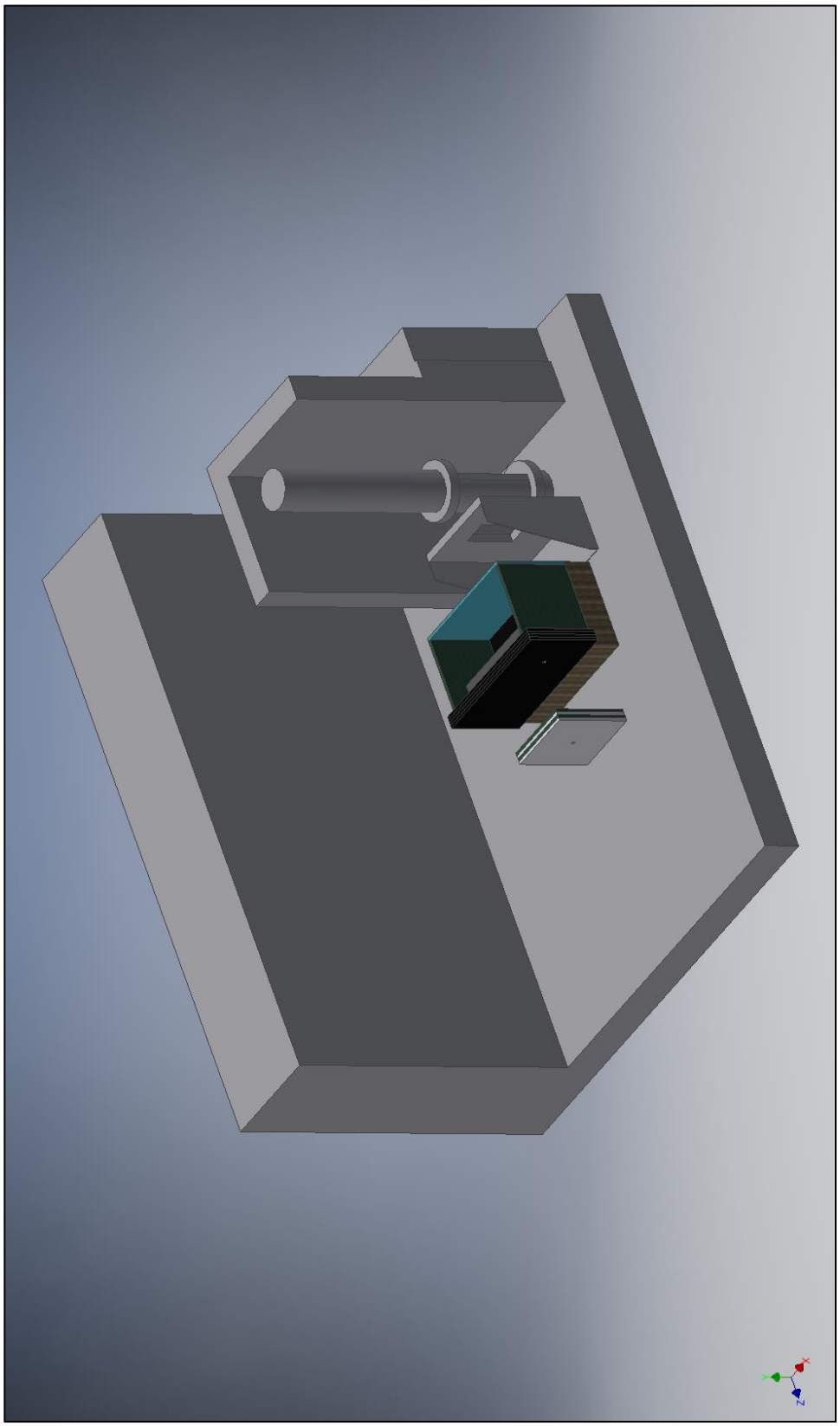

Figure 13. 3-D View of HPGe Detector Shielding Arrangement.

HPGe Detector Crystal

The next step in the gamma energy spectrum measurements is to obtain an understanding of what type of spectrum we can expect from this neutron beam. The most cost effective way of analyzing the spectrum is by using MCNP6. The detector that will be used for this experiment is an n-type, high purity germanium crystal that operates at a relative efficiency of about 15%. The crystal is one of Ortec's smaller models being only 50 mm wide and having a length of about 50 mm. The figures below show a screenshot of the Quality Assurance Data Sheet provided with the detector and the MCNP modeled HPGe crystal used for the gamma energy spectrum calculations.

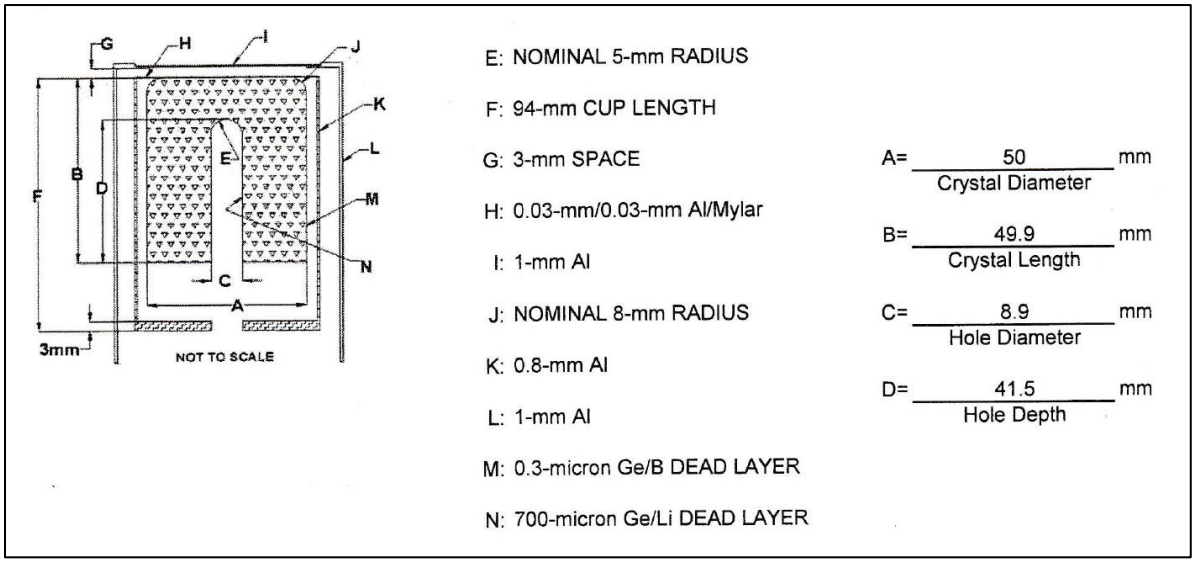

Figure 14. Dimensions and Material Composition of the HPGe Crystal.

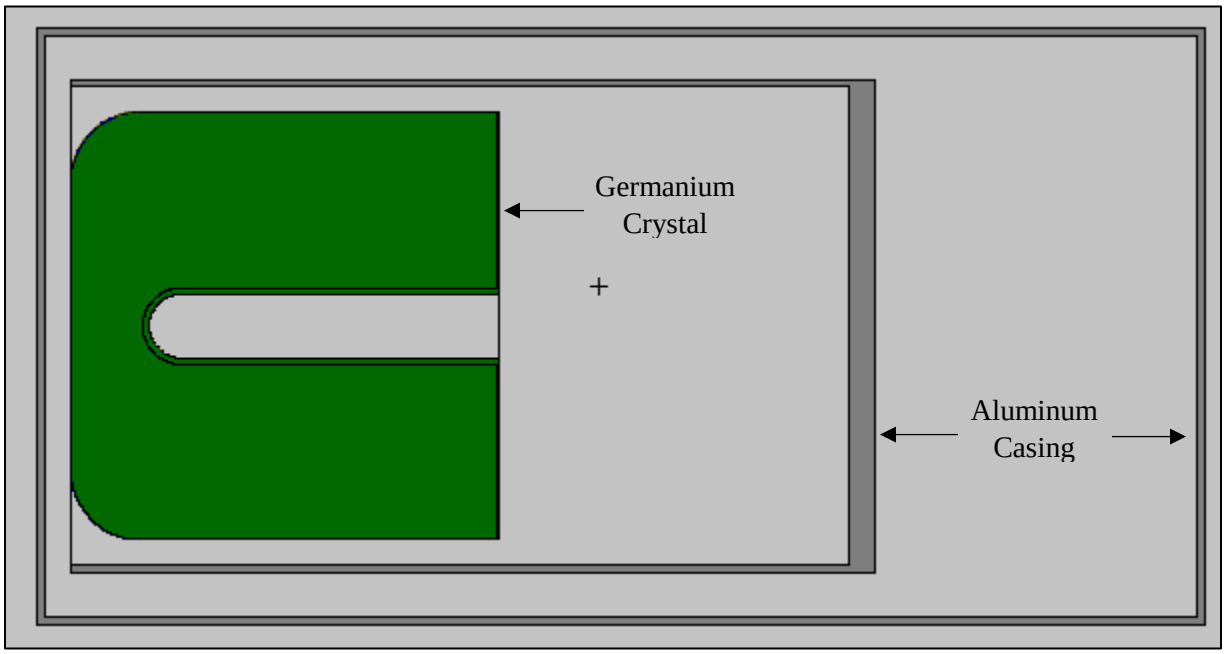

Figure 15. MCNP Model of HPGe Crystal.

Two types of pulse-height tallies (F8) were set up to be taken in the germanium crystal, a standard F8 tally and a special treated F8 tally (FT8). These tallies can be seen in Figure 16.

```
F18:p 6100
E18 0 1.75E-03 200ilog 3
C
F28:p 6100
E28   0 1.75E-03 200ilog 3
FT28  GEB 0.0 0.00125 0.0009 &
      PHL 1 16 1 HPG-1
F16:e 6100
```

Figure 16. F8 and FT8 tallies.

The F8 tally is pulse-height tally records the energy deposited in the cell of interest by the source particle as well as all secondary particles. The F8 was designed specifically for photon type problems that try to simulate the interactions in a detector. The PHL card in the F28 tally is a special treatment tally that models the detector with anticoincidence. A specific detector type can be specified in this card like HPG-1. When using the HPG-1, built-in particle dependent response functions are applied to the tallies resulting in more realistic results. The GEB special treatment tally provides an addition layer of realism when used with the F8 tally. GEB, stands for Gaussian Energy Broadening, and is based on the FWHM of the detector when exposed to photons. It requires three coefficients that are unique to each detector and can be measured by using the following equations [49]:

$$FWHM = a + b\sqrt{E + cE^2}$$

An MCNP simulation was conducted using $1x10^9$ particles and the two tallies shown above. Not a single value showed up for the F28 tally. This could mean not enough particles were making it to the detector or that the special treatment of the F8 tally is set up incorrectly.

Future work for this model should involve simulating more particles to produce tally detections in the detector cell. The coefficients for the GEB card should also be measured since they are unique to the detector and the application. A photon source should be created using the NRAD model to account for the photons emitted from the fuel in the core. This will result in two sources that required, the one just mentioned, and the neutron source used in the ERS model that produces secondary. A more powerful computer will be needed to simulate the number of particles required to produce data that is comparable to what will actually be measured.